Development of a Reduced Chemical Kinetic Model of n-Heptane–NG Blend for Homogeneous Charge Compression Ignition Engine Combustion

Keyvan Bahlouli

Submitted to the
Institute of Graduate Studies and Research
in partial fulfillment of the requirements for the Degree of

Doctor of Philosophy
in
Mechanical Engineering

Eastern Mediterranean University
January 2014
Gazimağusa, North Cyprus

Approval of the Institute of Graduate Studies and Research

Prof. Dr. Elvan Yılmaz
Director

I certify that this thesis satisfies the requirements as a thesis for the degree of Doctor of Philosophy in Mechanical Engineering.

Prof. Dr. Ugur Atikol
Chair, Department of Mechanical Engineering

We certify that we have read this thesis and that in our opinion it is fully adequate in scope and quality as a thesis for the degree of Doctor of Philosophy in Mechanical Engineering.

Assoc. Prof. Dr. Rahim Khoshbakhti Saray
Co-Supervisor

Prof. Dr. Ugur Atikol
Supervisor

Examining Committee

1. Prof. Dr. Ugur Atikol _____
2. Prof. Dr. Mustafa Canakci _____
3. Prof. Dr. Mehmet Akif Ceviz _____
4. Prof. Dr. Ibrahim Sezai _____
5. Assoc. Prof. Dr. Rahim Khoshbakhti Saray _____

ABSTRACT

As the transportation technologies move forward and the need of travelling becomes more important, the mankind is facing two major challenges, namely, emission of green-house gases and excessive fuel consumption. The homogeneous charge compression ignition (HCCI) engines have the well known benefits of emitting very low amounts of NO_x and soot, while producing higher efficiencies compared to the conventional engines. Computational modeling is a useful tool for engine design and optimization. The full chemical kinetic mechanisms to simulate the fuel oxidation consist of hundreds or thousands of species and reactions. Utilizing such a detailed mechanism requires extremely long computational time. In order to facilitate practical simulations, reduced mechanisms of smaller sizes are necessary. A three-stage reduction process is proposed in this research. The performance of the proposed method is investigated by producing reduced mechanisms of n-heptane fuel. This work is performed by using a validated single zone HCCI combustion model. To remove unimportant species at the first stage, the directed relation graph with error propagation (DRGEP) is applied. In the second stage, the computational singular perturbation (CSP) method is used to eliminate insignificant reactions. In the third stage, once again DRGEP is applied to the mechanism for further reduction. This combination of methods successfully reduced the comprehensive Curran's n-heptane mechanism (561 species and 2539 reactions) to a reduced mechanism with only 118 species and 330 reactions, while maintaining small errors (less than 2 percent) compared to the detailed mechanism in predicting selected representative parameters. The simulation time required for calculation is decreased from about 601

minutes when the detailed mechanism is used to 8 minutes by applying reduced mechanisms to the model.

Also, a reduced mechanism for a fuel blend of natural-gas and n-heptane is proposed. The approach is validated for the prediction of ignition timing in the HCCI combustion engine. A two-stage reduction process is used to produce two reduced mechanisms of existing detailed mechanisms for natural-gas and n-heptane fuels. The combination of the generated reduced mechanisms is used to develop a reaction mechanism for a fuel blend of natural-gas/n-heptane. Then, the genetic algorithm is used for optimization of reaction rate constants in the newly generated mechanism. The proposed mechanism includes only 41 species and 109 reactions. Simulation results agree well with the experimental results under various operating conditions, while maintaining small errors (less than 2 degrees) in predicting ignition timing.

Furthermore, effect of heat transfer through the boundaries in HCCI combustion simulation in generating reduced mechanism from the detailed mechanism is also investigated. A two-stage reduction process is used to produce reduced mechanisms of existing detailed GRI-Mech. 3.0 mechanism. Small differences observed in the developed reduced mechanisms for HCCI combustion model with considering heat transfer and in the adiabatic condition.

Keywords: HCCI engine, Ignition timing, Reduced mechanism, DRGEP, CSP, PCA, Blended fuel

ÖZ

Seyahat gereksinimleri nin önemi artıp ulaşım teknolojileri geliştikçe, insanoğlu iki büyük sorunla karşı karşıya kalmaktadır. Bunlar, sürekli artan sera gazlarının atmosfere salınımı ve aşırı miktarda yakıt kullanımı olarak kayıtlarda yer almaktadır. Homojen dolgulu sıkıştırma ile ateşlemeli (HCCI) motorlarının çok düşük seviyelerde NO_x ve kurum salınımları olması en bilinen faydalarındandır. Bu motorlar, bir yandan da geleneksel motorlara göre daha yüksek verimlilikte çalışmaktadır. Tasarım ve optimizasyon faaliyetlerinde en yararlı gereçlerin başında bilgisayarla modelleme yapmak gelmektedir. Yanmaya ait kimyasal kinetik mekanizmanın tamamı yüzbinlerce tür ve reaksiyondan oluşmaktadır. Böyle detaylı bir mekanizmayı kullanarak simülasyon yapmak için çok uzun bir bilgi işlem zamanına ihtiyaç duyar. Uygulanabilir simülasyonlar gerçekleştirebilmek için daha küçük boyutlara azaltılmış mekanizmalar kullanmak kaçınılmazdır. Bu araştırmada üç aşamalı bir azaltma süreci önerilmiştir. Önerilen yöntemin işleyişi n-heptan yakıtının azaltılmış mekanizmalarını oluşturarak incelemeye tabii tutulmuştur. Bu çalışma, geçerliliği isbat edilmiş tek bölgeli HCCI yanma modeli kullanılarak yürütülmüştür. İlk aşamada, önemsiz türleri mekanizmadan çıkarmak için hata yayılmalı yönlendirilmiş ilişki grafiği (DRGEP) uygulanmıştır. İkinci aşamada, hesaplamalı tekil karışıklık (CSP) metodu kullanılarak ilgisi olmayan reaksiyonlar elendmiştir. Üçüncü aşamada, daha fazla azaltma yapmak için DRGEP tekrar kullanılmıştır. Metodların bu şekilde birleştirilmesi Curran'ın (561 tür ve 2539 reaksiyondan oluşan) kapsamlı n-heptan modelini (sadece 118 tür ve 330 reaksiyondan oluşan) azaltılmış bir mekanizmaya düşürmeyi başarmıştır. Bunu yaparken de detaylı mekanizmaya göre temsili parametrelerin tahmininde yüzde

2’den daha az yanılgı payları elde edilmiştir. Hesaplamalar için detaylı mekanizma sırasında gereken simulasyon zamanı, 601 dakikadan, azatılmış mekanizmada 8 dakikaya kadar düşürülmüştür.

Doğal gaz ve n-heptandan oluşan bir yakıt karışımı için de bir azaltılmış mekanizma önerilmiştir. Bu yaklaşım, HCCI motorunun ateşleme zamanını tahmin etmek için kullanılmış ve geçerliliği sınanmıştır. Doğal gaz ve n-heptan yakıtlarına ait mevcut detaylı mekanizmalar iki aşamalı bir azaltma süreci kullanılarak iki azaltma mekanizması meydana getirilmiştir. Bu iki mekanizmanın birleştirilmesiyle doğal gaz ve n-heptan yakıtlarının karışımı için bir azaltılmış mekanizma geliştirilmiştir. Daha sonra, yeni üretilmiş mekanizmaların reaksiyon oranı katsayılarını optimize etmek için genetik algoritma kullanılmıştır. Önerilen mekanizmada sadece 41 tür ve 109 reaksiyon bulunmaktadır. Bir çok değişik çalışma şartlarında, simülasyon sonuçları, deneysel sonuçlarla iyi örtüşmektedir. Bu mekanizma ile ateşleme zamanını tahmin etmede çok düşük hata payları (yüzde 2’den az) elde edilmiştir.

Bir ileri tetkik olarak detaylı mekanizmadan azaltılmış mekanizma elde ederken HCCI yanma simülasyonu ile ilgili ısı kayıplarının etkisi sorgulanmıştır. Mevcut GRI-Mech 3.0 mekanizmasından azaltılmış bir mekanizma üretmek için iki aşamalı bir azaltma mekanizması kullanılmıştır. HCCI yanma modeli için geliştirilmiş azaltılmış mekanizmalarda ısı transferinin dikkate alınmasının çok az bir fark yarattığı gözlemlenmiştir.

Anahtar kelimeler: HCCI motoru, Ateşleme zamanı, Azaltılmş mekanizma, DRGEP, CSP, PCA, yakıt karışımı

To my Mother

ACKNOWLEDGMENTS

As I am sprinting towards the finishing line of my PhD study at Eastern Mediterranean University, I feel compelled to look back and thank all those who have helped and encouraged me along the way.

Firstly, I would like to acknowledge the unconditional support of my mother, Aghdas Forouzi, my sister, Sahar Bahlouli, and my brothers, Peiman, Arash, and Ramin Bahlouli, throughout my academic studies. Their enthusiasm for encouraging my pursuits in life has been extremely important to me. Without their love, I would not even dream of this day.

I would like to thank my wonderfully supportive and encouraging advisors, Prof. Ugur Atikol and Assoc. Prof. Rahim Khoshbakhti Saray. I always appreciated and benefited from the enthusiasm that they bring to research. I feel blessed to have had two advisors that I am happy to know as both colleagues and friends.

I also thank gratefully Professor M. D. Checkel for providing the permission to conduct experiments in Engine Research Laboratory of University of Alberta, Edmonton, Canada.

TABLE OF CONTENTS

LIST OF TABLES

LIST OF FIGURES

LIST OF ABBREVIATIONS & NOMENCLATURES

A	in-cylinder Surface area
C	species molar concentration
C_A	consumption of species A
$C_{P_{\text{int}}}$	specific heat constant (at constant pressure) of intake mixture (J/kg K)
c_{pk}	specific is heat constant of kth species
c_V	specific heat at constant volume (J/kg K)
c_1	heat transfer coefficient
c_2	heat transfer coefficient
D	cylinder bore (m)
E	activation energy
f	forward reaction
H	enthalpy
h	specific enthalpy
h_k	specific enthalpy of kth species
$(h_k)_0$	standard heat of formation of kth species at 0 K
I_K^i	importance index of the kth reaction to the ith species
L	instantaneous cylinder height (m)
m	total number of species
m	mass (kg)
m_{int}	intake mass (kg)
MW	molecular weight (kg/kmol)
n	total number of reactions

P	pressure (Pa)
P_A	production of species A
P_r	evaluated pressure at reference condition (Pa)
P_{mot}	motoring pressure (Pa)
Q	heat loss (J)
$\dot{Q}$	heat transfer rate (W)
$\dot{Q}_{real}$	real heat transfer rate (W)
$\dot{Q}_{\text{model}}$	Woschni's heat transfer rate (W)
R	ratio of connecting rod length to crank radius
R	column vector of reaction rates
$\overline{R}$	universal gas constant (kJ/kmol- K)
r	backward reaction
R_j	rate of the jth reaction
S	stoichiometric coefficient matrix
S_i^j	stoichiometric coefficient of the ith species in the jth reaction
S_{fast}	components of the stoichiometric vectors in the fast subspace
S_{slow}	components of the stoichiometric vectors in the slow subspace
T	temperature (K)
t	time (s)
T_{int}	temperature of intake mixture (K)
T_r	evaluated temperature at reference condition (K)
U	internal energy (J)
V	volume (m^3)
V_c	clearance volume (m^3)

V_d	displacement volume (m^3)
V_P	mean piston speed (m/s)
V_r	evaluated volume at reference condition (m^3)
v	stoichiometric coefficient
v'	reactants stoichiometric coefficients
v''	products stoichiometric coefficients
S_i^j	stoichiometric coefficient of the ith species in the jth reaction
Y_k	mass fraction of *k*th species

Greek

α	heat transfer coefficient
θ	crank angle (deg)
ϕ	Total equivalence ratio
τ	inverse of mixing time scale (1/s)
ω	reaction rate
$\dot{\omega}_k$	species molar production rate

Abbreviations

BMEP	brake mean effective pressure
CA	crank angle
CD	degrees crank angle
CI	compression ignition
CO_2	carbon dioxide
CNG	compressed natural gas
EGR	exhaust gas recirculation

EVO	exhaust valve opening
GA	genetic algorithm
HC	hydro-carbon
IC	internal combustion
IMEP	indicated mean effective pressure
IVC	inlet valve closing
LHV	low heating value
MHR	maximum heat release
MZCM	multi zone combustion model
NO_x	nitrogen oxides
PM	particulate matters
PRF	primary reference fuel
ODE	ordinary deferential equation
rpm	revolutions per minute
SI	spark ignition
SM	Smokes
SOC	start of combustion
SZCM	single zone combustion model

Chapter 1

INTRODUCTION

1.1 Internal Combustion Engine: A Short Brief

An internal combustion engine is the most common technology to power vehicles. In addition, it is also a main power generator for some industries, such as small scale electricity production. However, the use of internal combustion engines is considered as one of the main causes introducing two major challenges in recent years, i.e. high fuel consumption and toxic emissions such as green house gas (GHG) emissions, nitrogen oxides (NO_x), smokes (SM), particulate matters (PM), carbonmonoxide (CO), hydrocarbons (HC) and the other emissions. Stringent regulations on these issues lead to a significant amount of research to be conducted to reduce emissions in internal combustion engines.

Internal combustion engines have a long history. During its advancement, the spark ignition (SI) and compression ignition (CI) engines have emerged as the two most dominant technologies. Beau de Rochas (1862) developed the fundamental ideas of SI engine as early as 1860s. Diesel engine was introduced later by Akroyd Stuart (1890) and Rudolf Diesel (1892). Ever since, SI and CI engines have been the basis of the modern engines, on which numerous adjustments were made for enhancing their performance and emissions characteristics. The compression ratio of the SI engine is lower than that of the CI engines due to knocking taking place in SI engines with relatively high compression ratios. This results in reduction of mass and initial cost of the SI engines; however, their efficiencies will be less than that of the

CI engines. In the SI engines the particulate matter (PM) emissions are very low due to well premixed in-cylinder charge. Also, the reduction of other emissions such as unburned hydrocarbons (HC), carbon monoxide (CO) and nitrogen oxides (NO_x) is efficiently possible in SI engines by using three-way catalytic converters. In CI engines, however, the problem is that both NO_x and PM emissions show opposite behavior: conditions that reduce the formation of nitric oxides increase the production of soot, and vice versa. The cost of after-treatment devices is expensive and not easily available in the market. In order to reduce both soot and NO_x emissions simultaneously, a careful combination and adjustment of the different measures and after-treatment devices have to be applied. These improvements can be achieved by using a modern combustion system known as homogeneous charge compression ignition combustion (HCCI) engine which is a potential candidate for higher thermal efficiencies and lower emissions [1-3]

1.2 HCCI Combustion

HCCI combustion is an alternative and a promising technology utilized in internal combustion engines in order to save fuel while meeting emission standards. There are also other terminologies for HCCI combustion in the literature such as:

- Active Thermo Atmospheric Combustion (ATAC) [4]
- Active Radical Combustion (ARC) [5]
- Controlled Auto-Ignition (CAI) [6]
- Premixed Charge Compression Ignition (PCCI) [7]
- Premixed lean Diesel Combustion (PREDIC) [8]
- Compression Ignited Homogenous Charge (CIHC) [2]
- Modulated Kinetic (MK) [9]

1.2.1 HCCI Combustion Principle

HCCI combustion engines involve a process, which possess features of a combination of both spark ignition and diesel engines. The pre-mixed mixture of fuel and air are charged into the cylinder in the similar manner to SI engines while its charge is ignited due to compression in the same way to CI engines. Since there is no external ignition source in the HCCI engine, the auto-ignition of the cylinder charge will control the combustion.

1.2.2 Main Advantages of HCCI Combustion

HCCI combustion demonstrated that, under appropriate conditions of lean mixture and high residual content, a high compression ratio engine with a pre-mixed mixture can operate by auto-ignition. Also, low peak temperatures and well premixed lean mixture leads to negligible NO_x and soot emissions [1-3]. The capability of burning with various fuels that have different physical and chemical properties [10] and also the combination of different fuels as blends like n-butanol/n-heptane, natural gas/n-heptane, and ethanol/gasoline [11-13] are additional major advantages of HCCI engines.

1.2.3 Main Disadvantages of HCCI Combustion

A Limited operational range and the lack of any direct control on ignition timing are the two main challenges associated with HCCI combustion engine applications [14-16]. The operating range of HCCI engines is limited by knock phenomenon at high loads, and high cyclic variations at low loads [17, 18]. The high cyclic variations cause unstable combustion leading to limited operating range [18]. Also, the combustion take place due to the interaction between the temperature and pressure histories and the chemical processes without any control over the ignition timing [14-16].

1.3 Mechanism Reduction

Understanding fuel chemistry as well as producing a detailed model that properly describes fuel oxidation chemistry is critically important for HCCI engine design and optimization. However, real fuel is a complicated mixture to be modeled using a comprehensive chemical mechanism. Instead of this, a simpler surrogate fuel is used in numerical simulations. For example, since n-heptane has a cetane number of approximately 56, which is very similar to the cetane number of conventional diesel fuel, it can be considered as a good diesel fuel surrogate. A long list of detailed n-heptane mechanisms has been developed, such as the model of Nehse et al. [19], the model of Lindstedt and Maurice [20], the model of Held et al. [21], and the Golovitchev's mechanism, proposed by Golovitchev [22] at Chalmers University, containing 57 species and 290 reactions, and lastly the model of Curran et al. [23], which consists of 561 species and 2539 reactions.

The GRI Mech 3.0 mechanism [24], including 53 chemical species and 325 reactions, and the Konnov mechanism [25], containing 121 chemical species and 1027 reactions, were introduced for natural gas (NG) combustion.

For developing predictive combustion models, however, incorporating detailed chemistry into computational fluid dynamics (CFD) calculations is commonly assumed to be essential. A large system of nonlinear stiff ordinary differential equations (ODE) is produced by using detailed chemical kinetics mechanisms. The numerical solution of the large number of such systems within the CFD framework results in exceedingly long CPU times. Consequently, with most of the comprehensive kinetic mechanisms developed for hydrocarbon fuels, large scale three-dimensional reactive flow simulations are computationally unaffordable [26]. Therefore, reduction of the size of the detailed mechanism, keeping its essential

features, is found to be a viable solution to the problem of exceedingly long computational run-times.

1.4 Scope and Objectives

Transportation is a necessity of the modern life. However, it has been introducing two major challenges in the recent years, namely; emission of green-house gases and high fuel consumption. These problems may be resolved by using modern combustion systems, in which higher thermal efficiencies are achievable. Use of HCCI combustion, having two main advantages, i.e. ultra-low NOx and near-zero soot emissions and considerable reduction of fuel consumption, is one of the key approaches to reach the above-mentioned goals in the future [1-3]. Lack of direct control on ignition timing is one of the main challenges associated with homogeneous charge compression ignition (HCCI) combustion engine application. Merging two fuels with various fuel properties at a variety of ratios on a cycle-by-cycle basis is considered as a solution for this problem [27]. Accurate fuel oxidation chemistry models of such blended fuels offer great potential for HCCI engine design and optimization. On the other hand, utilizing a detailed mechanism in a complicated system model needs high demand of computational time. Therefore, to facilitate practical simulations, reduced mechanisms of smaller sizes are necessary. The main objectives in this work are:

- Development of combined reduction methods to extend the reduction of the mechanisms from detailed mechanisms
- Development of reduced mechanisms for PRF fuels and natural gas fuel
- Proposing a reduced mechanism of natural-gas/n-heptane fuel blend with the combination of two developed reduced mechanisms of natural gas and

n-heptane fuel, based on the GRI-Mech. 3.0 and Golovichev's mechanisms

- Investigating on effect of heat transfer on generating a reduced mechanism from detailed one for HCCI combustion mode through the analysis of adiabatic and non-adiabatic single zone HCCI combustion model

1.5 Organization of Thesis

The contents of this thesis are organized into six chapters.

Chapter 1 gives a brief information about HCCI engine and also, describes the objective of this thesis.

Chapter 2 reviews the mechanism reduction methods and the use of these methods in generating reduced mechanism from detailed one. Also, literature survey on the use of blend fuels in internal combustion engines is reported.

Chapter 3 describes the engine simulation model and the mechanism reduction procedures used in current work. Also, description on the utilization of Genetic Algorithm for the reaction constants optimization and the experimental set-up is presented.

Chapter 4 includes two parts: Development of a reduced mechanism from comprehensive mechanism of Curran for n-heptane fuel to demonstrate the ability of proposed DRGEP-CSP-DRGEP reduction method; Development of a reduced mechanism for prediction of combustion timing for a fuel blend of n-heptane and natural gas.

Chapter 5 studies the effect of heat transfer through the combustion chamber boundaries in generating reduced mechanism from detailed mechanism.

Chapter 6 presents conclusions of this study and proposes the area of possible future work.

Chapter 2

LITERATURE REVIEW

2.1 Mechanism Reduction

There are two main classes of reduction procedure, namely time scale analysis and skeletal reduction. Identifying and eliminating unnecessary species and reactions and producing computationally efficient reduced mechanisms, which are still able to reproduce the main features of their corresponding detailed mechanisms over the conditions of interest, are the aims of both methods.

The number of variables and the stiffness can be reduced by applying time scale analysis, as a result of eliminating short time scales associated with quasi-steady-state species or partial equilibrium reactions. In this regard, the intrinsic low-dimensional manifold (ILDM) performs eigenvalue analysis of the Jacobian matrix and assumes that the fast subspace disappears promptly [28]. On the other hand, in the theory of computational singular perturbation (CSP) which considers the time dependence of the Jacobian matrix, higher-order accuracy can be achieved [29]. A detailed comparison of CSP and ILDM methods can be found in ref. [30]. By using CSP it is possible to identify important species and reactions so that it can be used as a formal method for reducing reaction mechanisms [31]. Examples of elimination of reactions using CSP could be found in refs [32-34].

Different methods have been developed for skeletal reduction. Sensitivity analysis is one of the earliest methods developed for skeletal reduction [35]. It does not directly provide decoupled information about the reactions and species, however, and

further post-processing is necessary. The method of principal component analysis (PCA) [36], based on sensitivity analysis, operates on the sensitivity matrices and systematically identifies the redundant reactions. In recent works, the methods of directed relation graph (DRG) [37] and also directed relation graph with error propagation (DRGEP) [38] were developed to identify unimportant species by resolving species coupling with high efficiency and minimal requirement of system dependent knowledge. A review of the various methods for the identification of unimportant species was given by Nagy and Turanyi [39].

All of the above mentioned methods produce a single reduced mechanism from the detailed mechanism. The reduced mechanism is usually obtained by combining the important species at all sampling points in the parameter space. But at certain stage of the simulation, not all these species are actually active. This is a problem for all globally reduced mechanisms unless the method is used to reduce the mechanism dynamically. Examples of such dynamic methods are: He et al. [40] proposed an on the fly mechanism reduction, which analyses the reaction system and updates the reduced mechanism dynamically at each time step based on the local conditions. They used flux based methods in the adaptive chemistry approach for combustion simulations. In this method, locally accurate reduced mechanisms are developed for any condition. However, as mentioned by the authors, the discontinuity in species conversion rate, when mechanisms switch during the simulation in the fly scheme, may cause species composition oscillation and the possibility of ODE solver failure. Liang et al. [26, 41] used the same strategy in mechanism reduction by utilizing DRGEP method.

Increasing the extent of reduction could be achieved by using integrated reduction methods. Niemeyer et al. [42] integrated sensitivity analysis to DRGEP method.

Their work demonstrated weaknesses of DRGEP and DRGASA, and the subsequent improvement of DRGEPSA. Using the DRGEPSA method and an allowable 30% maximum error in ignition delay prediction, a final skeletal mechanism with 108 species and 406 reactions was obtained from the n-heptane detailed mechanism of Curran et al. [23]. In another work, Lu and Law [43] used different reduction methods for the reduction of Curran's mechanism. This approach used constant volume autoignition and perfectly-stirred reactor (PSR) in the reduction procedure. More specifically, using a two-stage DRG followed by sensitivity analysis a skeletal mechanism consisting of 78 species and 359 reactions was obtained with approximately 30% maximum error in ignition delay prediction. They further reduced the mechanism and showed that, while the reduction was based on autoignition and perfectly-stirred reactor (PSR) systems, the performance of the reduced mechanism in diffusive system was also good. However, they mention that in a worst case scenario the reduction error can accumulate through multiple reduction stages. Therefore, unless the reduced mechanism is appropriately validated, the worst-case accumulated error should be conservatively assumed in the prediction of new problems. Recently, Shi et al. [44] applied an automatic reduction scheme with combination of DRGEP and PCA methods for the reduction of large detailed kinetic mechanisms of hydrocarbon fuels for HCCI engines. This approach successfully reduced the comprehensive mechanisms of n-heptane (561 species and 2539 reactions) to reduced mechanisms with sizes of 140 species and 491 reactions.

2.2 Blend Fuels

Fuel blending is one of the approaches utilized for controlling HCCI combustion timing. Mixture ignitability can be adjusted on a cycle-by-cycle basis by mixing fuels

with various ignition properties and altering the blend ratio. Examples of such controlling method are given as follows:

Christensen et al. [45] used a variable compression ratio technique accompanied with different inlet temperature, various blends of n-heptane/iso-octane, and regular gasoline/diesel blends to adjust the start of combustion angle to the set points for a single-cylinder HCCI engine. In order to obtain auto-ignition at around TDC for a blended fuel of n-heptane/iso-octane with higher octane number, the engine should adjust to work with higher compression ratio. This work demonstrated that HCCI engine with variable compression ratio can run almost on any liquid fuel.

By altering the proportion of ethanol and n-heptane in the mixture, Olsson et al. [46] controlled the combustion timing for a given load and thereby extended the operating range for a turbocharged HCCI engine. Results indicate that at low loads, the ratio of n-heptane in the mixture was increased to advance the combustion timing, while this manner changes as the load increases.

Hosseini et al. [47] showed that adding Reformer gas (RG) to the n-heptane fuel causes reduction of heat release in the first stage of combustion in the well-known two-stage combustion of n-heptane fuel. It also shifts the second stage of combustion to a more optimized crank angle position, which increases the indicated power and fuel conversion efficiency.

Nathan et al. [27] studied the possibility of using the HCCI technology to exploit biogas effectively in IC engines. Biogas has a high self-ignition temperature and used as the main source of energy. Therefore, diesel fuel, with a low self-ignition temperature fuel was blended in for improved ignition and to control the start of combustion. The work demonstrated that the biogas–diesel HCCI mode can work at efficiencies close to that of diesel operation while attaining extremely low levels of

NO and smoke in a BMEP range of 2.5–4 bar. However, the amounts of HC emissions of biogas–diesel HCCI mode are significantly higher in comparison with the normal diesel mode.

Accurate fuel oxidation chemistry models of such a blended fuels offer great potential for HCCI engine design and optimization. However, there are fewer publications on studying of blended fuel combustion.

Brakora et al. [48] developed a reduced mechanism for combustion characteristics prediction of diesel/biodiesel blended fuel in a HCCI engine. The reduced mechanism of methyl butanoate, which was generated by applying reduction methods such as flux analysis, ignition sensitivity analysis, and optimization of reaction rate constants, was combined with the reduced mechanism for n-heptane oxidation. Reaction constants of specific reactions in the combined mechanism were then adjusted for the single zone combustion model to improve the performance of the mechanism for prediction of the ignition delay time.

Dagaut and Togbé [49] developed a detailed chemical mechanism of butanol/gasoline mixture by a combination of kinetic schemes for the oxidation of the pure components of the butanol/gasoline surrogate. In another work, Dagaut and Togbé [50] performed a kinetic modeling of ethanol/n-heptane mixtures oxidation by merging the kinetic mechanisms of n-heptane fuel and an ethanol oxidation sub-scheme. They showed that utilizing the resulting comprehensive chemical kinetic mechanisms in perfectly stirred reactor (PSR) systems have good accuracy in predicting the mole fractions of the fuel components and of the main products.

Most recently, Aggarwal et al. [51] studied the ignition behavior of heptane/methane fuel blends at conditions relevant to diesel/HCCI engines in a closed homogenous reactor. They showed that the termed Chalmers mechanism [22],

consisting of 42 species and 168 reactions, agreed with the shock tube ignition data for the mixtures of pure n-heptane with air and also for the mixture of pure methane with air. As a result, this mechanism has been selected to investigate the ignition behavior of n-heptane/methane fuel blends. It has been shown that the addition of n-heptane decreases the ignition delay for methane-air mixtures in both low and high temperature conditions. However, the authors have not provided any validation with respect to experimental data related to a natural-gas/n-heptane blend fueled HCCI engine.

Utilizing a detailed mechanism in a complicated system model needs high demand of computational time. Therefore, to facilitate practical simulations, reduced mechanisms of smaller sizes are necessary. Therefore in this study a reduced mechanism of natural-gas/n-heptane fuel blend with the combination of two developed reduced mechanisms of natural gas and n-heptane fuel, based on the GRI-Mech. 3.0 and Golovichev's mechanisms is developed. Also, a new methodology is introduced to extend the reduction of the mechanisms from detailed mechanisms.

Chapter 3

MODEL DESCRIPTION, MECHANISM REDUCTION PROCEDURE, OPTIMIZATION, AND EXPERIMENTAL SET-UP

The first part of this chapter presents the main governing equations used to estimate the in-cylinder variations of the gas properties during the closed part of the system. The calculations are based on the ideal gas equation, the chemical kinetics and the volume changes inside a piston-cylinder arrangement. The closed interval of the system from intake valve closing (IVC) to exhaust valve opening (EVO) includes the compression, combustion and expansion processes. To start this calculation, the IVC conditions must be specified, including average in-cylinder pressure, volume of a combustion chamber, concentrations of each species, average temperature of the mixtures and the total mixture mass in the cylinder.

In the second part the reduction methods and the algorithms which are used in this work for generating the reduced mechanisms are explained.

In the third part Genetic Algorithm which is used for the optimization of reaction constants for the proposed mechanism for the blended fuel is described.

The simulations are compared and validated with Fathi et al. [12] experimental work. Brief information about the experimental set-up is given at the end of this chapter.

3.1 Governing equations of single zone combustion model.

The modeling was performed for the closed part of the HCCI engine cycle where in-cylinder mass remains constant. Therefore:

$$\frac{dm}{dt} = \sum_{k=1}^{m} \dot{m}_k = 0 \tag{1}$$

Here m is mass of the in-cylinder charge, $\dot{m}_k$ is the rate of mass of kth species and also m in the sum denote the number of species.

The net production rate of the species is:

$$\frac{dm_k}{dt} = \dot{\omega}_k MW_k V \tag{2}$$

Here $\dot{\omega}_k$ is kth species molar production rate, MW_k is kth species molecular weight and V is volume.

The cylinder pressure is calculated at each CA step using the ideal gas state equation:

$$PV = \frac{m}{MW} \overline{R} T \tag{3}$$

Here P is pressure, $\overline{R}$ universal gas constant, and T is temperature.

Cylinder volume change equation relative to time is as follows:

$$\frac{dV}{dt} = V_C [\frac{1}{2}(r_C - 1)(\sin \theta \frac{d\theta}{dt} - \frac{1}{2}(R^2 - \sin^2 \theta)^{-\frac{1}{2}}(-\sin 2\theta)\frac{d\theta}{dt})] \tag{4}$$

Here V_C is clearance volume, r_C is compression ratio, θ is crank angle, and R is the ratio of connecting rod length to crank radius.

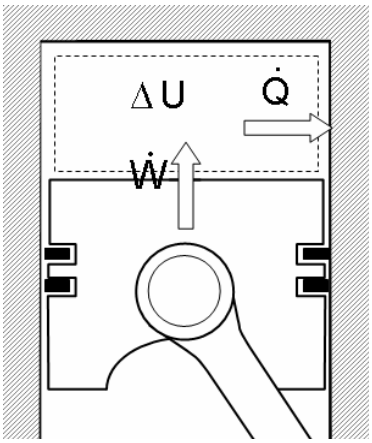

Figure 3. 1 Schematic of a Single Zone model [52]

The first law of thermodynamics, which balances internal energy changes with heat transfer to the wall and work done by the system (see Figure 3.1), is used to model the rate of mixture temperature change. Considering the classical first law equation,

$$\frac{dU}{dt} = \frac{dQ}{dt} - P\frac{dV}{dt} \tag{5}$$

Here U is internal energy and Q is heat transfer to the wall .The internal energy (the first term in Equation 5) is calculated as the sum of the internal energy of all species (Equation 6) with the derivative as shown in Equation 7.

$$U = \sum_{k=1}^{m} m_k u_k \tag{6}$$

$$\frac{dU}{dt} = \sum_{k=1}^{m} (m_k \frac{du_k}{dt} + u_k \frac{dm_k}{dt}) \tag{7}$$

Here u_k internal energy of kth species. The change in specific internal energy is calculated from Equation 8.

$$\frac{du_k}{dt} = c_{v,k} \frac{dT}{dt} \tag{8}$$

Here $c_{v,k}$ is kth species specific heat at constant volume. Finally, substituting Equations 7 and 8 back into Equation 5 yields, energy conservation equation given as:

$$m c_V \frac{dT}{dt} + \sum_{k=1}^{m} \dot{m}_k u_k = -P\frac{dV}{dt} + \frac{dQ}{dt} \tag{9}$$

Kongsereeparp and Checkel [53] after performing a detailed discussion about the mixing phenomenon and the heterogeneities existing inside the cylinder of HCCI combustion engine, have taken into account the mixture initial conditions and finally proposed the following relation as a modification to the selected heat transfer correlation:

$$\dot{Q}_{real} = \dot{Q}_{\mathrm{mod}\,el} - \tau\, m_{\mathrm{int}}\, C_{P_{\mathrm{int}}} \left(T - T_{\mathrm{int}}\right) \tag{10}$$

Here $\dot{Q}_{real}$ is the real heat transfer rate from the in-cylinder gases to the cylinder walls, which should be considered in the energy conservation equation, and $\dot{Q}_{\mathrm{mod}\,el}$ is the heat losses resulted from Woschni's heat transfer correlation [54]. $C_{P_{\mathrm{int}}}$ is specific heat constant (at constant pressure) of intake mixture. T_{int} is temperature of intake mixture, m_{int} is intake mass, and τ is inverse of mixing time scale. They performed their simulation for a NG-HCCI engine with compression ratio equal to 17 and also, an n-heptane-HCCI engine with compression ratio equal to 11.5.

As described by Kongsereeparp and Checkel, the coefficient τ may be adjusted according to the engine geometry and rotational speed. This coefficient has been specified to be $25\left(\frac{1}{s}\right)$ for the considered engine used by the researchers. By simulating the HCCI engine with various correlations during the compression stroke, it is determined by the authors that the heat transfer correlation proposed by Chang et al. [55] has the nearest prediction of in-cylinder pressure to the corresponding

experimental data and it needs minimum modification. This result may be due to the fact that this correlation has been basically developed for a HCCI engine. Therefore, the present study uses the heat transfer correlation developed by Chang et al. [55] and the modification term added by Kongsereeparp and Checkel to the heat transfer correlation. The final form of heat transfer equation for the current single-zone model is:

$$\dot{Q} = \left[\alpha\, P^{0.8}\, V_c^{0.8}\, L^{-0.2}\, T^{-0.73}\right] A - \tau\, m_{\text{int}}\, C_{P_{\text{int}}} \left(T - T_{\text{int}}\right) \tag{11}$$

and

$$V_c = c_1 \overline{V}_P + c_2 \left(\frac{V_d}{V_r}\right)\left(\frac{T_r}{P_r}\right)\left(P - P_{mot}\right) \tag{12}$$

Here, A is the heat transfer surface area, c_1, c_2, and α are the heat transfer coefficients. V_c is the clearance volume which is defined as the top dead center volume and that V is the in-cylinder volume as a function of CA. L is instantaneous cylinder height. V_d is the swept volume. $\overline{V}_P$ is mean piston speed. The subscript r denotes a reference crank angle, such as the one corresponding to the intake valve closing time. So, P_r, V_r, and T_r are pressure, volume and temperature at inlet valve closing condition, respectively. P is the firing pressure and P_{mot} is the motoring pressure. Generally, to modify the in-cylinder pressure in addition to the initial temperature and pressure adjustment, a set of parameters involving flow and heat transfer must be estimated due to the lack of detailed knowledge. These parameters include the heat transfer coefficients and the characteristic time scale (τ). In this work, the following values were considered for the aforementioned parameters:

$\alpha = 3.22160$, $c_1 = 2.30396$, $c_2 = 0.04917$ and $\tau = 32$.

Heat release rate (*HRR*) is defined as the change in enthalpy of in-cylinder mixture at each time step:

$$HRR = \frac{H_2 - H_1}{timestep} \tag{13}$$

Here H is the enthalpy of the mixture and time step is fixed at 0.1 CA.

$$H = m\,h \tag{14}$$

Here m is mass of mixture. h is specific enthalpy of the gas mixture. The specific enthalpy of the gas mixture is calculated through the following relations:

$$h = \sum_{k=1}^{m} h_k\, Y_k \tag{15}$$

and

$$h_k = (h_k)_0 + \int_{T_0}^{T} c_{pk}\, dT \tag{16}$$

Here m is number of species. h_k is specific enthalpy of kth species. Y_k is mass fraction of kth species. $(h_k)_0$ is the standard heat of formation of kth species. c_{pk} specific is heat constant of kth species. T_0 is temperature at 298 K [52].

3.2 Mechanism Reduction Procedure

3.2.1 Directed Relation Graph with Error Propagation (DRGEP).

The idea of Directed Relation Graph with Error Propagation (DRGEP) was introduced by Pepiot and Pitsch [38, 56] to overcome the shortcoming of directed Relation Graph (DRG) method. In the DRG method [37, 57], each node represents a species in the mechanism and there exists an edge from species A to B if there is an immediate dependence between them. The dependence is quantified by the normalized contribution of species B to A as:

$$r_{AB} = \frac{\sum_{j=1}^{n} \left| \nu_{A,j}\, \omega_j\, \delta_{Bj} \right|}{\sum_{j=1}^{n} \left| \nu_{A,j}\, \omega_j \right|} \tag{17}$$

Here $\delta_{Bj} = \begin{cases} 1 & \text{if the jth elementary} \\ & \text{reaction involve species B,} \\ 0 & \text{otherwise} \end{cases}$

$$\omega_j = \omega_{fj} - \omega_{rj} \tag{18}$$

$$\omega_{fj} = k_{fj} \prod_{i=1}^{m} C_i^{\nu'_{ij}} \tag{19}$$

$$\omega_{rj} = k_{rj} \prod_{i=1}^{m} C_i^{\nu''_{ij}} \tag{20}$$

$$k_{fj} = \left[A_j\, T^{n_j} \exp\left(-\frac{T_{aj}}{T} \right) \right] F_j \tag{21}$$

$$k_{rj} = \frac{k_{fj}}{k_{cj}} \tag{22}$$

Here the subscripts A and B specify the species identity. The subscripts j and i, respectively, designate the jth elementary reaction and the ith species, $\nu_{A,j}$ is the stoichiometric coefficient of species A, ω_j is the production rate, k_{fj} and k_{rj} are the forward and backward reaction rates, respectively, C_i is the molar concentration, ν'_{ij} and ν''_{ij}, are respectively the forward and backward stoichiometric coefficients. A, n, and T_a are the reaction parameters, and F is a correction term including the third body concentration, fall-off, and other special effects [37].

Therefore, r_{AB} is a measure of the error introduced to the production rate of A due to elimination of all the reactions that contain B. Once the search-initiating species are determined, the other species are eliminated if their contribution to the initial

species is less than a user-specified error tolerance. More detailed information about DRG method could be found in refs. [37, 38, 56, 57]. However, in the DRG selection procedure every species selected to be kept in the mechanism has equal importance and the set of strongly coupled species to which it belongs has to be kept entirely, which may not be necessary [38, 56].

The DRGEP method suggests that the effect of the error established by altering the concentration of a species or by eliminating the species entirely is damped as it propagates along the graph to reach the target species, a set of species deemed of interest to the investigator. Generally speaking, the species do not have equal importance, and the species directly linked to the target is of relatively high importance than those that are farther from the targets. In order to take into account this error propagation process, a geometric damping has been introduced by Pepiot and Pitsch [38, 56] in the selection procedure as follows:

$$r_{AB,P} = \prod_{i=1}^{m-1} r_{s_i s_{i+1}} \tag{23}$$

A path dependant coefficient $r_{AB,P}$ on path *i* from *A* to *B* is being the product of each primary interaction coefficient encountered on the path. The subscript s_i represents *i*th species and *m* is the number of species in the path. On Figure 3.2, for example, if path#1 is A→ B→ D, the coupling coefficient between *A* and *D* is:

$r_{AD,1} = r_{AB} . r_{BD}$

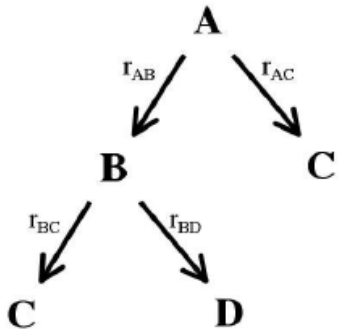

Figure 3. 2 Interaction graph between four species; coefficients *r* correspond to primary interactions. Species *A* depends on species *C* and *D* through its interaction with species *B* [56]

Finally, Pepiot and Pitsch [38, 56] introduced the generalized interaction coefficient of species with species *B* as the maximum path-dependant coefficient between *A* and *B* as follows:

$$R_{AB} = \max_{\text{All paths P}} \left[r_{AB,P} \right] \tag{24}$$

For example, on Figure 3. 2, *A* depends on *C* with coefficient

$$R_{AC} = \max\left[r_{AB} . r_{BC}, r_{AC} \right]$$

A new definition of the direct interaction coefficient is introduced by Pepiot and Pitsch [38], which is motivated by the shortcomings of earlier formulations, namely,

$$r_{AB} = \frac{\left| \sum_{j=1}^{n} v_{A,j}\, \omega_j\, \delta_{Bj} \right|}{\max\left(P_A, C_A\right)} \tag{25}$$

Here

$$P_A = \sum_{j=1}^{n} \max\left(0, v_{A,j}\, \omega_j\right) \tag{26}$$

$$C_A = \sum_{j=1}^{n} \max\left(0, -v_{A,j}\, \omega_j\right) \tag{27}$$

Here n is the number of reactions. P_A is production of species A and C_A is consumption of species A.

3.2.2. Computational Singular Perturbation (CSP) Method.

Detailed information about CSP can be found in refs. [29, 30]. It is briefly described as follows:

Simulating combustion process is accompanied by a set of ordinary differential equations,

$$\frac{d\mathbf{y}}{dt} = \mathbf{g}(\mathbf{y}) \tag{28}$$

Here **y** is the species concentrations and **g** is the species rate vector.

By utilizing CSP method the K-dimension of species rate vector of **g** could be decomposed to fast and slow subspaces as follows:

$$\mathbf{g} = \sum_{i=1}^{k} \mathbf{a}_i \, f^i \tag{29}$$

Here

$$f^i = \mathbf{b}^i \cdot \mathbf{g} \tag{30}$$

Here f is the modal amplitudes, $\mathbf{a}_i$ are the column basis vectors and $\mathbf{b}^i$ are the inverse row basis vectors.

Differentiating Equation 30 with respect to time:

$$\frac{df^i}{dt} = \sum_{j=1}^{K} \Lambda^i_j \, f^j, \qquad i = 1, 2, \ldots, \mathrm{K} \tag{31}$$

Here

$$\mathbf{\Lambda}_j^i = \left(\frac{d\mathbf{b}^i}{dt} + \mathbf{b}^i \cdot \mathbf{J} \right) \cdot \mathbf{a}_j, \qquad i, j = 1, 2, \ldots, \mathrm{K} \tag{32}$$

$$\mathbf{J} = \frac{d\mathbf{g}}{d\mathbf{y}} \tag{33}$$

and

$$\mathbf{a}_i = \left(\mathbf{b}^i \right)^{-1} \tag{34}$$

J is Jacobian matrix of **g**. Uncoupling the modes could be achieved by using ideal basis vectors, which transform the $\mathbf{\Lambda}$ matrix to a diagonal matrix. For linear systems, the Jacobian matrix is time independent such that $\frac{d\mathbf{b}}{dt}$ is unimportant and can be ignored. So, eigen-decomposition can be used to make the $\mathbf{\Lambda}$ matrix a diagonal matrix. For nonlinear systems, **J** is time-dependent in general, and as mentioned by Lam and Goussis [29], a set of basis vector pairs, $\mathbf{a}_i$ and $\mathbf{b}^i$, i = 1, 2, . . . , K, which make the $\mathbf{\Lambda}$ matrix block-diagonal, can be achieved by applying CSP refinement procedure. The first M pairs of basis vectors are for the M fast modes and the remaining (K–M) pairs are for slow modes.

The fast and slow subspaces are separated as follow:

$$\frac{d}{dt}\begin{pmatrix} \mathbf{f}_{fast} \\ \mathbf{f}_{slow} \end{pmatrix} = \begin{pmatrix} \mathbf{\Lambda}_{fast} & \\ & \mathbf{\Lambda}_{slow} \end{pmatrix} \cdot \begin{pmatrix} \mathbf{f}_{fast} \\ \mathbf{f}_{slow} \end{pmatrix} \tag{35}$$

Here $\mathbf{\Lambda}_{fast}$ are characterized with negative and significantly larger magnitudes of the eigenvalues while $\mathbf{\Lambda}_{slow}$ are characterized with the small eigenvalues. To distinguish between $\mathbf{\Lambda}_{fast}$ and $\mathbf{\Lambda}_{slow}$, a characteristic time scale τ_c associated with each sampled reaction state is defined. The modes, with time scales shorter than τ_c, belong to the fast space.

Using the above mentioned process the components of species rate vector **g** can be decomposed into two parts in fast and slow subspaces, respectively.

$$\mathbf{g} = \mathbf{S}\,\mathbf{R} = \mathbf{S}_{fast}\,\mathbf{R} + \mathbf{S}_{slow}\,\mathbf{R} \tag{36}$$

$$\mathbf{S}_{fast} = \left(\sum_{i=1}^{M} \mathbf{a}^i \mathbf{b}_i \right) \mathbf{S} \tag{37}$$

$$\mathbf{S}_{slow} = \left(\sum_{i=M+1}^{K} \mathbf{a}^i \mathbf{b}_i \right) \mathbf{S} \tag{38}$$

Here $\mathbf{S}$ is the stoichiometric coefficient matrix. $\mathbf{S}_{fast}$ is components of the stoichiometric vectors in the fast subspace and $\mathbf{S}_{slow}$ is components of the stoichiometric vectors in the slow subspace

According to Valorani et al. [58], the "fast" and "slow" importance indices which measure the importance of *k*th reaction to the *i*th species in fast and slow subspaces are introduced as follow:

$$\left(I_K^i\right)_f = \frac{\left(S_i^K\right)_f R_K}{\sum_{j=1}^{n} \left| \left(S_i^j\right)_f R_j \right|} \tag{39}$$

$$\left(I_K^i\right)_s = \frac{\left(S_i^K\right)_s R_K}{\sum_{j=1}^{n} \left| \left(S_i^j\right)_s R_j \right|} \tag{40}$$

Here the subscripts *f* and *s* indicate the fast and slow subspaces, respectively. A reaction *k* is considered important to a species *i* if I_K^i is not smaller than a user-specified threshold value in either the fast or the slow subspace.

3.2.3. Principal Component Analysis (PCA) Method

In the simulation of a combustion process a set of ordinary differential equations is used,

$$\frac{dc}{dt} = f(k,c) \tag{41}$$

Here *c (t)* is the concentration of any species and *k* is the kinetic parameter (such as rate constant). Any change in the kinetic parameters at time t_1, where $k = k^\circ$ and $c = c^\circ$, results in a change in the solution at time t_2(where $t_1 < t_2$). Regarding this fact, Turanyi et al. [36] introduced a reaction rate sensitivity gradient, which is the derivative of the deviation in the concentration of the species with respect to the rate constant as follows:

$$\widetilde{F}\left(k^\circ, c^\circ, t_2\right)_{ij} = \frac{\partial f_i(t_2)}{\partial k_j} \tag{42}$$

Non-dimensional sensitivity matrix equation (42) can be written as:

$$\widetilde{F}\left(k^\circ, c^\circ, t_2\right)_{ij} = \frac{k_j^\circ}{f_i(t_2)} \frac{\partial f_i(t_2)}{\partial k_j} \tag{43}$$

Since f_i is given by:

$$f_i(k,c) = \sum_{j=1}^{n} v_{ij} R_j = \sum_{j=1}^{n} v_{ij} k_j r_j(c) \tag{44}$$

Here R_j is the rate of reaction *j*, and v_{ij} is the stoichiometric coefficient for species *i* in reaction *j*, and n is the total number of reactions.

The elements of the log-normalized sensitivity matrix $\widetilde{F}$ can be written as:

$$\widetilde{F}_{ij} = \frac{k_j}{f_i(k,c)} \frac{\partial f_i(k,c)}{\partial k_j} = \frac{v_{ij} R_j(k,c)}{\sum_{j=1}^{n} v_{ij} R_j(k,c)} = \frac{v_{ij} R_j}{f_i} \tag{45}$$

In which $\widetilde{F}$ is considered as a ratio of the rate of formation or consumption of species *i* in reaction *j* and the net rate of the concentration change of species *i*. If the magnitude of $\widetilde{F}$ is equal to zero it means that species *i* does not exist in reaction *j*. As

mentioned by Vajda et al. [59] the kinetic information inherent in the matrix $\widetilde{F}$ is extracted by principal component analysis. The response function, which is the basic concept in the principal component analysis, is reformulated for reaction rate consideration as follows:

$$Q(\alpha,c)=\sum_{j=1}^{n}\left[\frac{f_j(\alpha,c)-f_j(\alpha^\circ,c)}{f_j(\alpha^\circ,c)}\right]^2 \tag{46}$$

$Q(\alpha,c)$ is a measure of deviation in a reaction rate caused by a parameter perturbation, $\alpha_j=\ln k_j$ and $\alpha_j^\circ=\ln k_j^\circ$. Vajda et al. [59] suggested that Equation 46 can be approximated by the simple quadratic expression:

$$\hat{Q}(\alpha)=(\Delta\alpha)^T\,\widetilde{F}^T\,\widetilde{F}(\Delta\alpha) \tag{47}$$

Here $(\Delta\alpha)=Q(\alpha,c)$ in the neighborhood of α°. Kinetic information comes by performing eigenvalue-eigenvector of the matrix $\widetilde{F}^T\widetilde{F}$, where $\widetilde{F}^T$ is the transpose matrix of $\widetilde{F}$. The important reactions can be defined as the significant eigenvector elements of reactions which are characterized by large eigenvalues. With providing the user-specified tolerances for these parameters, unnecessary reactions can be identified.

3.3 Description of Mechanism Reduction Process

In this thesis to generate reduced mechanism from detailed one two different method were used. The first method was proposed in this thesis and is based on DRGEP-CSP-DRGEP reduction method. The second scheme is based on DRGEP-PCA reduction method.

3.3.1 DRGEP-CSP-DRGEP Method

Now, the procedure used DRGEP and CSP reduction methods for generating the reduced mechanism are described. To do this, a Fortran code is developed which

utilized DRGEP reduction method for the first and third reduction stages and CSP reduction method for the second reduction stage. Also, the combustion system considered in this study is HCCI combustion modeled by a single zone combustion model.

For HCCI modeling, a sub-Fortran code coupled with DVODE solver [60] (Variable-coefficient Ordinary Differential Equation) to calculate the unknown variables (mass of species and mixture temperature and pressure), for a user defined time step. The calculation is based on ideal gas theory, specified heat transfer model, chemical kinetics mechanism and thermodynamic property models for gas mixtures. In order to reduce the time of computation, the chemical reactivity is considered to be negligible where the temperature is less than 500 K. User-defined time step is fixed at 0.1 CA for the compression, combustion and expansion processes.

The main program needs engine specifications, operating conditions, and a fuel chemical mechanism as inputs. Time steps corresponding to temperatures 600, 800, 1000, 1200, 1400, 1600K, and the cycle maximum temperature are selected as the sampling points in this study. At each sampling point, a set of important species and reactions is identified based on the thermal conditions and species mass fractions at that point. The summation of all these individual subsets constitutes the overall set of important species and reactions and the species are not involved in the overall set are specified as unimportant species. The validity of the generated mechanism is examined by comparing the output results such as peak pressure, crank angle where 50% of heat is released (CA50), and maximum total heat release with the corresponding results obtained from the detailed mechanism.

The program flowchart is illustrated in Figure 3.3. The reduction process is performed in a closed loop for each of the operating conditions. As observed from

this flowchart, firstly the reduction code calls the engine simulation subroutine, and reads the required inputs for DRGEP, such as pressure, temperature, as well as the mass fraction of each species and reaction rates for all reactions from the engine simulation code for all the sampling points. Then, with a small initial tolerance, DRGEP identifies unimportant species and stores them in a binary file. A Chemkin-II-library-based Fortran subroutine is developed to read this file and remove the specified unimportant species and their corresponding reactions from the detailed mechanism for the considered operating condition at the end of DRGEP reduction, thereby automating the reduced mechanism generation process. The result is the formation of a temporary reduced mechanism for the specified tolerance value.

Like Shi et al. [44] three operative parameters including peak pressure, crank angle where 50% of heat is released (CA50), and maximum heat release are selected as error specification parameters. The accurate prediction of the peak pressure is an important feature of the reduced mechanism for optimizing engines in HCCI simulations and it is a representative parameter for knock limit at high loads [18]. The amount of heat release is highly correlated to the peak pressure. However, to quantify the conversion of chemical energy of the reactants in the charge into thermal energy, the maximum heat release (cumulative heat release) is important. Turbulent mixing has little effect on the heat release process in HCCI combustion and there is no flame propagation in HCCI combustion [1, 61, 62], supporting the hypothesis that heat release is dominated by chemical kinetics. The CA50 represents a stable measure of the timing of combustion and it is used to investigate the cyclic variation that has specific implications for the control design used for stabilizing unstable HCCI operations near the misfire condition [18, 63]. Also, small changes in temperature as a result of overshooting low auto-ignition temperature can

dramatically affect CA50 [64]. If the differences between detailed and temporary reduced mechanisms, as reported by error specification parameters, are less than 3% for peak pressure and maximum heat release, and 1.5 degree of CA for CA50, the temporary reduced mechanism is regarded as a valid one [44].

The newly generated reduced mechanism is then returned to the engine simulation subroutine for further reduction. In the next generation, the tolerance value of DRGEP increases a little, and again a new mechanism is obtained. This loop is repeated until the allowable error tolerances reported by error specification parameters are exceeded. When the last valid reduced mechanism is obtained, this is used as an input for the second stage reduction with CSP method. This reduction stage is almost the same as previous stage except that, here a small error tolerance value for important index, which represents the importance of the reaction to the overall production of a species, is introduced to CSP. Unimportant reactions are identified by CSP method if their corresponding important index in slow or fast sub spaces is less than the error tolerance value from the generated reduced mechanism of the first stage.

Finally, the reduction stages are followed once again by employing DRGEP. The procedure is the same as the first DRGEP reduction procedure. The idea of using second DRGEP reduction is based on the fact that reduction is needed because the net production rates of the species are changed when the CSP method is applied to the mechanism, which affects the direct interaction coefficients (see equation 25).

3.3.2 DRGEP-PCA Method

The procedure used for this method, for generating the reduced mechanism, is almost similar to above mentioned method except that PCA is being used instead of CSP. Firstly, the unimportant species and related reactions are identified by

employing the directed relation graph with error propagation (DRGEP) reduction method and then, to extend reduction, the principal component analysis (PCA) method is utilized. To evaluate the validity of the reduced mechanism, representative engine combustion parameters such as peak pressure, maximum heat release, and CA50 are used. The program flowchart is illustrated in Figure 3.4.

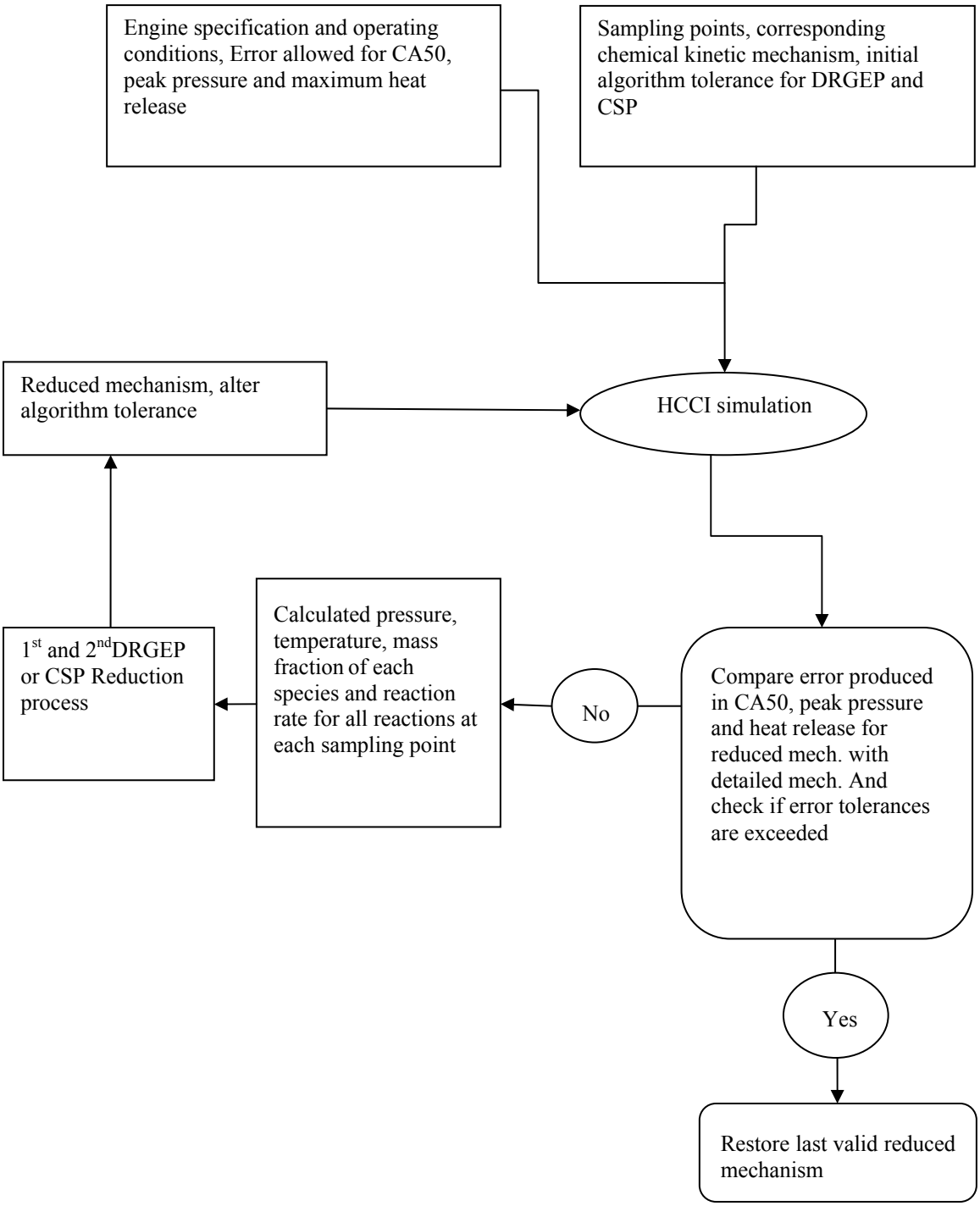

Figure 3. 3 Flowchart of mechanism reduction processes for DRGEP-CSP-DRGEP

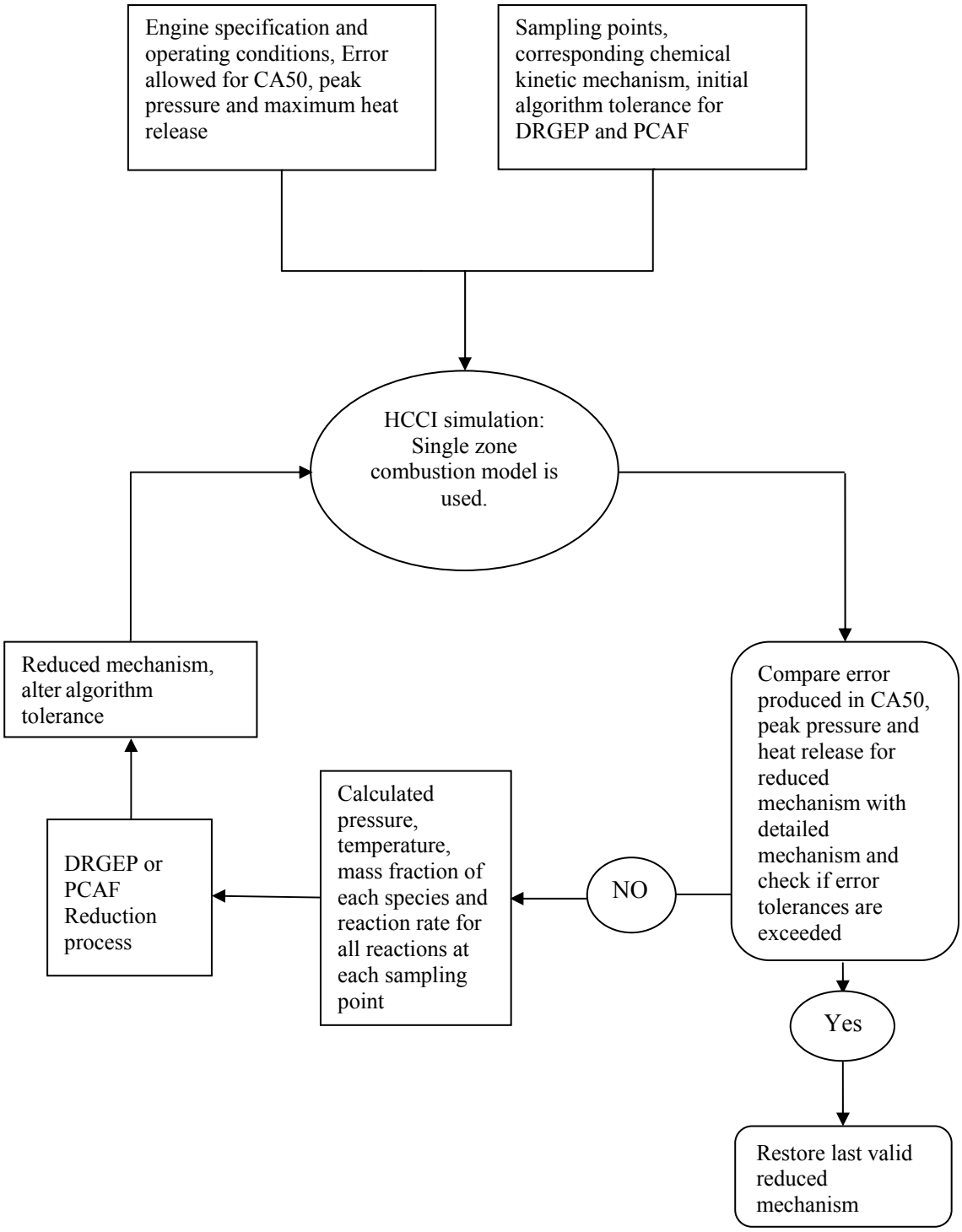

Figure 3. 4 Flowchart of mechanism reduction processes for DRGEP-PCA

3.4. Genetic Algorithm

As it will be discussed in chapter 4, an optimization of reaction constants is required for the blended fuel in the proposed mechanism for the blend fuel. This mechanism is the combination of generated reduced mechanism of natural gas and reduced mechanism of n-heptane. The present study uses a Fortran programming code, written by David L. Carroll, for GA algorithm implementation. The algorithm fetches the inputs from a file preparing a population (a set of possible solutions to the optimization problem) randomly in the range of +30% and -20% of the original values [65]. By utilizing the original population, it then recalls SZCM and makes a primary evaluation of fitness function.

The GA is put into practice by binary coding, tournament selection and functions computation procedures with weighting factors which are selected depending on the functions importance [66]. The definition of the Fitness function is:

$$\text{Fitness Function}= \sum_{i=1}^{n}\left[W_i \times \left| \frac{X_{i,code} - X_{i,test}}{X_{i,test}} \right| \right] \tag{48}$$

The term $\left| \frac{X_{i,code} - X_{i,test}}{X_{i,test}} \right|$ is the i^{th} target function in which, $X_{i,code}$ is an estimation of the corresponding i^{th} variable by using engine simulation model and $X_{i,test}$ represents the i^{th} variable obtained experimentally. In the case that more than one target functions are selected for optimization, W_i stands for weight coefficients of such parameters. However, in this work W_i is equal to 1. The SOC was selected as the target parameter in this work. The main purpose of this study is to produce a reduced chemical kinetic mechanism that provides the most accurate simulation of the ignition timing for natural gas and n-heptane blend fuel HCCI combustion. Timing of the SOC is an important feature of the HCCI engine. When the ignition

occurs too soon in the engine cycle, excessive rates of pressure-rise are produced, which may result in high combustion noise or engine damage. On the other hand, the combustion may be quenched because of too late ignition timing resulting in large amount of HC emission and no work output.

The following advantages are also achieved by selecting the ignition timing as the main feature of HCCI combustion characteristic:

1) It can be computed with SZCM.

2) It is a single output obtained from all the chemical reactions taken into account.

3) It can be correctly determined both experimentally and by simulations.

It would be more rational to use SZCM in GA optimization, since it is not only very accurate but also it takes less computational expenses than a multi-zone model. Besides, it is not possible to use the multi-zone model with the presently existing computer technology.

The optimized mechanism is obtained as the defined fitness function approaches to minimum. Other GA parameters used include the population number, crossover probability, mutation probability and maximum generation. In this study, these parameters are set to 50, 0.5, 0.02 and 1000, respectively. A genetic algorithm works by building a population of chromosomes which is a set of possible solutions to the optimization problem. Crossover probability is the probability that a pair of chromosomes will be crossed. Mutation probability is the probability that a gene on a chromosome will be mutated randomly. The maximum number of generations is a termination criterion which sets the maximum number of chromosome populations that will be generated before the top scoring chromosome will be returned as the search answer.

3.5 Experimental Set-Up and Engine Specifications

All experiments were carried out in the engine research facility of University of Alberta by using a Waukesha CFR single cylinder engine coupled to a DC dynamometer [12]. Engine specifications were presented in Table 3.1. The experimental set up is shown in Figure 3.5 [67].

The engine was run with an open throttle at a constant speed of 800 RPM. A 2.4 kW heater with PID temperature controller was used to pre-heat the intake air when required. Two types of fuel injectors, one for the n-heptane and the other for natural gas (NG), were located upstream of the intake valve to facilitate proper mixing. The control module of an AFS Sparrow-II engine was utilized to regulate the injection rate of each fuel separately or as a blend.

The external uncooled exhaust gas recirculation (EGR) line was connected to the intake after the heater and before the fuel injectors and was controlled by a manual butterfly valve. Intake gas was analyzed for the EGR fraction determination. A Vetronix PXA-1100 portable gas analyzer which is capable of measuring different gases was used in the intake system and EGR connection to the intake plenum to determine the CO_2 concentration in the intake mixture.

EGR was calculated using volume concentration measurement of CO_2 upstream and downstream of the engine. EGR was calculated as:

$$EGR = 100 \times \frac{CO_{2;up}}{CO_{2;down}} \tag{49}$$

To measure pressure signal in the combustion chamber on a resolution of 0.1 CAD, a Kistler 6043A pressure transducer was used. Experiments were monitored with the help of a personal computer with Labview software installed on it. Three NI

PCI-MIO-16E1 data acquisition cards with high sampling rates were used with the computational system.

The intake pressure at the IVC time was taken as the reference point for the pressure trace signal. The high frequency noise was filtered digitally from the pressure trace signal. The pressure traces measured over 100 successive cycles were averaged to avoid cyclic variations before they were used in calculations.

The parameters used in the present work were sorted into three groups, namely, primary, secondary and cyclic related. The error analysis was conducted differently for each group.

In the primary group, air and fuel flow rates, all measured temperatures, concentrations of exhaust gas species and intake and exhaust pressures were taken into account. Internal error analysis was performed for these parameters. In a steady-state engine operation the measurements were repeated 20 times for each parameter in this category.

The secondary parameters are defined to be those variables which were calculated from the primary parameters. Examples are indicated power and thermal efficiency. External error analysis was utilized for this group of parameters.

A reasonable number of the parameters, such as SOC, P_{max} etc., presented in the present study were averaged over 100 consecutive cycles. Cyclic variation in the HCCI combustion is less than that of the conventional combustion, but as far as the absolute estimated error from internal and external errors is concerned the deviation is significant. Averaging over 100 repeated cycles, the cyclic error related to each parameter was predicted. The uncertainty for engine parameters and combustion parameters are displayed in Table 3.2. The properties of natural gas and n-heptane are given in Table 3.3 and Table 3.4 [67].

Table 3. 1 Engine specifications

Parameter	Specification
Engine model	Waukesha CFR
Engine type	Water cooled, single cylinder
Combustion chamber	Disk cylinder head, flat-top piston
Throttle	Fully open
Bore	82.6 mm
Stroke	114.3 mm
Displacement	612 cc
IVC	146 CAD BTDC
EVO	140 CAD ATDC

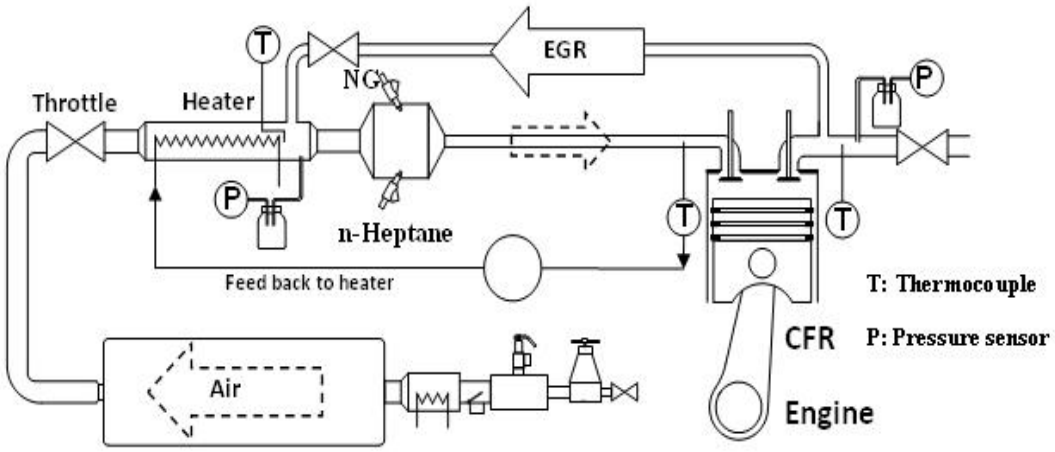

Figure 3. 5 Schematic of the engine lab hardware

Table 3. 2 Experimental uncertainty

Parameter	Uncertainty
Temperature	<1%
Crank angle position	<1%
Engine speed	<2%
Fuel Flow rate	<1%
Air flow rate	<1%
EGR	<1%
IMEP	<2%
SOC	< 2°
Pmax	<2%
MHR	<2%
CA50	<2°

Table 3. 3 Domestic natural gas properties

Property	Value
Normalized CH_4 dry molar fraction	95.39%
Normalized C_2H_6 dry molar fraction	1.90%
Normalized N_2 dry molar fraction	1.93%
Normalized CO_2 dry molar fraction	0.78%
Molar mass [g/mol]	16.76
Density at STP [kg/m³]	0.748
H/C ratio	3.92
LHV [kJ/kg]	44,818

Table 3. 4 n-Heptane properties

Property	Value
Molecular Formula	C_7H_{16}
Substance name	Normal heptane
Density @ 25 °C [g/cm³]	0.682
Enthalpy of combustion @ 77 °F [kJ/kg]	44558.1
H/C ratio	2.29

Chapter 4

REDUCED MECHANISMS FOR N-HEPTANE AND BLENDED FUEL OF N-HEPTANE&NATURAL GAS FUELS

The first part of this chapter examines the capability and the accuracy of the developed reduced mechanisms by the proposed method. In order to achieve this, the detailed mechanism of Curran's for n-heptane fuel is selected. The present method successfully reduced the comprehensive mechanism developed by Curran for n-heptane (561 species and 2539 reactions) to a reduced mechanism with only 118 species and 330 reactions, while obtaining small errors (less than 2 percent) compared to the detailed mechanism. The simulation time required for the calculations is decreased from about 601 minutes to 8 minutes in comparison to the detailed mechanism. In addition to matching the traces of pressure, temperature and heat release rate, the mass fractions of some important species calculated from the reduced mechanism agree closely with the results obtained from the detailed mechanism.

In the second part, to predict the combustion timing of the n-heptane-natural gas fueled HCCI engine, a reduced mechanism is proposed. A two-stage reduction process namely, DRGEP-PCA, is used to produce two reduced mechanisms of existing detailed GRI-Mech. 3.0 mechanism that contains 53 species and 325 reactions and Golovichev's mechanism consisting of 57 species and 290 reactions for natural gas and n-heptane fuels, respectively. The combination of the generated reduced mechanisms is used to develop a reaction mechanism for a fuel blend of

natural-gas/n-heptane. Then, the genetic algorithm is used to optimize the constants of the reaction rate in the newly generated mechanism. Simulation results agree well with the experimental results under various operating conditions, while maintaining small errors (less than 2 degrees) for the mentioned engine combustion parameter.

4.1 Development of a Reduced Mechanism for n-heptane Fuel

4.1.1 Mechanism Reduction

A detailed oxidation mechanism for n-heptane consisting of 561 species and 2539 reactions that is based on Curran's mechanism is used to describe the gas phase reactions of the HCCI combustion. Five cases are selected to cover practical operating conditions of the HCCI engine fueled by n-heptane as shown in Table 4.1. To reduce the proposed mechanism, a combination of three stage reduction methods, 1st and 2nd DRGEP and CSP methods, is used. At the first stage DRGEP identifies unimportant species and reactions and further reduction can be reached by considering the CSP method. Finally, 2nd DRGEP reduction method is applied to the mechanism.

For DRGEP reduction, like Liang et al. [26] and Shi et al.[44], fuel, HO_2, and CO are selected as the target species at each sampling point. As mentioned by Liang et al. [26] reactions in typical hydrocarbon oxidation mechanisms can be classified into three interacting groups: (1) hydrocarbon decomposition, (2) water production (or H_2–O_2 system), and (3) CO oxidation. To ensure that all significant reactions are taken into account, one or two key species from each group are selected to form the search-initiating set. Specifically, fuel is selected from the hydrocarbon decomposition group, HO_2 or H_2O_2 from the H_2–O_2 system, and CO from the CO oxidation group. At each sampling point, the important species are obtained by sum of three dependent sets corresponding to fuel, HO_2 and CO. The total important

species at each arbitrary operating condition are sum of the important species at all sampling points for that operating condition.

Two initial tolerance values are selected for the starting reduction of the detailed mechanism. For the DRGEP reduction method which was applied first, this value was equal to 10^{-5}. This tolerance value, which represents R_{AB} (overall interaction coefficient), is used to identify unimportant species in the DRGEP algorithm, such that species B is unimportant where R_{AB} is less than the tolerance value (and A is a target species). For the CSP method which followed the first reduction stage, a reaction is treated as important if its important index is over 0.05 percent. For evaluating performance of the reduced mechanism at each generation, the predicted CA50, peak pressure, and maximum heat release are selected to compare the performance of the reduced mechanisms in HCCI engine simulations with those of the detailed mechanism. In the present study, allowed differences in CA50, peak pressure, and maximum heat release are limited to 1.5-CA, 3%, and 3% between the detailed and reduced mechanisms. As a result, for the different test cases listed in Table 4.1, various reduced mechanisms with different final algorithm tolerances and different final sizes are produced. Table 4.2 shows reduced mechanisms results for n-heptane for five different considered operating conditions.

Table 4. 1 Operating conditions for considered cases of n-heptane

Case	1 (High-load with EGR)	2 (Mid-load with EGR)	3 (Mid-load with EGR)	4 (Mid-load with EGR)	5 (Low load without EGR)
Equivalence ratio (Φ)	0.68	0.41	0.43	0.38	0.26
n-heptane mass rate (mg/s)	103.43	75.52	89.69	92.40	79.23
Air mass rate (g/s)	2.28	2.77	3.11	3.66	4.57
T_{IVC} (K)	383	383	383	383	383
P_{IVC} (bar)	1.54	1.55	1.56	1.54	1.57
% EGR	51.01	40.69	31.66	19.79	0.0
Compression Ratio	11.5	11.5	11.5	11.5	11.5

Table 4. 2 Comparison of n-heptane skeletal mechanisms sizes generated at each operating conditions

Case	Species	Reactions	Allowable error tolerances are exceed?	Simulation time (min:sec)
Case 1	121	320	No	08:45
Case 2	114	382	Yes	07.38
Case 3	104	252	No	05:37
Case 4	118	330	No	07:52
Case 5	106	306	No	06:03

4.1.2 Reduction Process

Figure 4.1 shows the evolution of the reduction process for n-heptane fuel. The considered case in this figure is Case 4 of n-heptane fueled HCCI engine. In this figure, the 1st and 2nd DRGEP reduction stages are distinguished by the vertical lines. As expected, insignificant species and their corresponding reactions are effectively eliminated by using the DRGEP method at the first stage and then the reduction process is continued by reaction elimination through the CSP method. The reduction process is followed by a second DRGEP reduction step for further removing of species and reactions. Also, the errors in calculated CA50, peak pressure, and maximum heat release for the reduced mechanism, in comparison to the detailed one, at each reduction process are shown in this figure. It is evident that, by applying the 1st and 2nd DRGEP and CSP methods, a comprehensive mechanism of n-heptane including 561 species and 2539 reactions is reduced to a smaller mechanism containing 118 species and 330 reactions. The reduced mechanism (generated for Case 4) is included as Supplementary Material with this thesis in appendix A.

Case 4 as an engine operating condition is selected to discuss with more details on the performance of different employed methods in this study. The reason for this selection will be discussed later. Table 4.3 shows the size and results of the reduced mechanisms using DRGEP, DRGEP-CSP, and DRGEP-CSP-DRGEP for this case. It is clear from this table that DRGEP-CSP and DRGEP-CSP-DRGEP produce smaller skeletal mechanisms for the full range of error limits in comparison with DRGEP method alone. It is interesting that the smaller mechanism of DRGEP-CSP-DRGEP method has better performance results. Also, DRGEP increased the simulation speed by 53times, while simulation speed using reduced mechanism of DRGEP-CSP and DRGEP-CSP-DRGEP increase 57 and 79 times, respectively, in comparison to the

full mechanism. Furthermore, the computer time required to generate the reduced mechanism at the end of each reduction stage is shown in this table. The indicated CPU times include the accumulated computation time needed for the simulations and the error calculations. A major portion of this accumulated time is related to the first generation of DRGEP reduction stage that needs simulation with full mechanism. It is clear that the additional time required for DRGEP-CSP and DRGEP-CSP-DRGEP is a small value relative to the time consumed for DRGEP method.

Table 4. 3 Comparison of n-heptane skeletal mechanism generated by DRGEP, DRGEP-CSP, and DRGEP-CSP-DRGEP

Method	Species	Reactions	Error in Peak Press. (%)	Error in Max. HR (%)	Error in CA50 (Degree)	Simulation time (min:sec)	Cumulated time to develop the reduced mechanism (hr:min:sec)
DEGEP	135	509	0.69	0.18	1.3	11:12	18:51:21
DRGEP+CPS	135	370	0.69	0.16	1.3	10:38	19:17:09
DRGEP+CSP+DRGEP	118	330	0.03	0.18	0.2	07:52	19:44:31

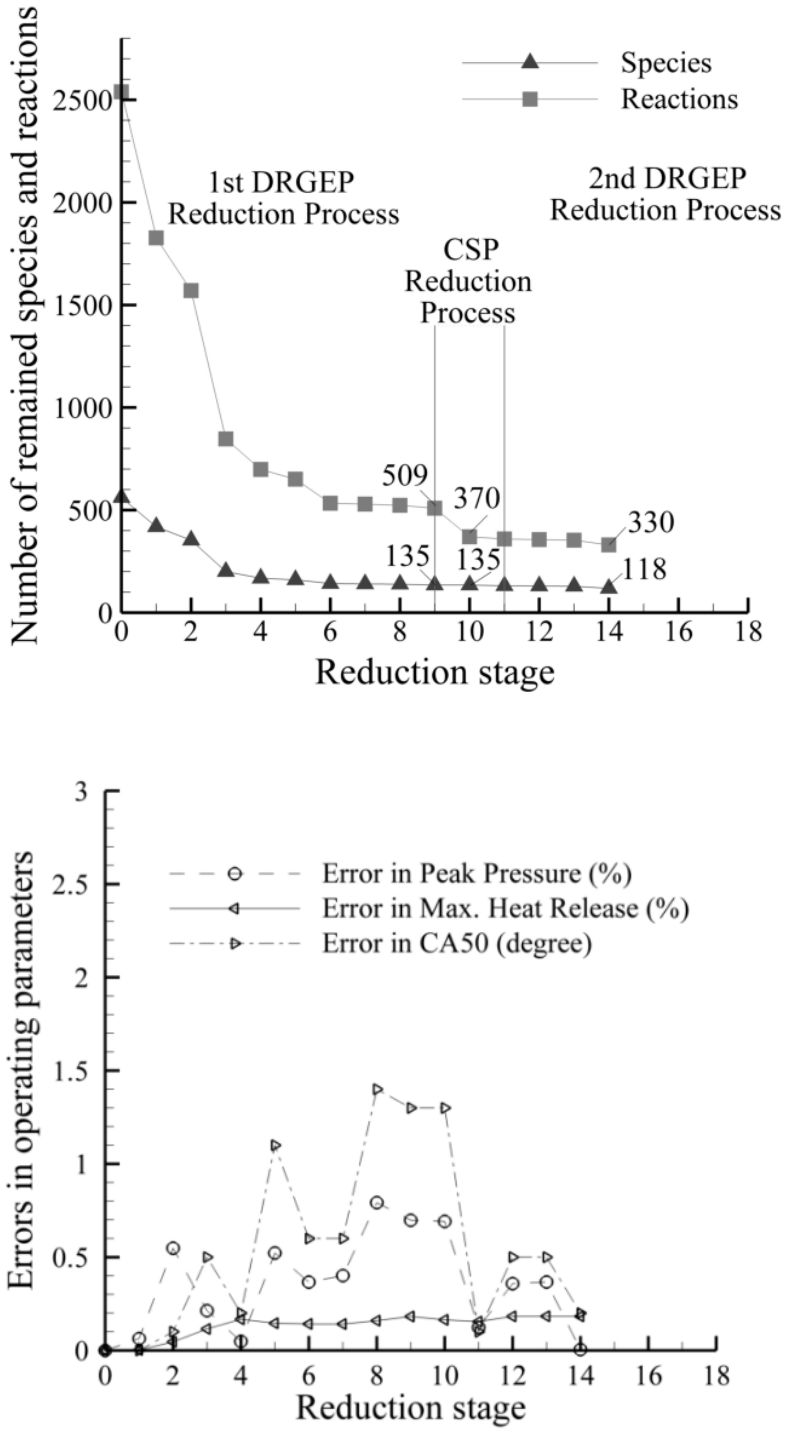

Figure 4. 1 Mechanism size and the corresponding error values at each reduction stage for Case 4 of n-heptane fueled HCCI engine

Figure 4.2 shows the algorithm error tolerances for each generation number of the mechanism reduction process. In this work, the subsequent reduced mechanism is created by gradually increasing the tolerances.

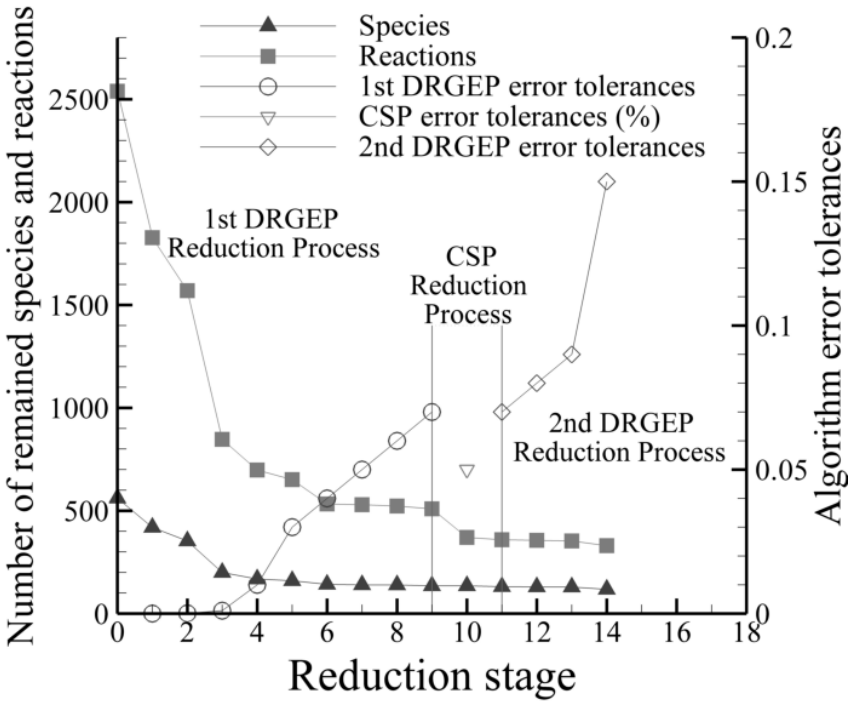

Figure 4. 2 Algorithm error tolerances for Case 4 of n-heptane fueled HCCI engine

4.1.3 Validity of Each Generated Reduced Mechanisms

While each reduced mechanism is generated by satisfying the user-specified error tolerances for a specific test condition, it is necessary to have a single reduced mechanism which may be applicable for all operating conditions of the engine. Commonly this goal is achieved by the combination of all the generated reduced mechanisms for each case. However, as mentioned by Shi et al. [44] and also it can be observed from Figure 4.3, this is not necessary that most of the generated reduced mechanisms in this work are able to predict selected representative combustion and performance parameters of the engine (Peak pressure, maximum heat release and CA50) in the error tolerances limit for all cases.

Each sub-figure of Figure 4.3 shows how the generated reduced mechanism of n-heptane fuel for a specific case can predict peak pressure, maximum heat release and CA50 for the other operating conditions. For example, the reduced mechanism generated for Case 1 (including 121 species and 320 reactions) is used to simulate

HCCI engine to predict the combustion and performance characteristics of the engine for all five different operating conditions. It means that five different reduced mechanisms were generated for each of five considered operating conditions. As it can be seen from this figure, the reduced mechanisms for Cases 1, 3, 4 and 5, in Figures 4.3a, 4.3c, 4.3d and 4.3e, can predict satisfactorily the combustion and performance characteristics of the engine compared to the detailed n-heptane mechanism for all other cases.

It may also be seen from Figure 4.3b that the reduced mechanism generated for Case 2 fails to predict satisfactorily the mentioned parameters for Case 1. It is interesting to note that the larger mechanism of Case 2 (including 114 species and 382 reactions) shows poorer performance than the smaller mechanism of Case 5 (including 106 species and 306 reactions) for all the investigated cases. It suggests that having a smaller mechanism does not always result in weaker performance. This behavior has been addressed by Niemeyer et al. [42] and Shi et al. [44]. As mentioned by Shi et al.[44] and evident in Figure 4.1, the errors between the detailed and reduced mechanisms do not necessarily monotonically increase as the algorithm error tolerances increase. For example, in Figure 4.1, the smaller reduced mechanism obtained at generation 14 is better than those of generations 8 to 10. However, this is not the case at generation 14, at the end of the reduction process when the absolute value of the user-specified tolerances becomes large, further mechanism reduction significantly deteriorates the accuracy of the reduced mechanism.

Although the reduced mechanism of Case 3 is the smallest generated reduced mechanism, in this study the reduced mechanism of Case 4 is selected as the final reduced mechanism. The reason is that by plotting the in-cylinder pressure development diagram for all the cases using the four valid generated mechanisms, it

is found that the reduced mechanism of Case 4 has the closest results to the corresponding experimental in-cylinder pressure traces.

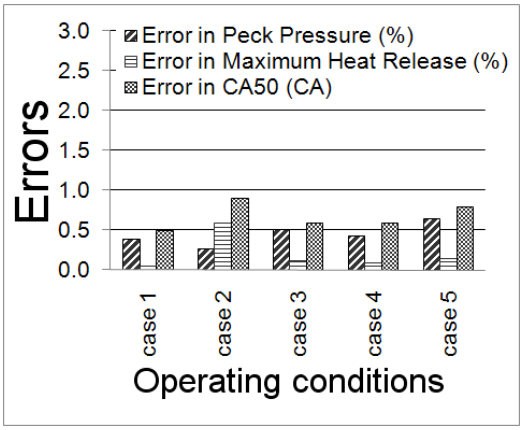

(a) Case 1

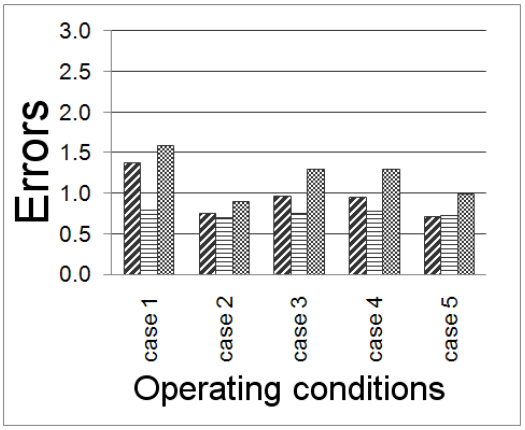

(b) Case 2

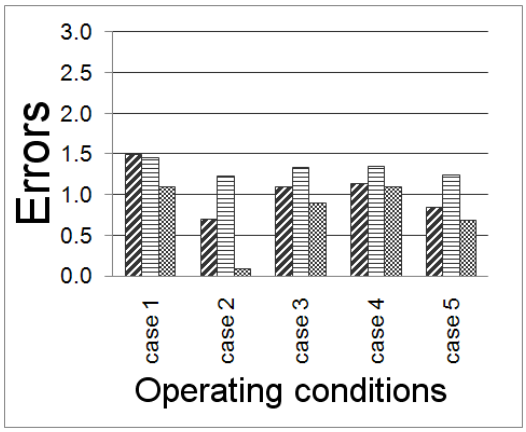

(c) Case3

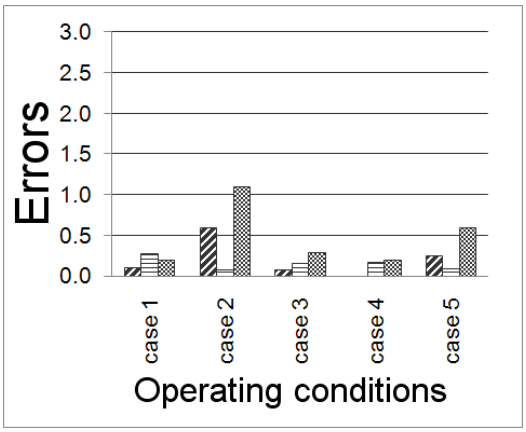

(d) Case 4

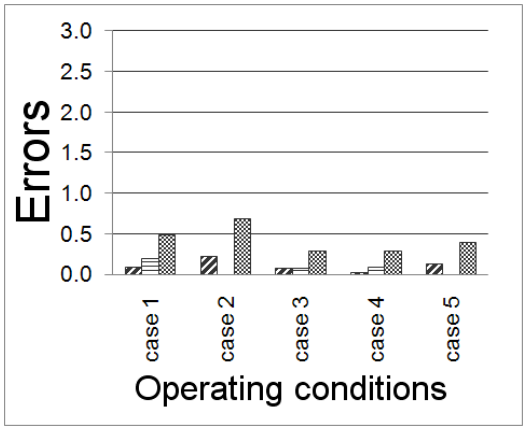

(e) Case 5

Figure 4. 3 Performance of each generated reduced mechanism of n-heptane for different operating conditions (different reduced mechanisms used for each of cases)

4.1.4 Reduced Mechanism Performance in Capturing in-cylinder Pressure and Temperature Traces

Figures 4.4 and 4.5 present a comparison between the pressure and temperature traces of HCCI combustion cycle by employing the detailed and reduced mechanisms for different operating conditions of n-heptane fuelled HCCI engine. It may be observed that the reduced mechanism accurately captures the in-cylinder pressure and temperature development during the compression, combustion, and expansion periods for all cases.

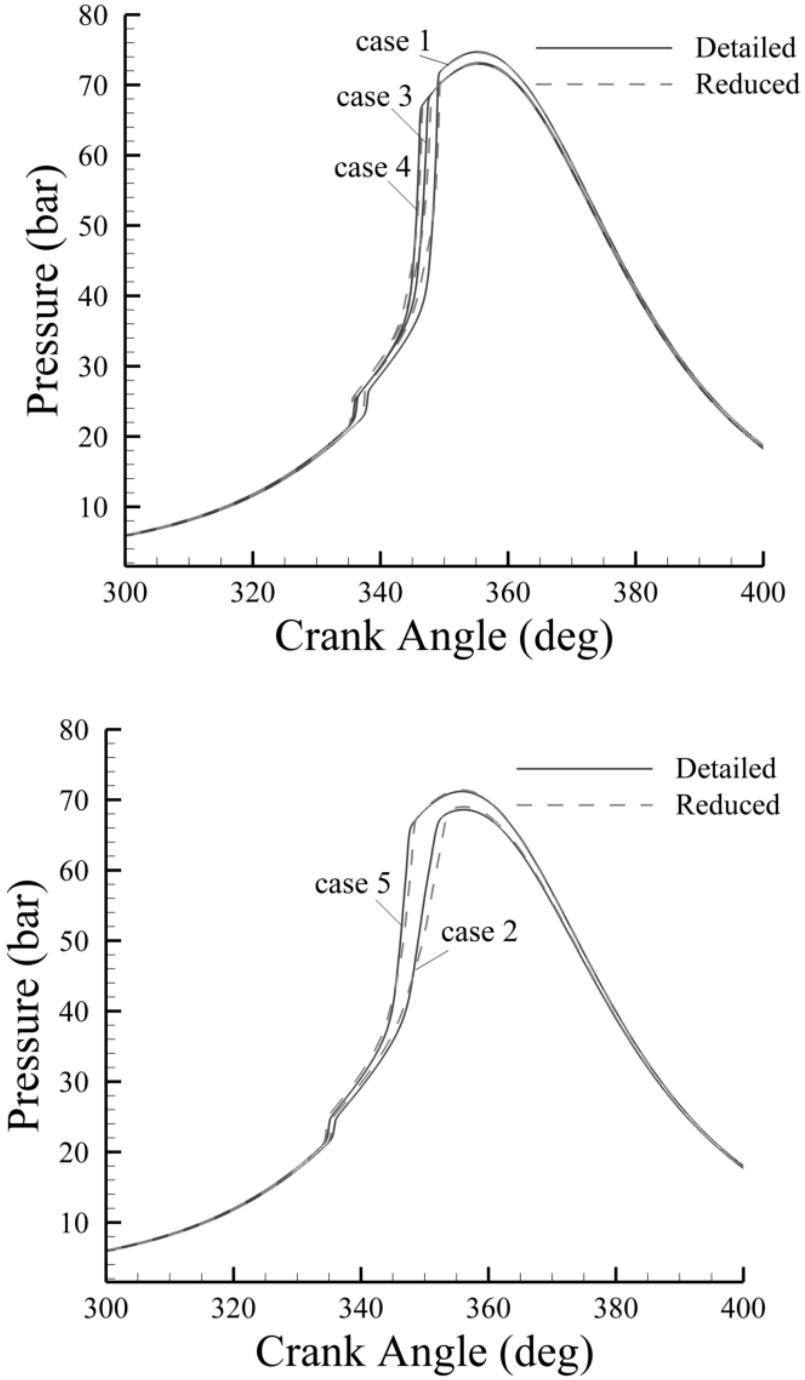

Figure 4. 4 Comparison of pressure traces by applying the detailed n-heptane mechanism and its reduced mechanism generated for Case 4 for different operating conditions

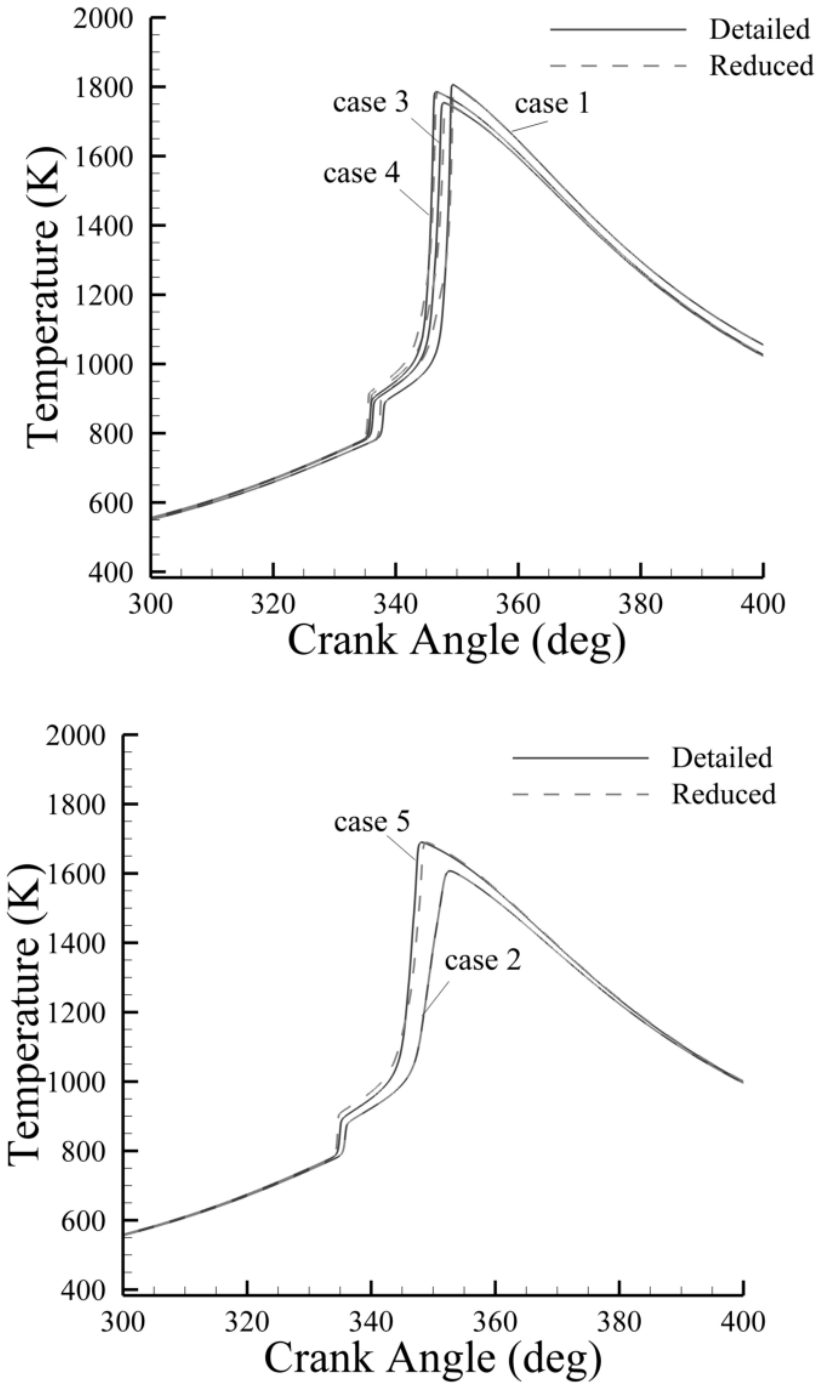

Figure 4. 5 Comparison of temperature traces by applying the detailed n-heptane mechanism and its reduced mechanism generated for Case 4 for different operating conditions

4.2.5 Reduced Mechanism Performance in Capturing in-Cylinder Heat Release Histories

A comparison of the heat release histories by applying the detailed and reduced mechanism in HCCI combustion cycle calculations is presented in Figure 4.6. In addition to good agreement between the obtained results, it can be seen from this figure that the well- known two stage combustion of n-heptane at all conditions are achievable for the reduced mechanism. The reduced mechanism accurately captures both stages of heat release associated with low temperature kinetic reactions (low temperature oxidation, LTO) and the much stronger one (main reactions) associated with high temperature oxidation (HTO).

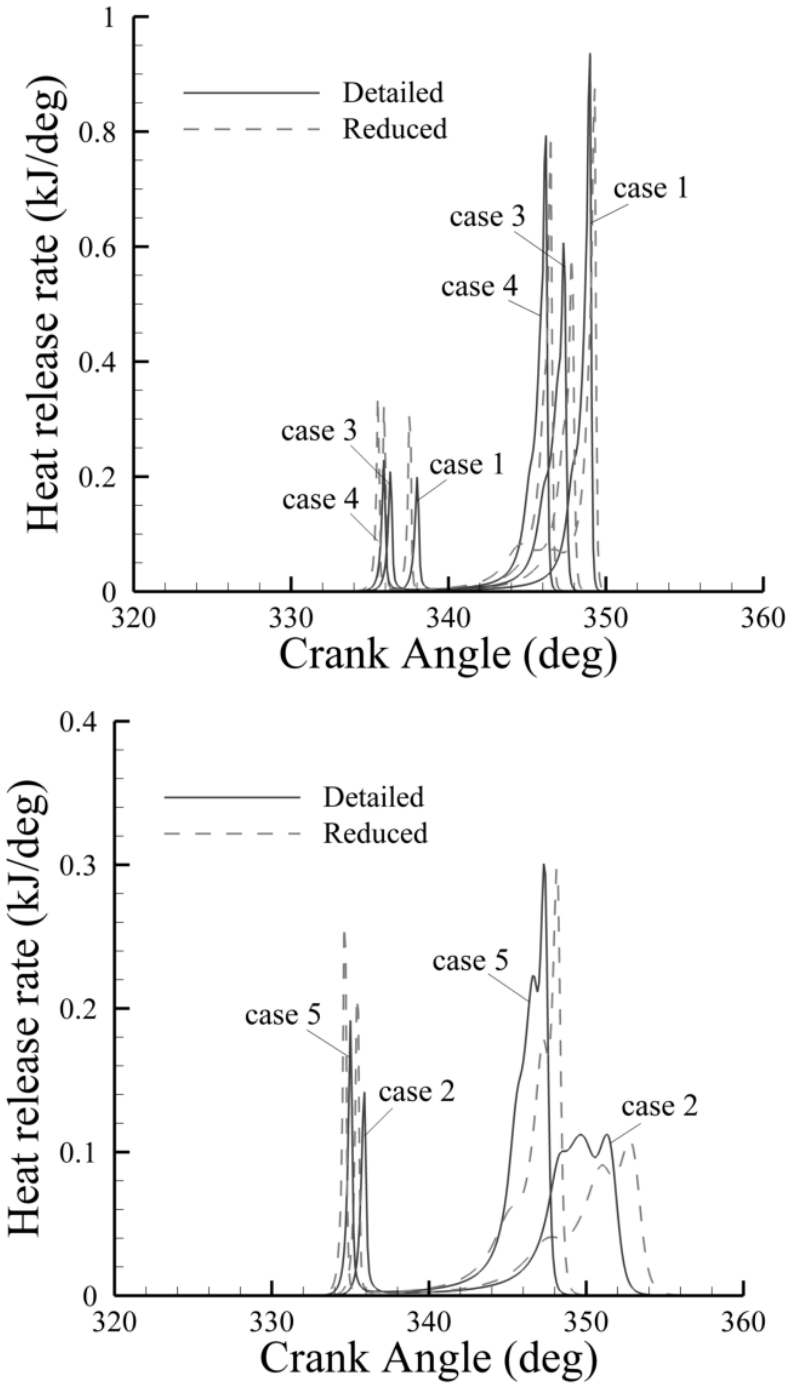

Figure 4. 6 Comparison of heat release rate histories by applying the detailed n-heptane mechanism and its reduced mechanism generated for Case 4 for different operating conditions

4.1.6 Reduced Mechanism Performance in Capturing the Mass Fraction of Species

In addition to matching pressure, temperature and heat release rate traces, the mass fractions of some important species calculated from the reduced mechanisms

are compared with the corresponding detailed mechanism results in Figure 4.7. It can be seen that there is a good agreement between the mass fractions of species such as O_2, CO and CO_2 obtained from applying both of detailed and reduced mechanisms to the HCCI engine cycle calculations.

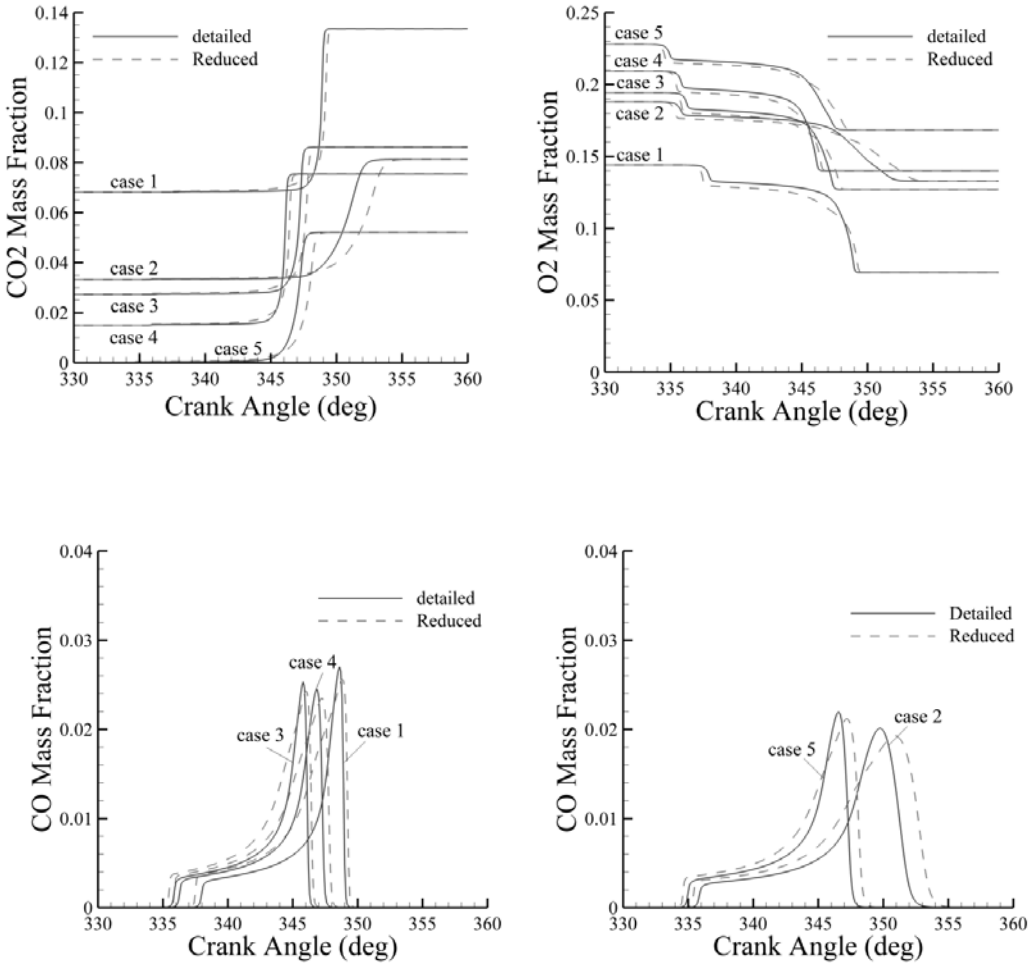

Figure 4. 7 Comparison of mass fraction for some selected species between the detailed n-heptane mechanism and its reduced mechanism generated for Case 4 at different operating conditions

4.1.7 Further Examine of the Validity of the Generated Mechanism

Cycle calculation time by employing the reduced mechanism is 79 times faster than the one employed detailed mechanism.

It should be emphasized here that in this work the reduced mechanism for each operating conditions is generated by combining sub-skeletal mechanisms generated for six sample points of the considered case. The validity of the reduced mechanism is then investigated within the investigated operating conditions (five different operating conditions mentioned in Table 4.1). It is well-described by Pepiot and Pitsch [38] that the accuracy of the reduced mechanism between the sample points is represented by the accuracy of the scheme at the sample points. Strictly, this validity should be ensured by a reliable method. Oluwole et al. [68, 69], for instance, have developed a reduction technique based on constrained optimization that guarantees the range of validity of the reduced scheme in steady-state problems. However, this approach is not applicable directly to the DRGEP method since engine simulation is a transient problem [38, 44].

To further examine the validity of the generated mechanism, the deviation of simulation results of the reduced mechanism from full mechanism for more sets of operating conditions was also investigated as shown in Figures 4.8 and 4.9. The results show that among almost all of the conditions the errors of the peak pressure, maximum heat release and CA50 are less than user specified tolerances.

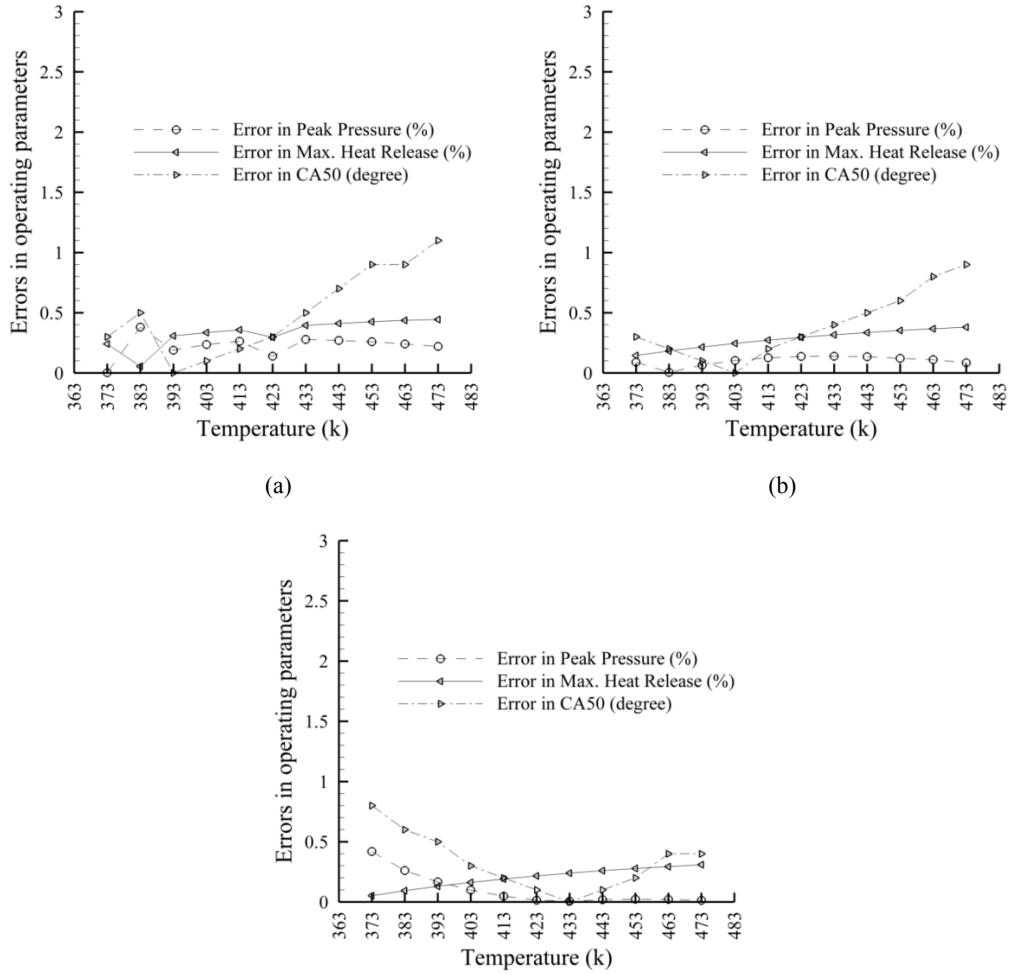

Figure 4. 8 Comparison of peak pressure, maximum heat release, and CA50 between the reduced mechanism generated for Case 4 and the detailed mechanism with various initial gas temperatures. a) Equivalence ratio= 0.68, PIVC=1.54 bar, EGR = 51.01 %. b) Equivalence ratio= 0.38, P_{IVC}=1.54 bar, EGR = 19.79 %. c) Equivalence ratio= 0.26, P_{IVC}=1.57 bar, EGR = 0.0 %

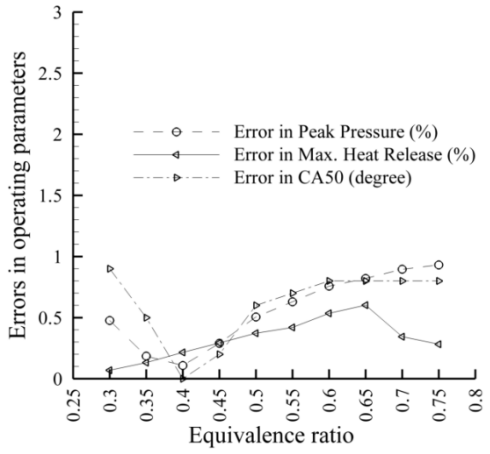

(a)

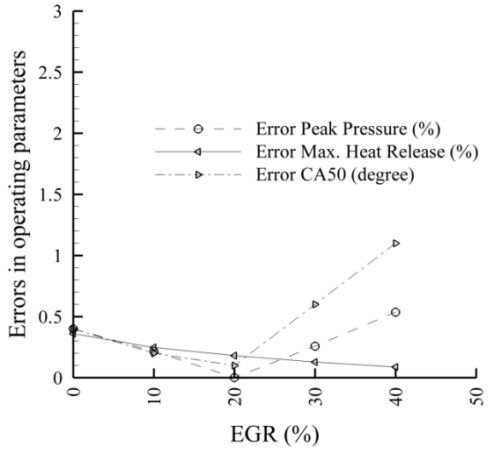

(b)

Figure 4. 9 Comparison of peak pressure, maximum heat release, and CA50 between the reduced mechanism generated for Case 4 and the detailed mechanism. a) With various equivalence ratio. b) With various EGR

4.2 A Reduced Mechanism for a Fuel Blend of Natural-Gas and n-Heptane

4.2.1 Performances of the Golovichev's and Curran's Mechanisms in Predicting n-Heptane-Natural-Gas Fueled HCCI Engine Combustion

Five different engine operating conditions are selected for combustion analysis for each of natural gas and n-heptane fuels listed in Tables 4.4 and 4.1, respectively. Figure 4.10 demonstrates the validity of the single zone combustion model utilized in this work in capturing in-cylinder pressure comparable with experimental data through the compression stroke and estimation of start of combustion (SOC) for n-heptane fueled HCCI engine and natural gas fueled HCCI engine at some selected operating conditions. Tables 4.5 and 4.6 show the error between the measured and predicted SOC of the model for natural gas fueled HCCI engine and n-heptane fueled HCCI engine, respectively. It is clear that the applied single zone combustion model is in good agreement with experimental data and the error in prediction of SOC is less than 2 degrees. Since the Golovichev's mechanism already includes the sub-mechanism for methane, the validity of this mechanism is questioned for the blend fuel of n-heptane and natural gas. Figure 4.11 shows a comparison of predicted in-cylinder pressure traces during the compression stroke resulting from the single-zone combustion model for n-heptane and natural gas blends combustion in HCCI engine with the corresponding experimental data for some selected operating conditions. It is clear that by using this mechanism, the predicted in-cylinder pressure cannot follow the corresponding experimental data as well as SOC. Figure 4.11 also points out that the Curran's mechanism, with 560 species and 2539 reactions, shows remarkable discrepancies in prediction of the above mentioned parameter with respect to the experimental data for the blend fuel.

As a result, in this work, two reduced mechanism of n-heptane and natural gas fuels, which represent the main features of the corresponding detailed mechanism, are generated and a combination of these two mechanisms is tested to represent the combustion of a fuel blend of n-heptane and natural gas. Therefore, at first step two reduced mechanisms of n-heptane and natural gas are developed.

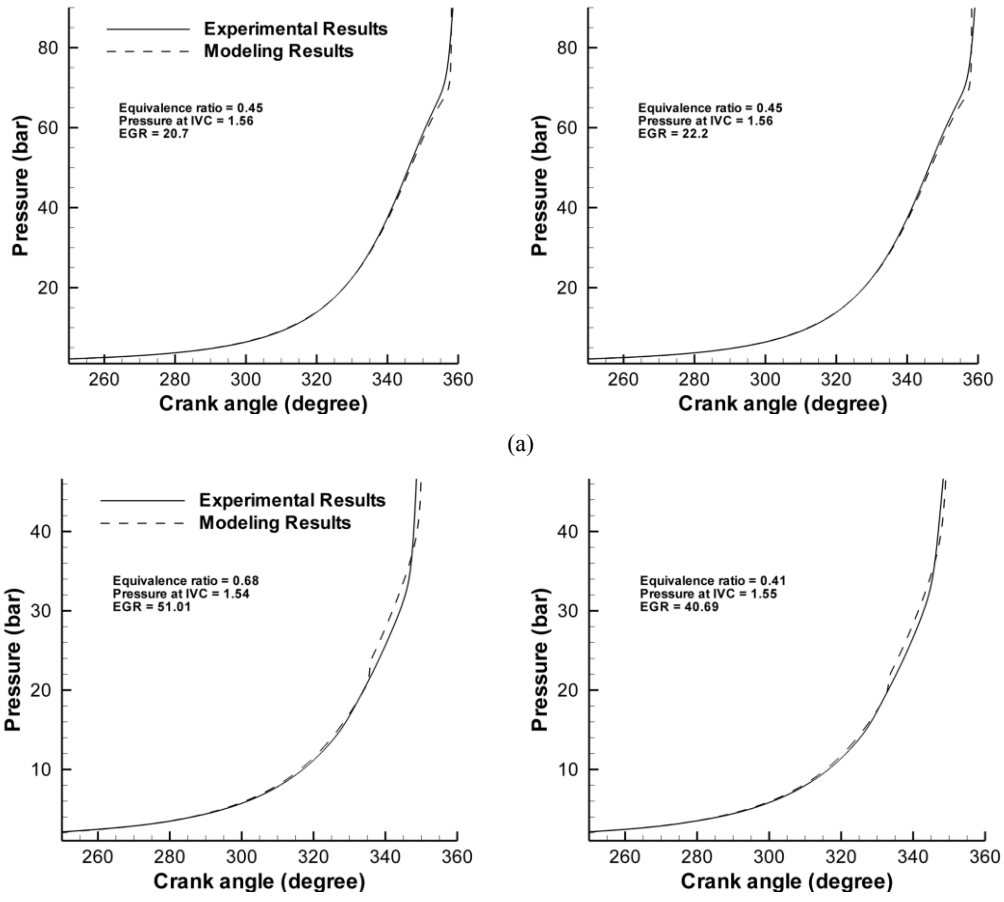

Figure 4. 10 Comparison of predicted in-cylinder pressure traces during the compression stroke resulted from the single-zone combustion model with the corresponding experimental data (a) pure natural gas fuel (b) pure n-heptane fuel

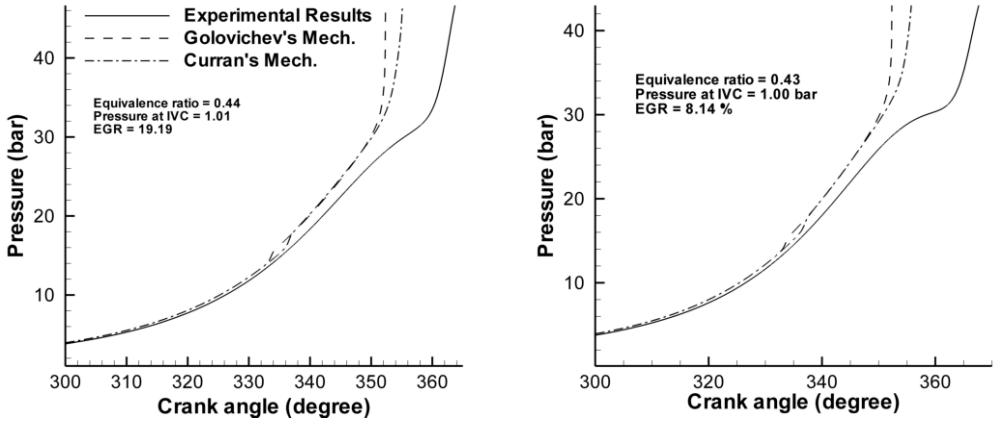

Figure 4. 11 Comparison of predicted in-cylinder pressure traces during the compression stroke resulted from the single-zone combustion model utilizing the Golovichev's mechanism and the Curran's mechanism with the corresponding experimental data

4.2.2 Mechanism Reduction

The GRI-Mech. 3.0 [24] and an updated version of Golovichev's [22] kinetic reaction mechanisms, consisting of 53 species and 325 reactions and 57 species and 290 reactions respectively, are chosen for the oxidation of natural-gas (NG) and n-heptane fuels.

The reduction process, which is used in the present work, is based on a two-stage reduction method which utilizes DRGEP and PCA methods, successively. More specifically, DRGEP identifies and eliminates unimportant species and reactions. Then, in the second stage, the PCA method is applied to improve the process by eliminating redundant reactions. For DRGEP reduction, like Liang et al. [26] and Shi et al. [44] , fuel, HO_2, and CO are selected as the target species at each sampling point. Species that are reachable from the target species are identified at each sampling point and the collection of all of these species sets constitutes the final important species set for a specific operating condition. The rest of the species are considered unimportant species, and reactions that include any of these species are eliminated from the final mechanism.

An initial tolerance value to start the DRGEP reduction process was 10^{-5} and the tolerance value for PCA reduction process that follows the DRGEP process was 10^{-3}. The selected representative parameters for investigating the validity of the reduced mechanism in this work are the predicted CA50, peak pressure, and maximum heat release. At each generation, these parameters are calculated using the HCCI engine simulation code and compared to the results obtained by using the detailed mechanism for the considered cases. The generated reduced mechanism is considered as valid one if the errors in predicted CA50, peak pressure, and maximum heat release using reduced mechanism do not exceed 1° CA, 1%, and 1% respectively, with those of the detailed mechanism. Therefore, for each operating condition mentioned in Table 4.4 and 4.1, the developed reduced mechanisms are in different final sizes as can be seen in Table 4.7.

Table 4. 4 Operating conditions for considered cases of natural gas

Case	1	2	3	4	5
Equivalence ratio (Φ)	0.69	0.53	0.45	0.45	0.42
NG mass rate (mg/s)	107	95.49	92.43	92.43	85.59
Air mass rate (g/s)	2.51	2.94	3.35	3.30	3.33
T_{IVC} (K)	413	413	413	413	413
P_{IVC} (bar)	1.57	1.56	1. 56	1. 56	1. 56
% EGR	41.1	30.5	20.7	22.2	22.2
Compression Ratio	17.25	17.25	17.25	17.25	17.25

Table 4. 5 Comparison between simulated and experimental SOC of a natural gas fueled HCCI engine

Case	Simulation	Experimental	Error (degree)
Case 1	3.8 ATDC	3.0 ATDC	0.8
Case 2	0.5 BTDC	2.2 BTDC	1.7
Case 3	2.1 BTDC	2.6 BTDC	0.5
Case 4	2.0 BTDC	2.1 BTDC	0.1
Case 5	1.6 BTDC	0.0 TDC	1.6

Table 4. 6 Comparison between simulated and experimental SOC of a n-heptane fueled HCCI engine

Case	Simulation	Experimental	Error (degree)
Case 1	13.4 BTDC	13.5 BTDC	0.1
Case 2	16.5 BTDC	17.4 BTDC	0.9
Case 3	17.3 BTDC	18.5 BTDC	1.2
Case 4	19.3 BTDC	20.3 BTDC	1.0
Case 5	19.2 BTDC	21 BTDC	1.8

Table 4. 7 Comparison of natural gas and n-heptane skeletal mechanisms sizes generated at each operating conditions

For natural gas fuel				**For n-heptane fuel**			
Case	Species	Reactions	Allowable error tolerances are exceed?	Case	Species	Reactions	Allowable error tolerances are exceed?
Case 1	19	37	No	Case 1	38	65	No
Case 2	19	36	No	Case 2	40	95	No
Case 3	19	41	No	Case 3	36	104	No
Case 4	19	35	No	Case 4	38	74	Yes
Case 5	19	39	No	Case 5	38	85	No

4.2.3 Reduction Process

Figures 4.12 and 4.13 show the mechanism size and the interfered errors in calculation of CA50, peak pressure, and maximum heat release because of elimination of insignificant species and reactions and algorithm error tolerances at each generation during DRGEP and PCA reduction processes, which are distinguished with a vertical line. The considered cases in these figures are test condition 5 and test condition 2 for natural gas and n-heptane fuels, respectively. For the first reduction stage, which utilizes DRGEP reduction method, insignificant species and their corresponding reactions are identified and eliminated effectively from the mechanism. Following the first stage, PCA reduction is applied to the mechanism to remove further reactions in the second stage. By applying this two-stage reduction method, a detailed mechanism used for modeling the combustion of natural gas comprising 53 species and 325 reactions, is reduced to a smaller mechanism containing 19 species and 39 reactions. Also, a detailed mechanism of n-heptane including 57 species and 290 reactions is cut down to a more concise mechanism consisting of 40 species and 95 reactions. The reduced mechanisms, generated for Case 5 of natural gas-fueled HCCI engine and Case 2 of n-heptane-fueled HCCI engine, are provided as Additional Information for the present work in Appendix B and Appendix C, respectively.

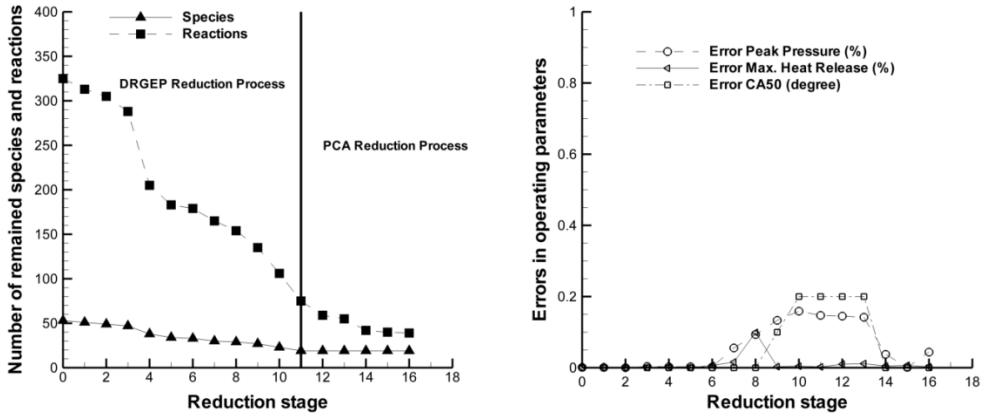

(a)

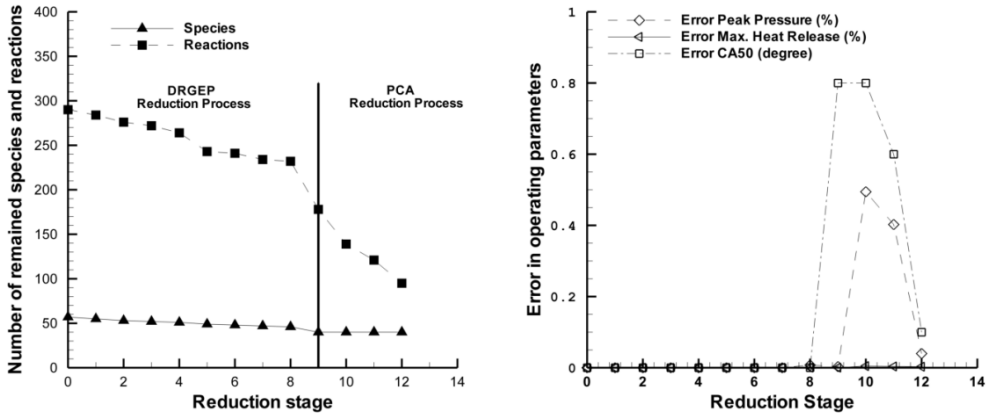

(b)

Figure 4. 12 Mechanism size and the corresponding error values at each reduction stage for (a) natural gas (Case 5) and (b) n-heptane (Case 2)

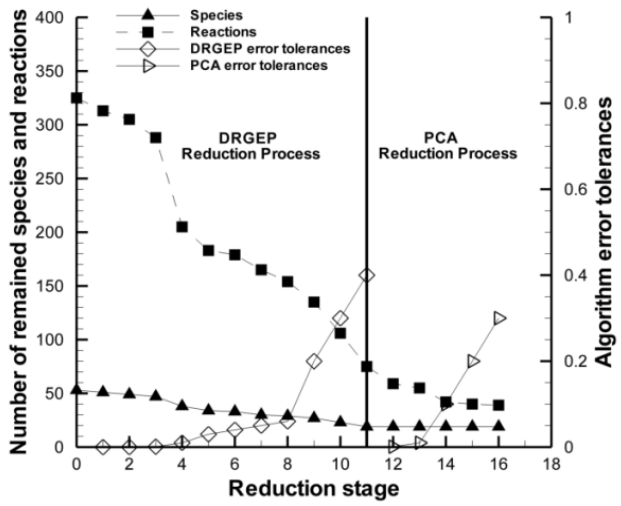

(a)

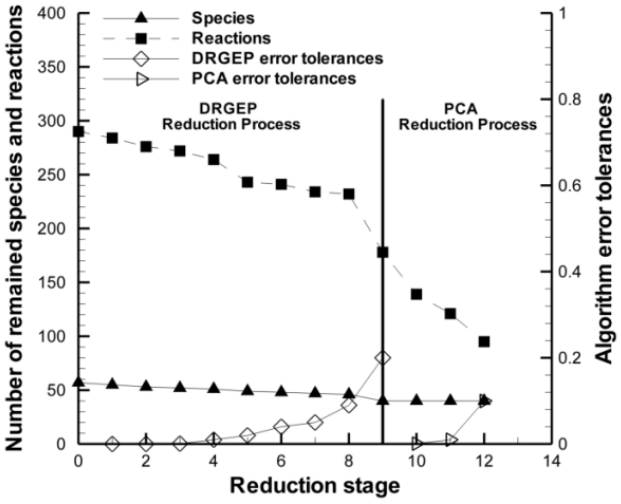

(b)

Figure 4. 13 Algorithm error tolerances. (a) for Case 5 of the NG fueled HCCI engine and (b) for Case 2 of the n-heptane fueled HCCI engine

4.2.4 Validity of Each Generated Reduced Mechanisms

By utilizing the specified reduction processes for each of the operating conditions, the corresponding reduced mechanism is generated. However, it is required to have a single reduced mechanism. Normally, as explained in previous section, this final reduced mechanism can be developed by the combination of all the generated mechanisms for each case. Another alternative solution for this goal as mentioned in ref.[44], and also can be seen in Figures 4.14 and 4.15, is to evaluate the performance of each of the reduced mechanisms at different operating conditions. It can be seen

that most of the generated mechanisms can be used for all other cases while predicting the representative parameters in the error tolerance limits. For example, the generated reduced mechanism for Case 1 for natural gas fuel is used to simulate the combustion phase of the natural gas-fueled HCCI engine in different considered cases in Table 4.4. The calculated errors in predicting peak pressure, maximum heat release, and CA50 between reduced and detailed mechanisms are less than the user specified error tolerance values. However, the developed reduced mechanism of Case 4 for n-heptane is unable to accurately predict some of these parameters for operating conditions of Case 1, Case 2, and Case 3. Therefore it is not considered as a valid one.

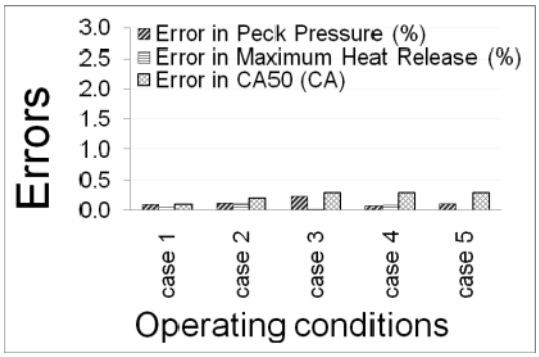

(a) Case 1

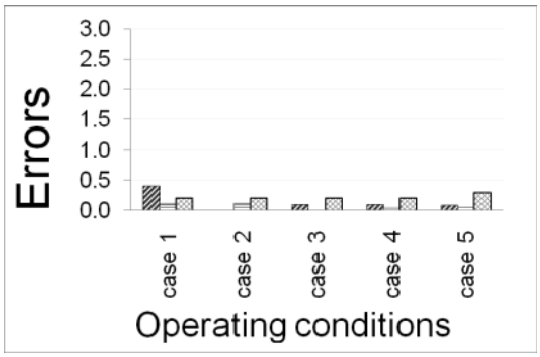

(b) Case 2

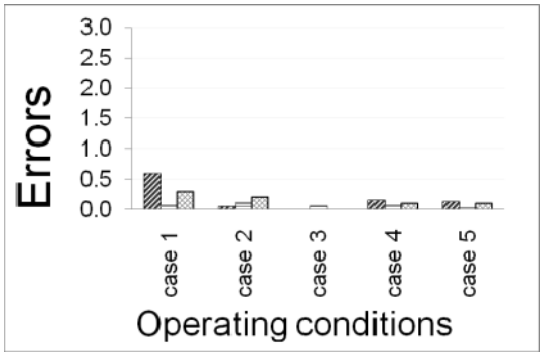

(c) Case 3

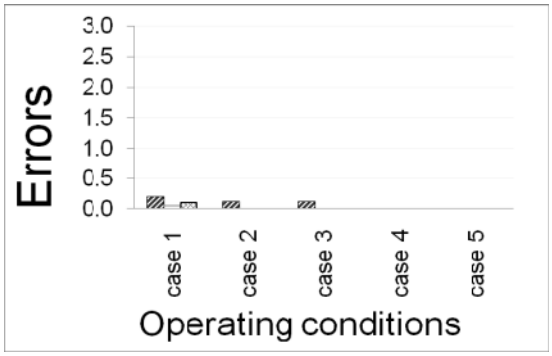

(d) Case 4

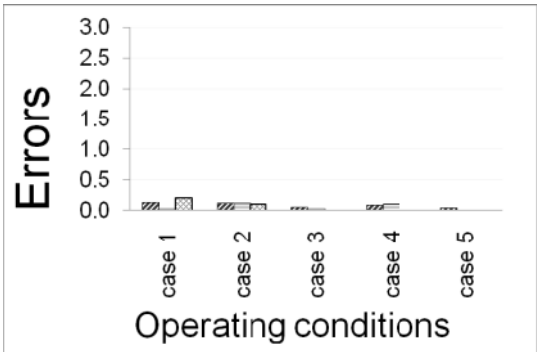

(e) Case 5

Figure 4. 14 Performance of each generated reduced mechanism for natural gas fuel at different operating conditions

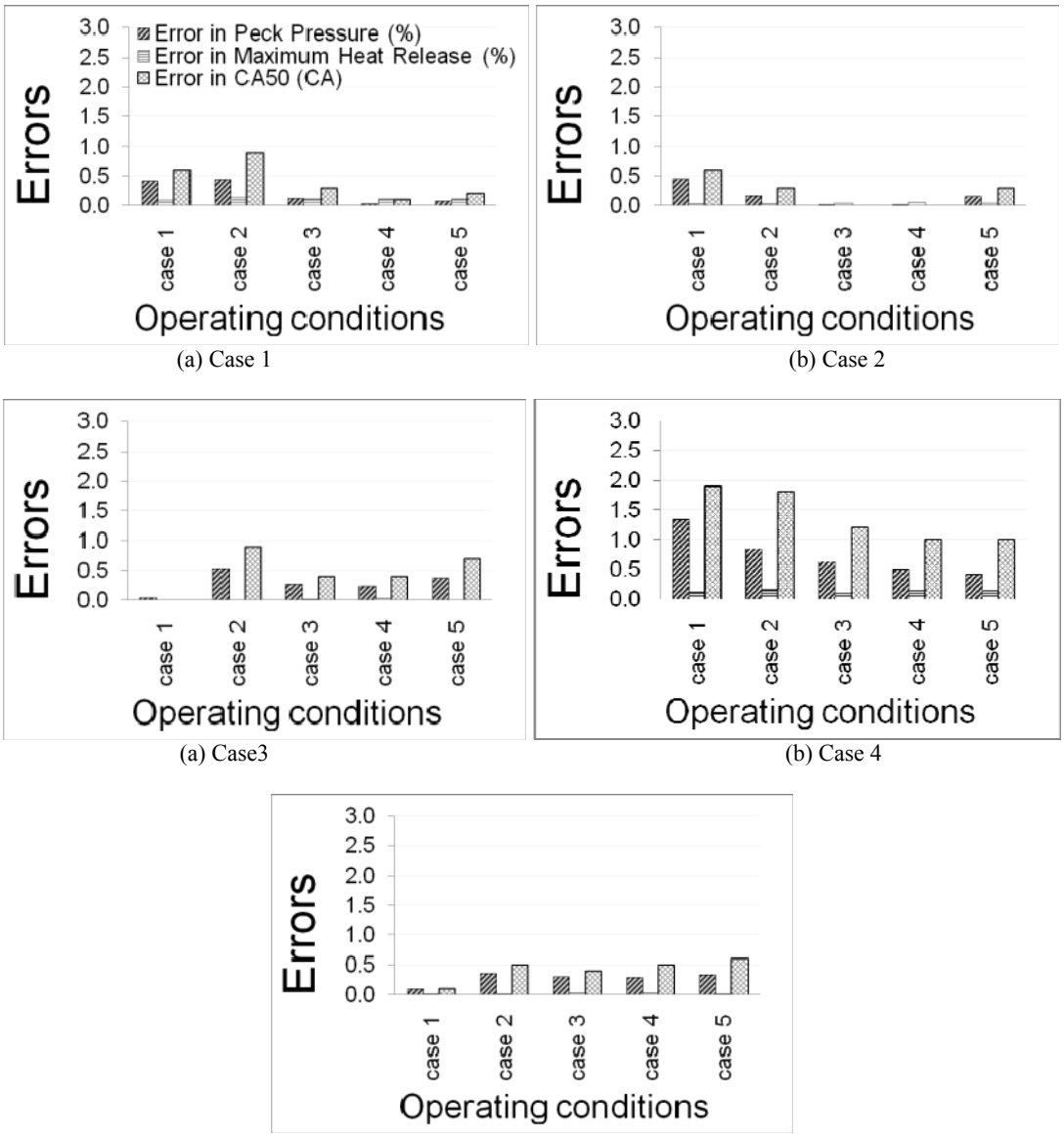

(a) Case 1 (b) Case 2

(a) Case3 (b) Case 4

(e) Case 5

Figure 4. 15 Performance of each generated reduced mechanism for n-heptane fuel at different operating conditions

4.2.5 Reduced Mechanisms Performance in Capturing Pressure and Heat Release Traces for Both Natural Gas-Fueled and n-Heptane-Fueled HCCI Engines

To verify the ability of the reduced mechanism in predicting the pressure traces and heat release rate histories, a comparison of these parameters between reduced and detailed mechanisms are depicted in Figure 4.16 for different operating conditions of both natural gas-fueled and n-heptane-fueled HCCI engine. As

indicated in this figure, simulation using reduced mechanism is in good agreement with the simulation utilizing detailed mechanism. Furthermore, the two-stage combustion behavior of n-heptane fuel is accurately captured by the reduced mechanism for all cases.

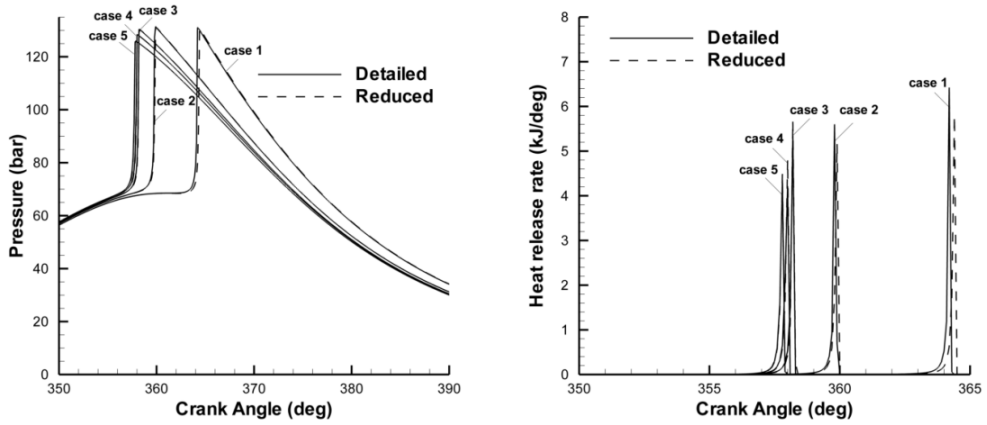

(a)

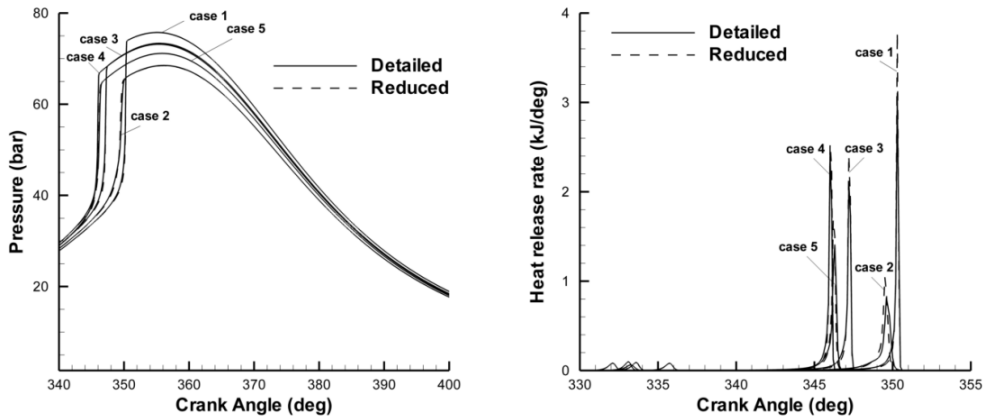

(b)

Figure 4. 16 Comparison of pressure traces and heat release rate histories (a) by applying the detailed GRI mechanism and its reduced mechanism generated for Case 5 at different operating conditions and (b) by applying the detailed Golovichev's mechanism and its reduced mechanism generated for Case 2 at different operating conditions

4.2.6 Reduced Mechanisms Performance in Capturing SOC Calculated for Both Natural Gas-Fueled and n-Heptane-Fueled HCCI Engines

The definition of SOC adopted here is the point at which 10 percent of total heat is released. Figure 4.17 evaluates SOC for both reduced and detailed mechanisms for both natural gas-fueled and n-heptane-fueled HCCI engines. Combustion in HCCI engines is governed by the chemical kinetics. It is observed that the SOC is predicted accurately for all considered cases.

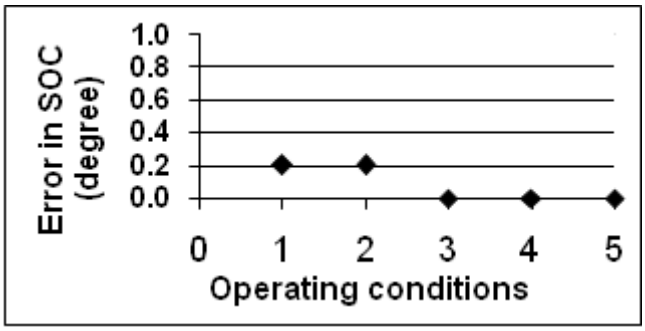

(a)

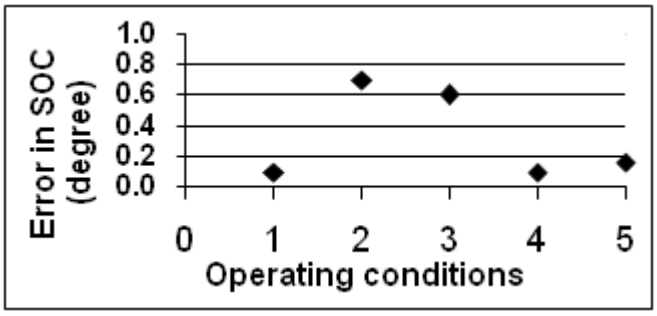

(b)

Figure 4. 17 Error in prediction of SOC for (a) natural gas (b) n-heptane fuels in HCCI combustion engine for reduced mechanisms relative to the detailed ones at all

4.2.7 Reduced Mechanisms Performance in Capturing the Mass Fraction of Species for Both Natural Gas-Fueled and n-Heptane-Fueled HCCI Engines

Finally, a comparison of the simulation results for the mass fraction profiles of some major species such as fuels and CO using the reduced mechanisms and the detailed mechanisms are shown in Figure 4.18. The results show that the calculated

mass fraction of these species using the reduced mechanisms agrees very well with the simulation results utilizing the detailed mechanisms for both fuels.

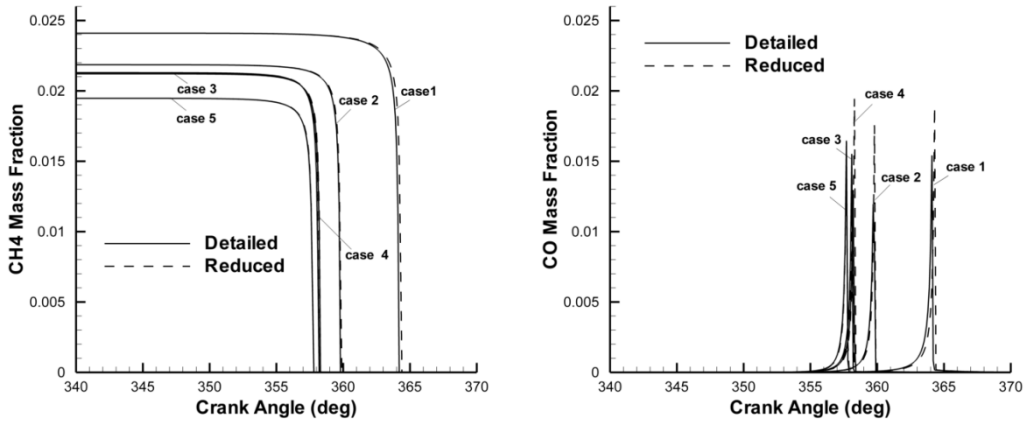

(a)

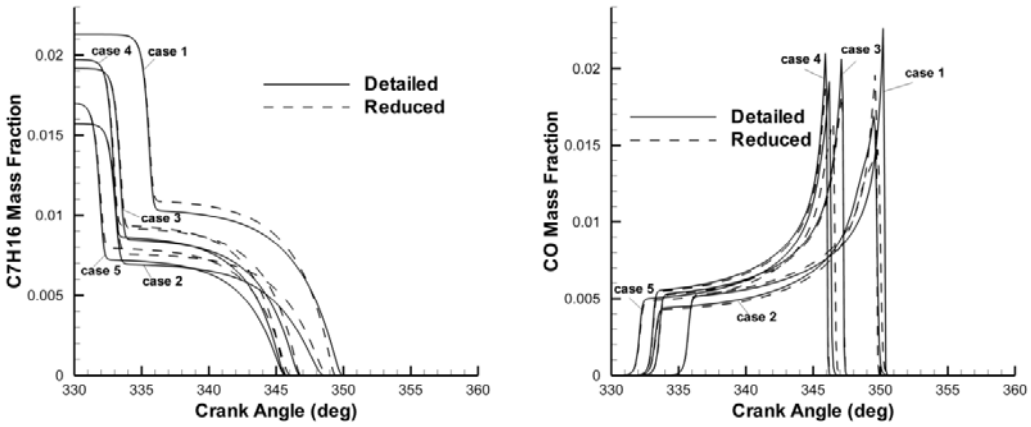

(b)

Figure 4. 18 Comparison of mass fraction for some selected species between (a) the detailed natural gas mechanism and its reduced mechanism generated for Case 5 (b) the detailed n-heptane mechanism and its reduced mechanism generated for Case 2

4.2.8 Validation of Combined Chemical Kinetics Mechanism

As mentioned before, the purpose of this study is to generate a proper reduced chemical kinetic mechanism for oxidation of fuel blend of natural-gas and n-heptane using HCCI combustion model. To do this, two developed reduced mechanisms of n-heptane and natural gas are combined. The combined mechanism is based on natural gas mechanism in which species and corresponding reactions that are unique to the n-heptane mechanism are added to the natural gas mechanism. The resultant mechanism includes 41 species and 109 reactions. A set of different experimental

conditions mentioned in Table 4.8 over wide ranges of equivalence ratios, intake pressures, and EGR rates are selected to evaluate the validity of this mechanism.

Table 4. 8 Operating conditions for considered cases of natural gas/n-heptane blend fuel

Case	Case 1	Case 2	Case 3	Case 4	Case 5	Case 6	Case 7	Case 8	Case 9
Equivalence ratio (Φ)	0.44	0.43	0.61	0.32	0.48	0.91	0.76	0.63	0.86
NG mass rate (mg/s)	21.70	28.68	45.96	42.25	24.18	45.97	42.25	40.33	29.79
n-heptane mass rate (mg/s)	37.74	35.57	41.06	39.36	39.99	41.06	39.36	36.94	49.26
Air mass rate (g/s)	2.08	2.33	1.50	1.68	2.07	1.50	1.68	1.90	1.43
T_{IVC} (K)	393	393	393	393	393	393	393	393	393
P_{IVC} (bar)	1.01	1.00	1.01	1.00	1.00	1.01	1. 01	1. 01	1. 01
% EGR	19.19	8.14	34.56	28.03	19.02	34.56	28.03	21.81	37.38
Compression Ratio	13.8	13.8	13.8	13.8	13.8	13.8	13.8	13.8	13.8

Figure 4.19 displays the prediction of SOC for original combined mechanism. Significant disagreement is observed by utilizing original combustion parameters related to experimental results. Therefore, to improve the combustion prediction of the original mechanism, the optimization of the reaction rate constants is vital.

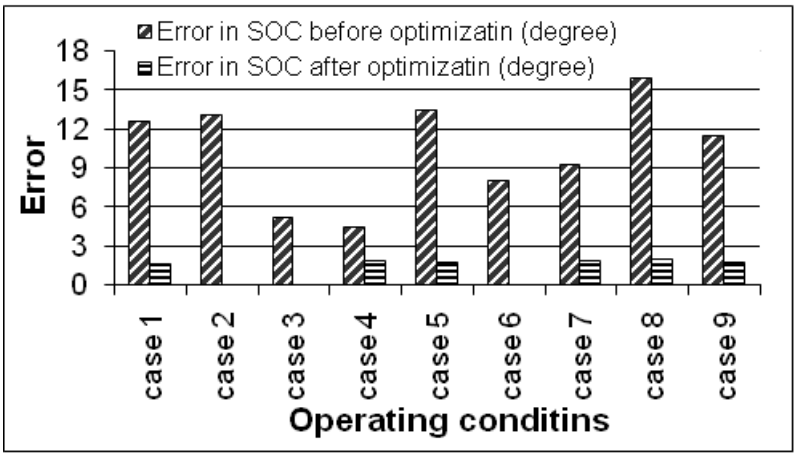

Figure 4. 19 Error in prediction of SOC for fuel blend of natural gas/n-heptane in HCCI combustion engine for reduced mechanisms relative to experimental ones at all considered cases

Genetic algorithm is used to optimize the constants of the reaction rates in the combined reduced mechanism. A Fortran code was developed which firstly utilized the GA code to produce a population randomly and then, by recalling the SZCM, the start of combustion was calculated for each of the considered operating conditions. Then an initial estimate of the fitness function was performed using this original population. This loop was repeated, if necessary, until the fitness function, the average error between the predicted and the measured ignition timing over the entire operating conditions of interest, was less than a specified tolerance.

It should be noted that only the Arrhenius coefficients were changed in the optimization process. The other parameters such as the enhanced factors and the Troe parameters were unaltered from their values in the original mechanisms (i.e. the GRI-Mech 3.0 and Golovitchev mechanisms).

To optimize the constants of reaction rates, the four different operating conditions considered in Table 4.8 (Cases 1 to 4) are applied to the GA. The optimized mechanism reduced the error in prediction of the ignition timing less than 2 degrees for all of the operating conditions. To further examine the validity of the optimized mechanism, the deviation of simulation results of the reduced mechanism from experimental data for five different operating conditions presented in Table 4.8 (Cases 5 to 9) are also investigated as shown in Figure 4.19. This figure demonstrates the differences between the predicted results for start of combustion by utilizing the optimized combined chemical kinetics mechanism and the experimental data. It can be seen that for all cases, this parameter is predicted accurately within the defined tolerances.

Figure 4.20 shows a comparison of predicted in-cylinder pressure traces during the compression stroke resulted from the single-zone combustion model before and after optimization, along with the corresponding experimental data for some selected operating conditions mentioned in Table 4.8. These graphs demonstrate that the ability of the model using optimized mechanism in predicting the in-cylinder pressure in comparison with experimental data through the compression stroke is reasonably well and also it provides accurate prediction of ignition timing. Of course the SZCM over-estimates combustion rates after ignition due to its assumptions. This is a well-known limitation of single-zone combustion models. If the rest of the cycle is needed to be analyzed, thermal and composition distributions of cylinder charge should be considered. This goal is achieved by employing multi-zone combustion models but take a large amount of simulation time in comparison with SZCM. A large number of simulations are required to optimize the mechanism using GA optimization, and the use of Multi-zone models is prohibitive. It is observed that

SZCM is exceedingly accurate for the purpose of this thesis. As a result, in this study, single-zone modeling was adequate for following the auto-ignition process up to the point of main combustion. From this figure it is evident that a significant discrepancy is observed when applying mechanism with the original combustion parameters to the model with the experimental results. Thus, the optimization is necessary. The proposed reduced mechanism for the present study is provided as additional Information in appendix D.

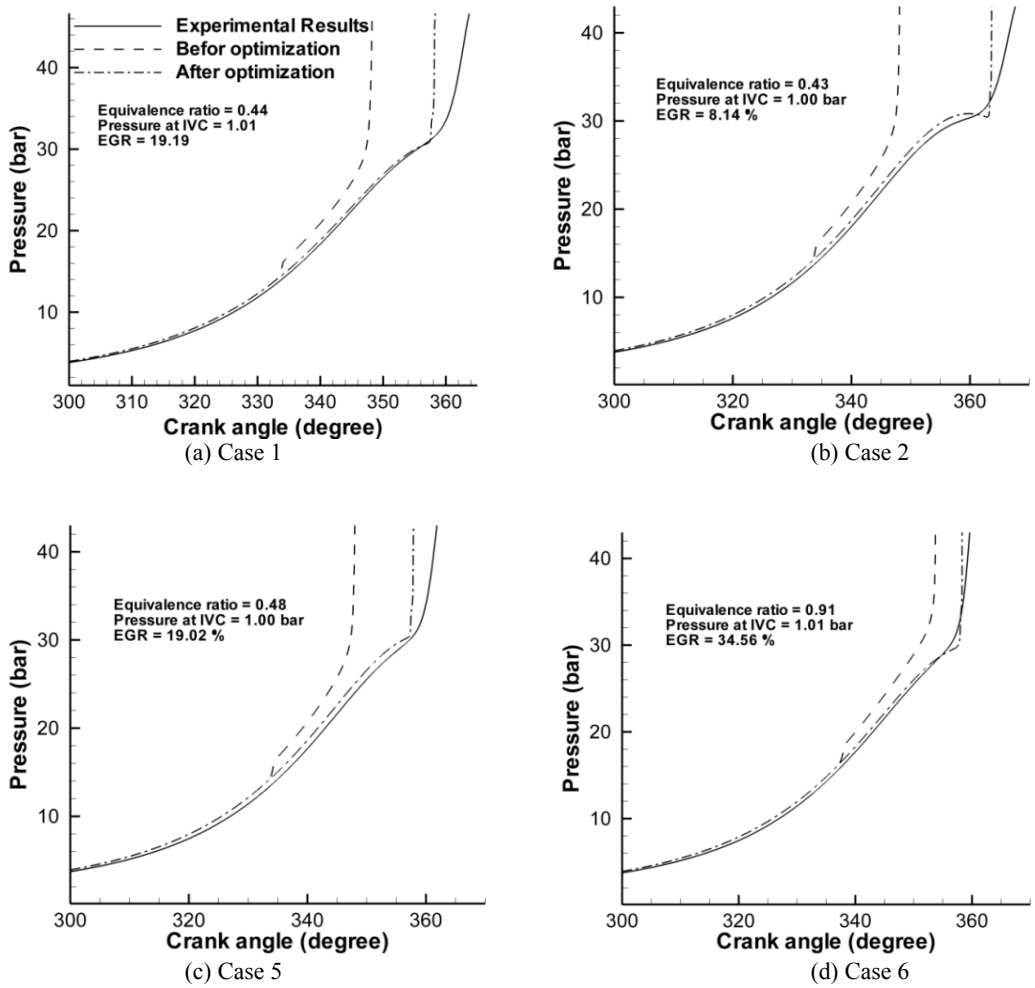

Figure 4. 20 Comparison of predicted in-cylinder pressure traces during the compression stroke resulted from the single-zone combustion model before and after optimization with the corresponding experimental data

Figure 4.21 compares the predicted pressure trace obtained experimentally with those of using the Golovichev's, Curran's and proposed mechanisms. While both the Golovichev's and Curran's mechanisms exhibit discrepancies in predicting ignition timing, the proposed mechanism provides reasonable agreement with corresponding measurements for predicting the ignition timing.

Table 4.9 shows the ability of the above mentioned mechanisms in predicting SOC. The proposed mechanism increased the simulation speed by 57 times in comparison with Golovichev's mechanism and 99.9 times in comparison with Curran's mechanism.

Table 4. 9 Comparison of proposed mechanism, Golovichev's mechanism, and also Curran's mechanism

mechanism	Species	Reactions	Error in SOC for Case 1 (Degree)	Error in SOC for Case 2 (Degree)	Simulation time (hr:min:sec)
Curran	561	2539	10.0	12.0	10:01:21
Golovichev	57	290	10.8	13.6	00:01:24
This work	41	109	1.7	0.1	00:00:36

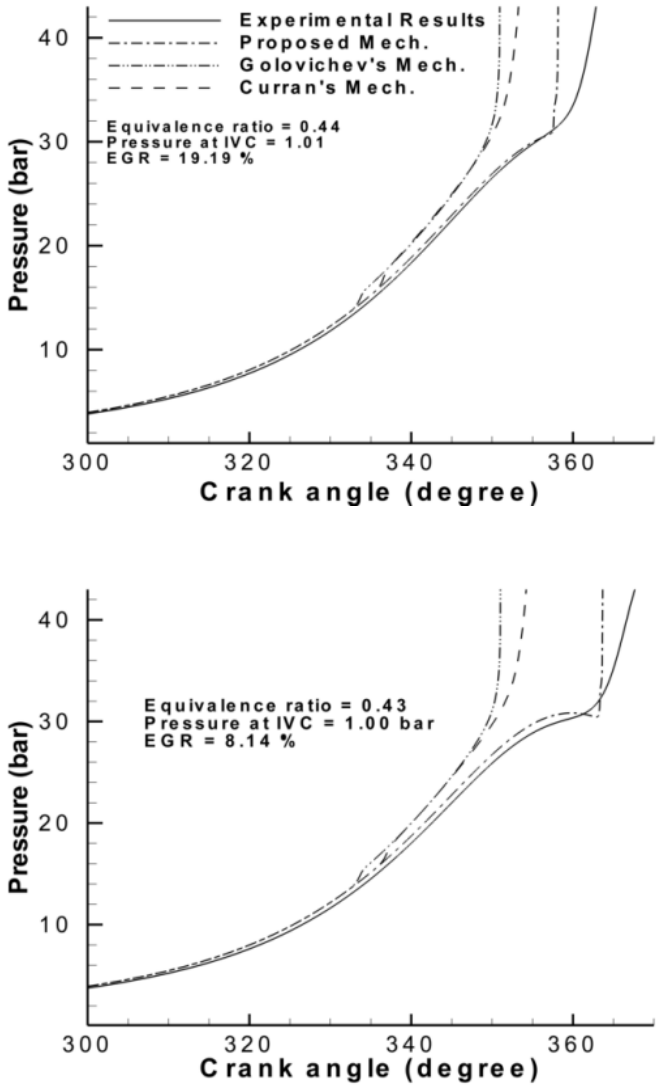

Figure 4. 21 Comparison of predicted in-cylinder pressure traces resulting from the single-zone combustion model employing the Golovichev's mechanism, the Curran's mechanism, and the proposed mechanism with the corresponding experimental data

Chapter 5

EFFECTS OF HEAT TRANSFER ON THE REDUCTION OF DETAILED KINETIC CHEMICAL MECHANISM IN HCCI COMBUSTION ENGINE

The heat loss from the hot combustion gases to the surroundings deteriorates the thermal conditions in the cylinder. These conditions are governed by the interaction of the chemical processes with the temperature and pressure changes in the cylinder. As a result, the heat release rate and heat transfer inside the combustion chamber play a significant role in the HCCI combustion mode. However, in developing reduced chemical kinetic mechanism from the detailed chemical kinetic mechanism it is common not to consider the role of heat transfer and to focus only on the kinetics aspects of HCCI. In this chapter the effect of heat transfer (through the boundaries of HCCI combustion chamber) on the development of reduced mechanisms from the detailed mechanisms is discussed.

5.1 Heat Transfer from In-Cylinder Gas to the Boundaries

Since there is no external ignition source in the HCCI engine, the auto-ignition of the cylinder charge will determine the start of the combustion. Combustion initiation and promotion of appropriate chemical kinetics strongly depend on the gas temperature [70].

In all IC engines, regardless of the combustion type (compression ignition, spark ignition or homogeneous charge compression ignition) or any type of engine configuration (conventional or free-piston engine [71-73]) a significant portion of the released fuel energy is lost in the form of heat [74-77]. In HCCI engines the heat

transfer from the bulk of the gas to the piston crown and the cylinder walls has an effect on the in-cylinder pressure and temperature. This in return will influence both fuel consumption and the pollutant emissions. Generally, chemical kinetics are strongly associated with the heat transfer process in HCCI engines [78]. Several different models have been proposed in the literature to predict the heat transfer from the in-cylinder gases to the combustion chamber walls such as the ones by Annand [79], Woschni [54] and Hohenberg [80]. It is necessary to mention that in the development of these correlations, they have considered engine design and operating conditions that differ significantly from those in HCCI combustion. In this regard, the works of Ognik et al. [81], Soyhan et al. [78], and Chang et al.[55] were dedicated to heat transfer modeling of HCCI engines.

Computational modeling is a useful tool for engine design and optimization. The full chemical mechanisms to simulate the fuel oxidation consist of hundreds or thousands of species and reactions. Utilizing such a detailed mechanism requires extremely long computational time. In order to facilitate practical simulations, reduced mechanisms of smaller sizes are necessary.

In many studies, the heat transfer from the in-cylinder gas of the HCCI engines to the surroundings was disregarded in the development of reduced chemical kinetic mechanisms from the detailed chemical kinetic mechanisms. Instead they intensified their work on the kinetics aspects of the HCCI combustion. For example, Liang et al. [26, 41] developed a dynamic adaptive chemistry (DAC) scheme based on the DRGEP method. In their study, a simplified single zone engine model with adiabatic boundary conditions is assumed where the main focus was on the kinetics aspects of the HCCI combustion using a detailed n-heptane mechanism (578 species). Shi et al. [44] applied an automatic reduction scheme with a combination of DRGEP and PCA

methods for the reduction of large detailed kinetic mechanisms of hydrocarbon fuels for HCCI engines. In the simulations, they used single zone combustion model.

On the other hand, some researchers took into account the effect of heat transfer in their analysis of reactive systems for generating reduced mechanisms [82, 83].

Notwithstanding the numerous amount of research work in this field, little is known about the importance of thermal systems heat transfer in the development of reduced mechanisms. Therefore, the objective of this chapter is to investigate the consequences of including heat transfer in the generation of reduced mechanisms for HCCI engines. It is preferred to use a single-zone combustion model since the computation time with this model is considerably less compared to the multi-zone modeling. Single-zone combustion model assumes that the combustion is homogenous throughout the combustion chamber and for this reason it has been shown that the single-zone simulations would not represent all aspects of the real HCCI engine operation where charge and temperature stratification exist. However, recent studies have revealed that single-zone simulations with high-fidelity fuel mechanisms can adequately reproduce the chemical kinetics characteristics of real fuels in HCCI engine over a wide range of operating conditions [47, 83]. Therefore, such a SZCM was considered as an effective tool for the purpose of the present work, because other models are time consuming. This is in agreement with the published works in the literature [26, 41, 44, 82, 83].

5.2 Engine Simulation Strategy

The purpose of this work is to study the effect of heat transfer from in-cylinder charge to the combustion camber walls during generating a reduced mechanism from the detailed mechanism. For this reason, a single zone natural gas fuelled HCCI combustion model is used as described in chapter 3. The heat transfer model is based on Woschni's heat transfer coefficients.

A direct comparison can be made by simulating the cyclic process for the engine, both by using the Wosheni heat transfer model and by using the adiabatic conditions. The rate coefficients that obey the Arrhenius law, is vigorously dependent on temperature in a non-linear manner, which is a characteristic of chemical reactions. Variation in the mixture temperature inside the combustion chamber at each specific engine simulation time step, as a result of adiabatic and non-adiabatic assumption, may influence the species concentrations which are inputs for the mechanism reduction methods. The chemical kinetic reaction mechanism which describes the oxidation of natural gas (NG) contains 53 species and 325 reactions based on the GRI-Mech. 3.0 kinetic reaction mechanism. This matches the works of Zheng and Caton [84, 85]. GRI-Mech. 3.0 was subject matter to mechanism reduction simulations in many publications [68, 86-89]. Table 4.4 represents the considered operating conditions of the engine for combustion analysis of natural gas fuel.

5.3 Mechanism Reduction

A multiple reduction process based on DRGEP and PCA reduction schemes are used for simplifying the detailed mechanism. In this work the overall performance of the skeletal mechanism is estimated by the peak pressure, at crank angle where 50% of heat is released (CA50), and with maximum heat release. In the generation of the reduction process, more than 200 sampling points associated with the time steps

between the times of intake valve closing (IVC) and exhaust valve opening (EVO), are sampled. At each sampling point, a set of important species and reactions is identified based on the thermal conditions and the mass fractions of the species at that point.

First, the DRGEP method is applied using an initial tolerance value, R_{AB}, of 10^{-5}, which generates a reduced mechanism as unimportant species and reactions containing unimportant species are removed. In the process of identifying the unimportant species in the DRGEP algorithm, the species *B* is unimportant where R_{AB} is less than the tolerance value and *A* is a target species. The representative parameters calculated by applying the reduced mechanism in HCCI engine simulation code are compared with those obtained using the detailed mechanism in the simulation code. Then, by increasing the tolerance value the procedure is repeated until errors which are specified by the user for peak pressure, CA50, and maximum heat release (In this work: 1%, 1° CA, and 1% respectively) are exceeded. For further simplification, in the second stage, PCA method is applied to the final valid reduced mechanism developed in the first stage with an initial tolerance value equal to 10^{-3}.

By applying the reduction process for each operating condition presented in Table 4.4 two reduced mechanisms; one associated with non-adiabatic and the other with adiabatic simulations for HCCI combustion are generated. The mechanism sizes and the estimated errors for the selected representative parameters for each operating condition at the end of DRGEP and DRGEP-PCA reduction processes are provided in Table 5.1. It is well known that in some cases DRGEP species and PCA reaction removal can even decrease the error values. The implication of this observation is that it is useful to continue the DRGEP reduction or PCA based reaction elimination

even on the skeletal mechanisms just above the prescribed thresholds. However, this is not the case for the generated reduced mechanisms shown in Table 5.1, since at the end of each reduction process further mechanism reduction significantly deteriorates the accuracy of the reduced mechanism, as the absolute value of the user-specified tolerances becomes large.

For each considered case, the numbers of species is approximately equal to each other, while the numbers of reactions vary in small amounts. The engine simulation results for the selected representative parameters are below the user specified error-tolerance values. More specifically, except for Case 2 in which there are very small variations, at the end of DRGEP reduction process, not only the number of species and reactions in both of the generated reduced mechanism are equal, but also the species and reactions themselves are the same for both adiabatic and non-adiabatic conditions. A more comprehensive investigation of the DRGEP reduction process reveals interesting results. In this work for the mechanism reduction procedure a dense set of sampling points, more than 200 points, are selected. Each of these sampling points correspond to a specific crank angle during compression, combustion, and expansion processes of the engine cycle with related temperature and pressure and species concentrations. At each sampling point, a set of important species and reactions is identified and the union of all these individual subsets forms the overall set of important species and reactions. However, almost all of the species for the overall set are included in the summation of those subsets related to the sampling points which are associated with the compression stroke where the differences between temperature histories of the engine simulation for adiabatic and non-adiabatic conditions are very low. This simply means that considering heat transfer in such simulations does not have significant effect on the selection of the

species by DRGEP method. This is not the case for PCA method which was used to identify the important reactions. The results of reduction process show that some parts of the identified important reactions are associated with the sampling points during the combustion and expansion processes where the differences between the temperature traces for adiabatic and non-adiabatic conditions are significant. This will affect the rate of reactions and the elements of the log-normalized rate sensitivity matrix. As a result, although the size of the two generated reduced mechanisms are the same, even in the operating condition of Case 3, this does not mean that all of the reactions are exactly the same.

Figure 5.1 shows the temperature histories of the engine cycle for both of the adiabatic and non-adiabatic conditions for operating condition of Case 4. The figure demonstrates that the differences in temperature during the expansion process are greater than the ones obtained during the compression process. The final reduced mechanisms for both of the considered conditions are only slightly different than each other; however, the performances of these reduced mechanisms are compared with that of the detailed mechanism for the corresponding operating conditions.

Table 5. 1 Comparison of natural gas skeletal mechanisms generated by DRGEP, DRGEP-PCA with and without considering heat transfer

DRGEP	**Case 1**		**Case 2**		**Case 3**		**Case 4**	
	adiabatic	**non-adiabatic**	**adiabatic**	**non-adiabatic**	**adiabatic**	**non-adiabatic**	**adiabatic**	**non-adiabatic**
Species	19	19	22	21	20	20	20	20
Reactions	144	144	169	154	144	144	144	144
Error in Peak Press. (%)	0.547	0.021	0.005	0.003	0.000	0.000	0.003	0.003
Error in Max. HR (%)	0.048	0.225	0.199	0.007	0.007	0.043	0.011	0.100
Error in CA50 (Degree)	0.3	0.1	0.1	0.1	0.0	0.2	0.0	0.0
DRGEP + PCA	**Case 1**		**Case 2**		**Case 3**		**Case 4**	
Species	19	19	22	21	20	20	20	20
Reactions	90	64	83	83	66	66	64	74
Error in Peak Press. (%)	0.564	0.466	0.876	0.058	0.015	0.092	0.016	0.013
Error in Max. HR (%)	0.044	0.106	0.031	0.006	0.008	0.057	0.068	0142
Error in CA50 (Degree)	0.2	0.7	0.4	0.3	0.4	0.5	0.4	0.1

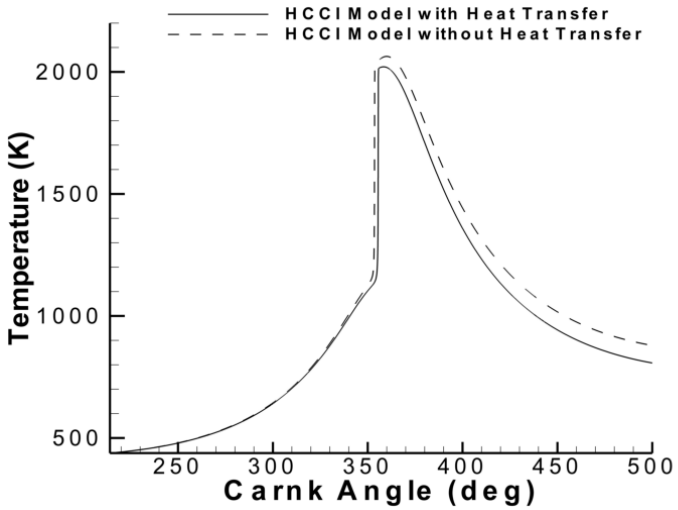

Figure 5. 1 Comparison of the temperature traces by applying the detailed GRI mechanism to the single zone HCCI combustion model by considering heat transfer and without heat transfer for operating condition of Case 4

5.4 Performance of the Developed Reduced Mechanisms for Adiabatic and Non-Adiabatic Conditions

To verify the ability of the reduced mechanisms in predicting the pressure trace, accumulated heat release, and temperature histories, a comparison of these parameters by applying the reduced and detailed mechanisms to the SZCM are depicted in Figures 5.2 , 5.3, and 5.4 for different operating conditions of the natural gas-fuelled HCCI engine. As indicated in these figures, simulations using both of the reduced mechanisms are in good agreement with the simulations employing the detailed mechanism.

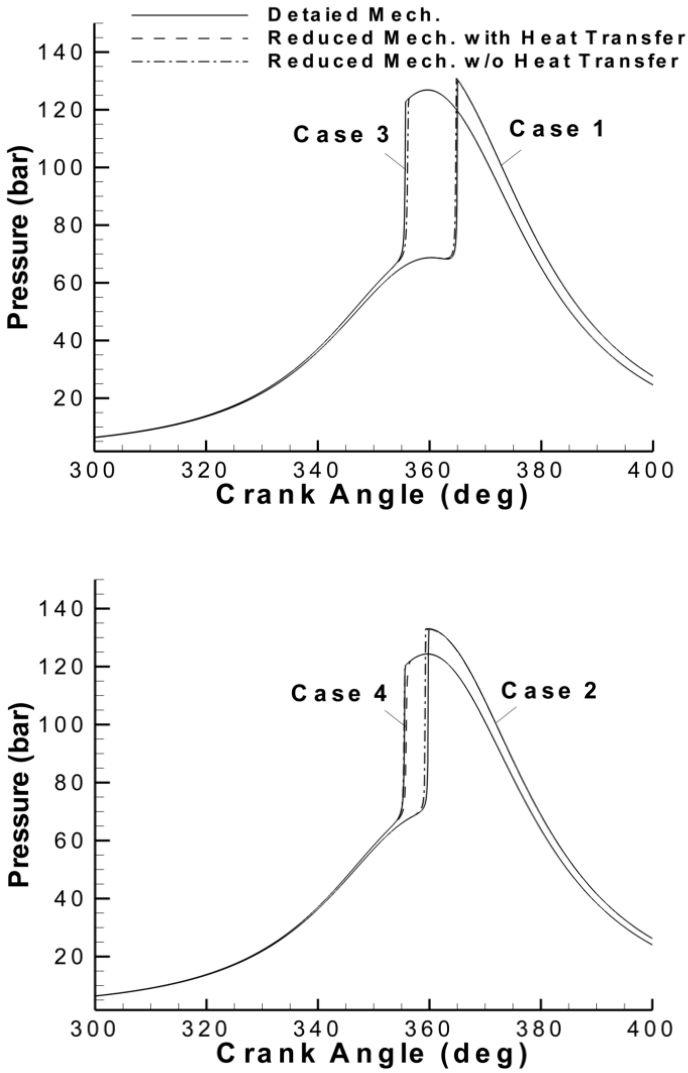

Figure 5. 2 Comparison of the pressure traces generated by applying the detailed GRI mechanism and corresponding reduced mechanisms with and without heat transfer

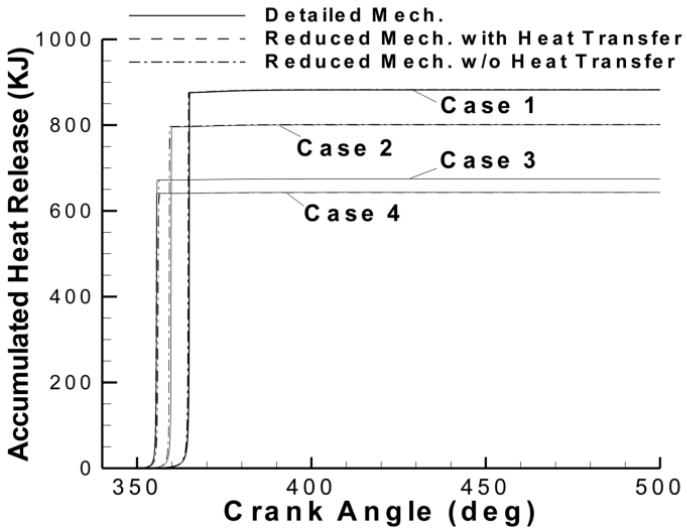

Figure 5. 3 Comparison of the accumulated heat-release generated by applying the detailed GRI mechanism and corresponding reduced mechanisms with and without heat transfer

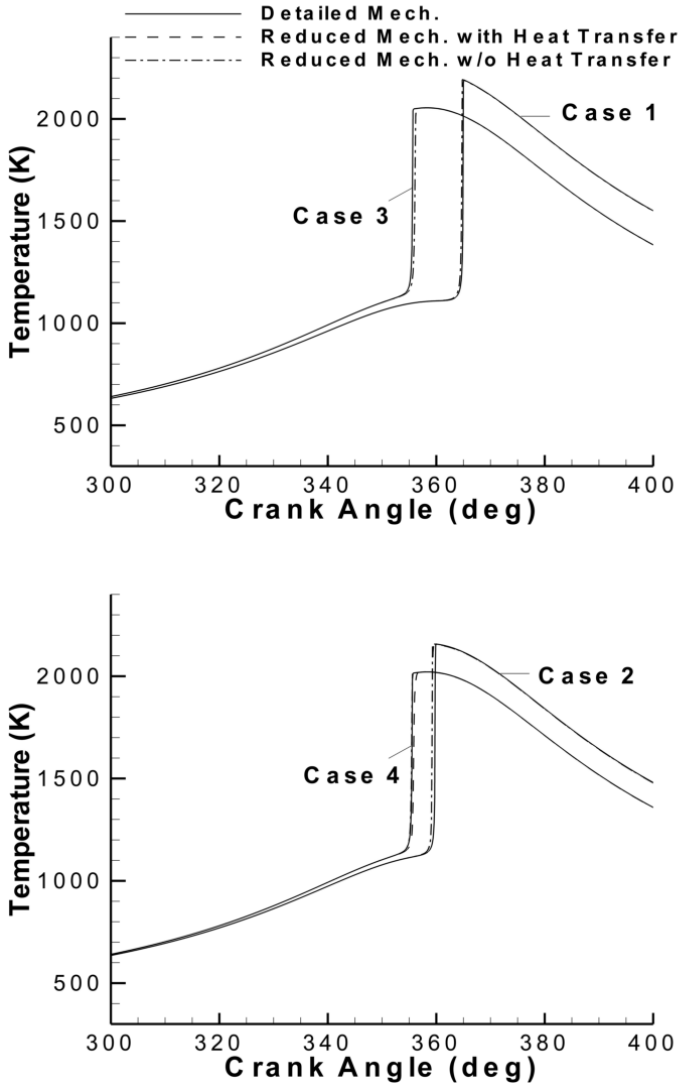

Figure 5. 4 Comparison of the temperature traces generated by applying the detailed GRI mechanism and corresponding reduced mechanisms with and without heat transfer

Finally, the mass fraction profiles of some major species (such as the fuels and CO) obtained by using both of the reduced mechanisms and the detailed mechanism are compared as shown in Figure 5.5. The results show that the calculated mass fractions of these species employing the reduced mechanisms agree very well with those of detailed mechanism and therefore it can be concluded that the effect of heat transfer is negligible.

These results demonstrate that the impact of considering heat transfer in HCCI engines during generating reduced mechanisms is very low and in both conditions, either adiabatic or non-adiabatic, the HCCI combustion model can perform satisfactory.

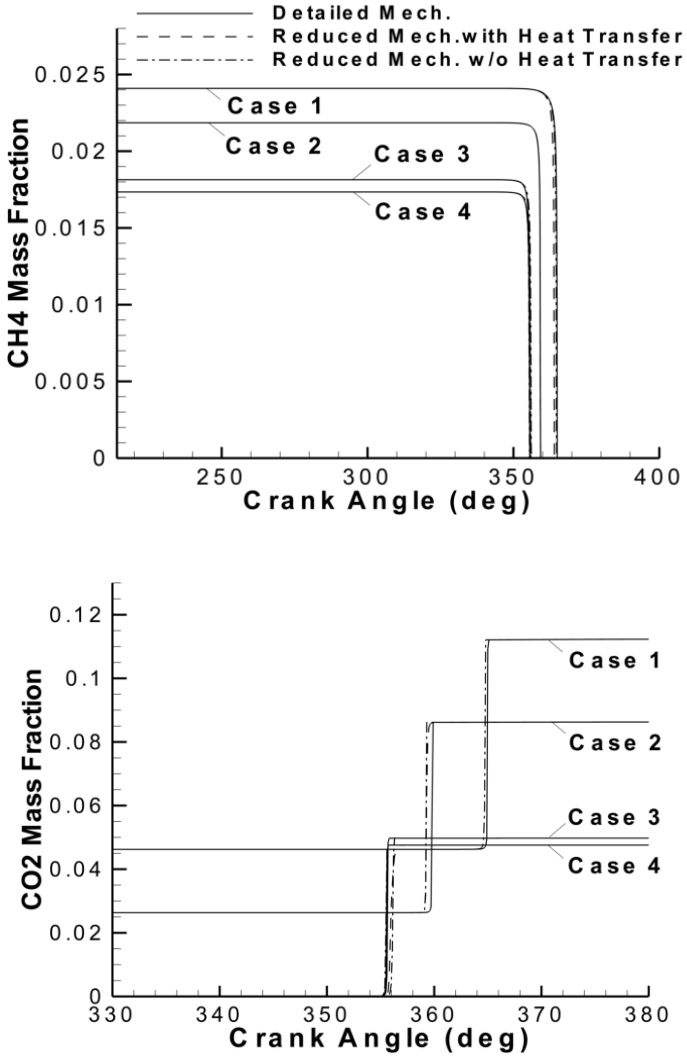

Figure 5. 5 Comparison of the mass fraction for some selected species generated by applying the detailed GRI mechanism and corresponding reduced mechanisms with and without heat transfer

Chapter 6

CONCLUSION AND FUTURE WORK

6.1 Conclusion of Work

In the present work, the combination of directed relation graph with error propagation (DRGEP) method (applied twice) and computational singular perturbation (CSP) method for generating a reduced mechanism of n-heptane, based on the Curran's mechanism, was used and discussed. The reduced mechanism achieved reduction ratios of 79 percent for the number of species and also 87 percent for the number of reactions, while the differences in the CA50, peak pressure, and maximum heat release between the original and reduced mechanisms are less than 1.5 CA, 2 percent and 2 percent, respectively. The reduced mechanism has great ability in the prediction of combustion phasing for n-heptane fuel in investigated operating conditions for a HCCI engine. Also, there is a good agreement between the mass fractions of species such as O_2, CO and CO_2 obtained from applying both detailed and reduced mechanisms to the HCCI engine cycle calculations. Also, cycle calculation time by employing the reduced mechanism is 79 times faster than the one employed detailed mechanism.

Also, in the current study, a reduced mechanism of natural-gas/n-heptane fuel with the combination of two developed reduced mechanisms of natural gas and n-heptane fuel, based on the GRI-Mech. 3.0 and Golovichev's mechanisms, was proposed. Reduction procedure to develop the reduced mechanisms was based on an integrated method that utilizes DRGEP and PCA reduction methods. The mechanism

reduction achieved reduction ratios of 64 and 30 percents for the number of species and also 88 and 67 percents for the number of reactions (for the natural gas and n-heptane mechanisms respectively). These were achieved within tight error limits for prediction of CA50, peak pressure, and maximum heat release. The combination of the generated reduced mechanisms is used to develop a reaction mechanism for a fuel blend of natural-gas/n-heptane. The combined mechanism was optimized using Genetic Algorithm and validated against experimental data for predicting ignition timing in the natural-gas/n-heptane fuelled HCCI engine. The proposed reduced mechanism for fuel blends of natural-gas and n-heptane contains 41 species and 109 reactions.

Furthermore, a simulation study has been carried out to provide better understanding of the effect of heat transfer on generating a reduced mechanism from detailed one for HCCI combustion mode. An investigation was conducted by employing the single-zone combustion model with adiabatic and non-adiabatic conditions. The heat transfer model used here is based on the Wosheni heat transfer model. Several different operating conditions were considered. For each considered case, the results show that the sizes of the reduced mechanisms developed for the adiabatic and non-adiabatic HCCI model are very close to each other. However, the mechanisms are not exactly the same even when the sizes are identical. A comparison of the simulation results using the reduced mechanisms and the detailed mechanism shows that both of the reduced mechanisms are in good agreement with the detailed mechanism.

6.2 Future Works

1. Applying the reduced mechanism developed for n-heptane fuel in multi zone and multi-dimensional models to verify their applicability for prediction of HCCI engines combustion, performance and emission characteristics.
2. Utilizing the proposed reduction procedure to develop reduced mechanisms from other comprehensive chemical kinetic mechanisms.
3. Applying the reduced mechanism of natural-gas/n-heptane fuel in multi zone and multi-dimensional models to verify their applicability for prediction of HCCI engines combustion, performance and emission characteristics.
4. Investigating the NO_x emission behaviour at high loads for HCCI engines.

REFRENCES

[1] Onishi S, Jo SH, Shoda K, Jo PD, Kato S. Active thermo-atmosphere combustion (ATAC) - A new combustion process for internal combustion engines. SAE paper 790501. 1979.

[2] Najt PM, Foster DE. Compression-ignited homogeneous charge combustion. SAE paper 830264. 1983.

[3] Thring RH. Homogeneous charge compression ignition (HCCI) engines. SAE paper 892068. 1989.

[4] Iida N. Combustion Analysis of Methanol-Fueled Active Thermo-Atmosphere Combustion (ATAC) Engine Using a Spectroscopic Observation. SAE Paper 940684. 1994.1250-7.

[5] Yamaguchi J. Honda readies activated radical combustion two-stroke engine for production motorcycle. CAutomotive Engineering. 1997.90–2.

[6] Cao L, Zhao H, Jiang X, Kalian N. Investigation into the Effect of Injection Timing on Stoichiometric and Lean CAI Operations in a 4-Stroke GDI Engine. SAE Paper 2006-01-0417. 2006.

[7] Aoyama T, Hattori Y, Mizuta J, Sato Y. An Experimental Study on Premixed-Charge Compression Ignition Gasoline Engine. SAE Paper 960081. 1996.

[8] Shimazaki N, Akagawa H, Tsujimura K. An experimental study of premixed lean diesel combustion process. SAE Paper, 1999-01-0181. 1999.

[9] Kimura S, Aoki O, Kitahara Y, Aiyoshizawa E. Ultra-clean combustion technology combining a low-temperature and premixed combustion concept for meeting future emission standards. SAE 2001-01-0200. 2001.

[10] Yao M, Zheng Z, Liu H. Progress and recent trends in homogeneous charge compression ignition (HCCI) engines. Progress in Energy and Combustion Science. 2009;35(5):398-437.

[11] Saisirirat P, Togbé C, Chanchaona S, Foucher F, Mounaim-Rousselle C, Dagaut P. Auto-ignition and combustion characteristics in HCCI and JSR using 1-butanol/n-heptane and ethanol/n-heptane blends. Proceedings of the Combustion Institute. 2011;33(2):3007-14.

[12] Fathi M, Saray RK, Checkel MD. The influence of Exhaust Gas Recirculation (EGR) on combustion and emissions of n-heptane/natural gas fueled Homogeneous Charge Compression Ignition (HCCI) engines. Appl Energ. 2011;88(12):4719-24.

[13] Wu H-W, Wang R-H, Ou D-J, Chen Y-C, Chen T-y. Reduction of smoke and nitrogen oxides of a partial HCCI engine using premixed gasoline and ethanol with air. Appl Energ. 2011;88(11):3882-90.

[14] Santoso H, Matthews J, Cheng WK. Managing SI/HCCI dual-mode engine operation. SAE paper 2005-01-0162. 2005.

[15] Weinrotter M, Wintner E, Iskra K, Neger T, Olofsson J, Seyfried H, et al. Optical Diagnostics of Laser-Induced and Spark Plug-Assisted HCCI Combustion. SAE paper 2005-01-0129. 2005.

[16] Urushihara T, Yamaguchi K, Yoshizawa K, Itoh T. A study of a gasoline-fueled compression ignition engine expansion of HCCI operation range using SI combustion as a trigger of compression ignition. SAE paper 2005-01-0180. 2005.

[17] Warnatz J, Maas U, Dibble RW. Combustion: Physical and Chemical Fundamentals, Modeling and Simulation, Experiments, Pollutant Formation. 4th ed. Berlin: Springer, 2006.

[18] Ghazimirsaied A, Shahbakhti M, Koch CR. HCCI engine combustion phasing prediction using a symbolic-statistics approach. Journal of Engineering for Gas Turbines and Power. 2010;132(8).

[19] Nehse M, Warnat J, Chevalier C. Kinetic modeling of the oxidation of large aliphatic hydrocarbons. Symposium (International) on Combustion. 1996;26(1):773-80.

[20] Lindstedt RP, Maurice LQ. Detailed kinetic modelling of n-heptane combustion. Combust Sci Technol. 1995;107(4-6):317-53.

[21] Held TJ, Marchese AJ, Dryer FL. A semi-empirical reaction mechanism for n-heptane oxidation and pyrolysis. Combustion Science and Technology. 1997;123(1-6):107-46.

[22] Golovitchev VI. Mechanisms (Combustion Chemistry). http://www.tfd.chalmers.se/~valeri/MECH.html.

[23] Curran HJ, Gaffuri P, Pitz WJ, Westbrook CK. A comprehensive modeling study of n-heptane oxidation. Combustion and Flame. 1998;114(1-2):149-77.

[24] Smith GP, Golden DM, Frenklach M, Moriarty NW, Eiteneer B, Goldenberg M, et al., http://www.me.berkeley.edu/gri_mech/.

[25] Konnov A. A. Detailed reaction mechanism for small hydrocarbons combustion. http://homepages.vub.ac.be/,akonnov.

[26] Liang L, Stevens JG, Farrell JT. A dynamic adaptive chemistry scheme for reactive flow computations. Proceedings of the Combustion Institute. 2009;32 I:527-34.

[27] Swami Nathan S, Mallikarjuna JM, Ramesh A. An experimental study of the biogas–diesel HCCI mode of engine operation. Energy Conversion and Management. 2010;51(7):1347-53.

[28] Maas U, Pope SB. Simplifying chemical kinetics: Intrinsic low-dimensional manifolds in composition space. Combustion and Flame. 1992;88(3-4):239-64.

[29] Lam SH, Goussis DA. CSP method for simplifying kinetics. International Journal of Chemical Kinetics. 1994;26(4):461-86.

[30] Zagaris A, Kaper HG, Kaper TJ. Analysis of the computational singular perturbation reduction method for chemical kinetics. Journal of Nonlinear Science. 2004;14(1):59-91.

[31] Tomlin AS, Turanyi T, Pilling MJ. Mathematical tools for the construction, investigation and reduction of combustion mechanisms. In: Pilling MJ, Hancock G, editors. Low-Temperature Combustion and Autoignition. Amsterdam: Elsevier; 1997. p. 293-437.

[32] Massias A, Diamantis D, Mastorakos E, Goussis DA. Global reduced mechanisms for methane and hydrogen combustion with nitric oxide formation constructed with CSP data. Combustion Theory and Modelling. 1999;3(2):233-57.

[33] Massias A, Diamantis D, Mastorakos E, Goussis DA. An algorithm for the construction of global reduced mechanisms with CSP data. Combustion and Flame. 1999;117(4):685-708.

[34] Lu T, Ju Y, Law CK. Complex CSP for chemistry reduction and analysis. Combustion and Flame. 2001;126(1-2):1445-55.

[35] Hwang YT. On the proper usage of sensitivities of chemical kinetics models to the uncertainties in rate coefficients. Proceedings of the National Science Council B ROC. 1982;6:270-8.

[36] Turányi T, Bérces T, Vajda S. Reaction rate analysis of complex kinetic systems. Int J Chem Kinet. 1989;21(2):83-99.

[37] Lu T, Law CK. A directed relation graph method for mechanism reduction. Proceedings of the Combustion Institute. 2005;30(1):1333-41.

[38] Pepiot-Desjardins P, Pitsch H. An efficient error-propagation-based reduction method for large chemical kinetic mechanisms. Combustion and Flame. 2008;154(1-2):67-81.

[39] Nagy T, Turányi T. Reduction of very large reaction mechanisms using methods based on simulation error minimization. Combustion and Flame. 2009;156(2):417-28.

[40] He K, Androulakis IP, Ierapetritou MG. On-the-fly reduction of kinetic mechanisms using element flux analysis. Chemical Engineering Science. 2010;65(3):1173-84.

[41] Liang L, Stevens JG, Raman S, Farrell JT. The use of dynamic adaptive chemistry in combustion simulation of gasoline surrogate fuels. Combustion and Flame. 2009;156(7):1493-502.

[42] Niemeyer KE, Sung CJ, Raju MP. Skeletal mechanism generation for surrogate fuels using directed relation graph with error propagation and sensitivity analysis. Combustion and Flame. 2010;157(9):1760-70.

[43] Lu TF, Law CK. Strategies for mechanism reduction for large hydrocarbons: n-heptane. Combustion and Flame. 2008;154(1-2):153-63.

[44] Shi Y, Ge HW, Brakora JL, Reitz RD. Automatic chemistry mechanism reduction of hydrocarbon fuels for HCCI engines based on DRGEP and PCA methods with error control. Energy and Fuels. 2010;24(3):1646-54.

[45] Christensen M, Hultqvist A, Johansson B. Demonstrating the Multi Fuel Capability of a Homogeneous Charge Compression Ignition Engine with Variable Compression Ratio. SAE paper 1999-01-3679. 1999.

[46] Olsson J, Tunestal P, Haraldsson G, Johansson B. A Turbocharged dual-fuel HCCI engine. SAE Paper 2001-01-1896. 2001.

[47] Hosseini V, Stuart Neill W, David Checkel M. Controlling n-heptane HCCI combustion with partial reforming: Experimental results and modeling analysis. Journal of Engineering for Gas Turbines and Power. 2009;131(5).

[48] Brakora JL, Ra Y, Reitz RD, McFarlane J, Daw CS. Development and validation of a reduced reaction mechanism for biodiesel-fueled engine simulations. SAE International Journal of Fuels and Lubricants. 2009;1(1):675-702.

[49] Dagaut P, Togbé C. Oxidation kinetics of butanol-gasoline surrogate mixtures in a jet-stirred reactor: Experimental and modeling study. Fuel. 2008;87(15-16):3313-21.

[50] Dagaut P, Togbé C. Experimental and modeling study of the kinetics of oxidation of ethanol-n-heptane mixtures in a jet-stirred reactor. Fuel. 2010;89(2):280-6.

[51] Aggarwal SK, Awomolo O, Akber K. Ignition characteristics of heptane-hydrogen and heptane-methane fuel blends at elevated pressures. Int J Hydrogen Energ. 2011;36(23):15392-402.

[52] Kongsereeparp P. Chemical Kinetic Based Simulation for an HCCI Engine and Its Combustion. Edmonton, Alberta: University of Alberta, 2008.

[53] Kongsereeparp P, Checkel MD. Novel method of setting initial conditions for multi-zone HCCI combustion modeling. SAE Paper 2007-01-0674. 2007.

[54] Woschni G. A universally applicable equation for the instantaneous heat transfer coefficient in the internal combustion engine. SAE Paper 670931. 1967.

[55] Chang J, Güralp O, Filipi Z, Assanis D, Kuo TW, Najt P, et al. New heat transfer correlation for an HCCI engine derived from measurements of instantaneous surface heat flux. SAE paper 2004-01-2996. 2004.

[56] Pepiot-Desjardins P, Pitsch H. Systematic Reduction of Large Chemical Mechanisms. Presented at the 4th Joint Meeting of the US Sections of the Combustion Institute. Drexel University, Philadelphia, 2005.

[57] Lu T, Law CK. On the applicability of directed relation graphs to the reduction of reaction mechanisms. Combustion and Flame. 2006;146(3):472-83.

[58] Valorani M, Creta F, Goussis DA, Lee JC, Najm HN. An automatic procedure for the simplification of chemical kinetic mechanisms based on CSP. Combustion and Flame. 2006;146(1-2):29-51.

[59] Vajda S, Valko P, Turanyi T. Principal Component Analysis of Kinetic-Models. International Journal of Chemical Kinetics. 1985;17(1):55-81.

[60] Brown PN, Byrne GD, Hindmarsh AC. VODE: A variable-coefficient ODE solver. SIAM J Sci Stat Comput. 1989;10(5):1038-51.

[61] Richter M, Franke A, Aldén M, Hultqvist A, Johansson B. Optical diagnostics applied to a naturally aspirated homogeneous charge compression ignition engine. SAE paper 1999-01- 3649. 1999.

[62] Hultqvist A, Christensen M, Johansson B, Richter M, Nygren J, Hult J, et al. The HCCI combustion process in a single cycle-high fuel tracer LIF and chemiluminescence imaging. SAE paper 2002-01-0424. 2002.

[63] Bengtsson J. Closed-loop control of HCCI engine dynamics. Lund, Sweden: Lund University, 2004.

[64] Mack JH, Flowers DL, Buchholz BA, Dibble RW. Investigation of HCCI combustion of diethyl ether and ethanol mixtures using carbon 14 tracing and numerical simulations. Proceedings of the Combustion Institute. 2005;30 II:2693-700.

[65] Elliott L, Ingham DB, Kyne AG, Mera NS, Pourkashanian M, Whittaker S. Reaction mechanism reduction and optimisation for modelling aviation fuel oxidation using standard and hybrid genetic algorithms. Comput Chem Eng. 2006;30(5):889-900.

[66] Goldberg DE. Genetic Algorithms in Search, Optimization and machine Learning. Boston: Addison-Wesley Longman Publishing Co., 1989.

[67] Hosseini V. Reformer Gas Application in HCCI Combustion Engine. Edmonton, Alberta: University of Alberta, 2008.

[68] Oluwole OO, Bhattacharjee B, Tolsma JE, Barton PI, Green WH. Rigorous valid ranges for optimally reduced kinetic models. Combustion and Flame. 2006;146(1-2):348-65.

[69] Oluwole OO, Barton PI, Green WH. Obtaining accurate solutions using reduced chemical kinetic models: A new model reduction method for models rigorously validated over ranges. Combustion Theory and Modelling. 2007;11(1):127-46.

[70] Garcia MT, Aguilar FJJE, Villanueva JAB, Trujillo EC. Analysis of a new analytical law of heat release rate (HRR) for homogenous charge compression ignition (HCCI) combustion mode versus analytical parameters. Appl Therm Eng. 2011;31(4):458-66.

[71] Mikalsen R, Jones E, Roskilly AP. Predictive piston motion control in a free-piston internal combustion engine. Appl Energ. 2010;87(5):1722-8.

[72] Mikalsen R, Roskilly AP. A computational study of free-piston diesel engine combustion. Appl Energ. 2009;86(7-8):1136-43.

[73] Mikalsen R, Roskilly AP. Coupled dynamic-multidimensional modelling of free-piston engine combustion. Appl Energ. 2009;86(1):89-95.

[74] Rakopoulos CD, Giakoumis EG, Rakopoulos DC. Cylinder wall temperature effects on the transient performance of a turbocharged Diesel engine. Energy Conversion and Management. 2004;45(17):2627-38.

[75] Rakopoulos CD, Mavropoulos GC. Experimental instantaneous heat fluxes in the cylinder head and exhaust manifold of an air-cooled diesel engine. Energy Conversion and Management. 2000;41(12):1265-81.

[76] Rakopoulos CD, Giakoumis EG, Rakopoulos DC. Study of the short-term cylinder wall temperature oscillations during transient operation of a turbocharged diesel engine with various insulation schemes. International Journal of Engine Research. 2008;9(3):177-93.

[77] Komninos NP, Kosmadakis GM. Heat transfer in HCCI multi-zone modeling: Validation of a new wall heat flux correlation under motoring conditions. Appl Energ. 2011;88(5):1635-48.

[78] Soyhan HS, Yasar H, Walmsley H, Head B, Kalghatgi GT, Sorusbay C. Evaluation of heat transfer correlations for HCCI engine modeling. Appl Therm Eng. 2009;29(2-3):541-9.

[79] Annand WJD. Heat transfer in the cylinders of reciprocating engines. Proc Inst Mech Eng. 1963;177(3).

[80] Hohenberg GF. Advanced Approaches for Heat Transfer Calculations. SAE Paper 790825. 1979.

[81] Ogink R, Golovitchev V. Gasoline HCCI modeling: computer program combining detailed chemistry and gas exchange processes. SAE Paper 2001-01-3614. 2001.

[82] Bahlouli K, Saray RK, Atikol U. Development of a Reduced Mechanism for n-Heptane Fuel in HCCI Combustion Engines by Applying Combined Reduction Methods. Energ Fuel. 2012;26(6):3244-56.

[83] Andrae JCG, Head RA. HCCI experiments with gasoline surrogate fuels modeled by a semidetailed chemical kinetic model. Combustion and Flame. 2009;156(4):842-51.

[84] Zheng J, Caton JA. Use of a single-zone thermodynamic model with detailed chemistry to study a natural gas fueled homogeneous charge compression ignition engine. Energy Conversion and Management. 2012;53(1):298-304.

[85] Zheng J, Caton JA. Effects of operating parameters on nitrogen oxides emissions for a natural gas fueled homogeneous charged compression ignition engine (HCCI): Results from a thermodynamic model with detailed chemistry. Appl Energ. 2012;92(0):386-94.

[86] Xin Y, Song Z, Tan YZ, Wang D. The directed relation graph method for mechanism reduction in the oxidative coupling of methane. Catalysis Today. 2008;131(1–4):483-8.

[87] Leroy V, Leoni E, Santoni P-A. Reduced mechanism for the combustion of evolved gases in forest fires. Combustion and Flame. 2008;154(3):410-33.

[88] Lu T, Law CK. A criterion based on computational singular perturbation for the identification of quasi steady state species: A reduced mechanism for methane oxidation with NO chemistry. Combustion and Flame. 2008;154(4):761-74.

[89] Nikolaou ZM, Chen J-Y, Swaminathan N. A 5-step reduced mechanism for combustion of CO/H2/H2O/CH4/CO2 mixtures with low hydrogen/methane and high H2O content. Combustion and Flame. 2013;160(1):56-75.

APPENDICES

APPENDIX A:

Reduced mechanism for Curran's n-heptane fuel

Rate coefficients are expressed in the form:

$$K = A \times T^b \times \exp(-\frac{E}{RT})$$

For concentration units mol/cm3 and time in s. E is given in cal/mol.

Species:

NC7H16, CO, HO2, H2O, H2, N2, O2, CO2, AR, H2O2, H, O, OH, HCO, CH3, CH2O, C6H11OOH1-5, CH3O, C2H4, C2H5, CH2, C2H2, C2H3, CH3OH, CH2OH, CH2CO, HCCO, PC2H4OH, SC2H4OH, CH3CO, CH2CHO, CH3CHO, C3H4-A, C3H4-P, C3H6, C4H6, NC3H7, C4H7, C4H8-1, PC4H9, CH3COCH3, CH3COCH2, C2H5CHO, C2H5CO, C5H9, C5H10-1, C5H11-1, C2H5O, CH3O2, C2H5O2, C2H4O2H, O2C2H4OH, CH3CO3, C3H6OOH1-2, NC3H7O2, C4H8OOH1-3O2, C4H8OOH1-3, PC4H9O2, CH3COCH2O2, C3H5-A, C3H5-T, C3H3, C3H2, CH2(S), NC4KET13, TC3H6OH, IC3H5OH, NC3H7CHO, NC3H7CO, CH2CH2COCH3, C2H5COCH2, C2H5COCH3, CH3CHCOCH3, C2H3COCH3, CH3CHCO, C2H5COC2H4P, NC3H7COCH2, NC4H9CHO, NC4H9CO, HOCHO, C6H12-1, C7H15-1, C7H15-2, C7H15-3, C7H15-4, C7H15O2-1, C7H15O2-2, C7H15O2-3, C7H15O2-4, C7H14OOH1-3, C7H14OOH1-4, C7H14OOH2-4, C7H14OOH2-5, C7H14OOH3-1, C7H14OOH3-5, C7H14OOH3-6, C7H14OOH4-2, C7H14OOH1-3O2, C7H14OOH2-4O2, C7H14OOH2-5O2, C7H14OOH3-1O2, C7H14OOH3-5O2, C7H14OOH3-6O2, C7H14OOH4-2O2, C7H14O1-4, C7H14O2-4, C7H14O2-5, NC7KET13, NC7KET24, NC7KET25, NC7KET35, NC7KET36, NC7KET42, NC4H9COCH3, NC4H9COCH2, C5H9OOH1-4, C5H9OOH1-5, C6H11OOH1-4

Reaction number	Reaction	A	b	E
1	HCO+OH = CO+H2O	1.02E+14	0	0
2	CO+OH = CO2+H	1.40E+05	1.95	-1344.6
3	H+O2 = O+OH	1.97E+14	0	16511.36
4	O+H2 = H+OH	5.08E+04	2.67	6281.12
5	O+H2O = 2OH	2.97E+06	2.02	13376.8
6	OH+H2 = H+H2O	2.16E+08	1.51	3424.08
7	HCO+M = H+CO+M	1.86E+17	-1	16970.56
8	H2O2+OH = H2O+HO2	1.00E+12	0	0
9	C2H4+O = CH3+HCO	1.02E+07	1.88	178.68
10	H+C2H4(+M) = C2H5(+M)	1.08E+12	0.45	1818.8

11	CH3OH(+M) = CH3+OH(+M)	1.90E+16	0	91570.89
12	CH3OH+HO2 = CH2OH+H2O2	3.98E+13	0	19366.4
13	CH3+HO2 = CH3O+OH	1.10E+13	0	0
14	CO+HO2 = CO2+OH	3.01E+13	0	22960.15
15	H2O+M = H+OH+M	1.84E+27	-3	122387.4
16	H+O2(+M) = HO2(+M)	1.48E+12	0.6	0
17	CO+O(+M) = CO2(+M)	1.80E+10	0	2379.84
18	CO+O2 = CO2+O	1.62E+13	0	47617.28
19	CH2O+OH = HCO+H2O	3.43E+09	1.18	-446.2
20	CH2O+H = HCO+H2	9.33E+08	1.5	2970.88
21	CH2O+O = HCO+OH	4.16E+11	0.57	2757.2
22	CH3+OH = CH2O+H2	2.25E+13	0	4292.48
23	CH3+O = CH2O+H	8.00E+13	0	0
24	CH3+O2 = CH3O+O	2.00E+18	-1.57	29159.32
25	CH3O(+M) = CH2O+H(+M)	5.45E+13	0	13476.64
26	C2H4(+M) = C2H2+H2(+M)	1.80E+13	0	75868.19
27	HO2+O = OH+O2	3.25E+13	0	0
28	HCO+HO2 = CH2O+O2	2.97E+10	0.33	-3854.28
29	CH3O+O2 = CH2O+HO2	5.50E+10	0	2419.84
30	HCO+O2 = CO+HO2	7.58E+12	0	409.36
31	HO2+H = H2+O2	1.66E+13	0	818.56
32	HO2+OH = H2O+O2	2.89E+13	0	-499.2
33	H2O2+O2 = 2HO2	5.94E+17	-0.66	53057.82
34	2OH(+M) = H2O2(+M)	1.24E+14	-0.37	0
35	H2O2+H = H2O+OH	2.41E+13	0	3963.12
36	CH2O+HO2 = HCO+H2O2	5.82E-03	4.53	6545.64
37	OH+M = O+H+M	3.91E+22	-2	105117.4
38	O2+M = 2O+M	6.47E+20	-1.5	121289.3
39	C2H2+H(+M) = C2H3(+M)	3.11E+11	0.58	2584.52
40	C2H4+H = C2H3+H2	8.42E-03	4.62	2578.52
41	C2H4+OH = C2H3+H2O	2.05E+13	0	5939.68
42	C2H2+O2 = HCCO+OH	2.00E+08	1.5	30047.82
43	CH2+O2 = CO+H2O	7.28E+19	-2.54	1805.8
44	C2H2+O = CH2+CO	6.12E+06	2	1896.64
45	CH2+O2 = HCO+OH	1.29E+20	-3.3	283.52
46	CH2+O2 = CO2+2H	3.29E+21	-3.3	2863.04
47	CH3OH+OH = CH2OH+H2O	7.10E+06	1.8	-595.04
48	CH3OH+H = CH2OH+H2	1.44E+13	0	6084.44
49	CH3OH+O = CH2OH+OH	3.88E+05	2.5	3074.72

50	CH2OH+O2 = CH2O+HO2	6.51E+05	2.27	-768.72
51	CH2OH(+M) = CH2O+H(+M)	2.80E+14	-0.73	32763.05
52	C2H3+O2 = C2H2+HO2	2.12E-06	6	9467.52
53	H2O2+O = OH+HO2	9.55E+06	2	3963.12
54	C2H2+O = HCCO+H	1.43E+07	2	1896.64
55	C2H2+OH = CH2CO+H	2.19E-04	4.5	-998.24
56	CH2CO+O = CH2+CO2	1.75E+12	0	1347.6
57	CH2+O2 = CH2O+O	3.29E+21	-3.3	2863.04
58	CH2CO(+M) = CH2+CO(+M)	3.00E+14	0	70856.89
59	CH2CO+O = HCCO+OH	1.00E+13	0	7986.08
60	CH2CO+OH = HCCO+H2O	1.00E+13	0	1996.48
61	CH2CO+H = HCCO+H2	2.00E+14	0	7986.08
62	HCCO+OH = 2HCO	1.00E+13	0	0
63	HCCO+H = CH2(S)+CO	1.10E+14	0	0
64	HCCO+O = H+2CO	8.00E+13	0	0
65	CH2+O2 = CO2+H2	1.01E+21	-3.3	1505.44
66	CH3OH+OH = CH3O+H2O	1.00E+06	2.1	495.9
67	C2H3+O2 = CH2O+HCO	1.70E+29	-5.31	6488.77
68	PC2H4OH = C2H4+OH	1.29E+12	-0.37	26803.44
69	SC2H4OH+M = CH3CHO+H+M	1.00E+14	0	24956.64
70	CH3CO(+M) = CH3+CO(+M)	3.00E+12	0	16691.04
71	CH3CHO = CH3+HCO	2.61E+15	0.15	80410.29
72	CH3CHO+OH = CH3CO+H2O	2.00E+06	1.8	1297.76
73	CH3CHO+H = CH3CO+H2	1.34E+13	0	3294.24
74	CH3CHO+O = CH3CO+OH	5.94E+12	0	1864.8
75	CH3CHO+HO2 = CH3CO+H2O2	3.01E+12	0	11899.36
76	C3H5-A = C2H2+CH3	2.40E+48	-9.9	81937.66
77	C3H6 = C2H3+CH3	2.73E+62	-13.28	122986.3
78	C3H6 = C3H5-A+H	2.01E+61	-13.26	118294.5
79	C3H6+O = CH2CO+CH3+H	2.50E+07	1.76	75.84
80	C3H6+O = C2H5+HCO	1.58E+07	1.76	-1213.92
81	C3H6+O = CH3CHCO+2H	2.50E+07	1.76	75.84
82	C3H6+HO2 = C3H5-T+H2O2	3.00E+09	0	9912.72
83	C3H6+OH = C3H5-A+H2O	3.12E+06	2	-297.52
84	C4H6 = 2C2H3	4.03E+19	-1	97979.77
85	C4H6+OH = CH2O+C3H5-A	1.00E+12	0	0
86	C4H6+O = C2H4+CH2CO	1.00E+12	0	0
87	C4H6+O = CH2O+C3H4-A	1.00E+12	0	0
88	CH2O+M = CO+H2+M	1.83E+32	-4.42	86968.89

89	NC3H7 = CH3+C2H4	2.28E+14	-0.55	28350.72
90	NC3H7 = H+C3H6	2.67E+15	-0.64	36756.16
91	C3H6+OH = C3H5-T+H2O	1.11E+06	2	1448.44
92	C3H6+O = C3H5-A+OH	5.24E+11	0.7	5873.76
93	C3H6+O = C3H5-T+OH	6.03E+10	0.7	7618.72
94	C3H6+H = C3H5-A+H2	1.73E+05	2.5	2487.68
95	C5H9 = C3H5-A+C2H4	2.50E+13	0	44921.94
96	C5H9 = C4H6+CH3	1.34E+15	-0.52	38253.55
97	C4H7 = C4H6+H	1.20E+14	0	49214.5
98	C4H7 = C2H4+C2H3	1.00E+11	0	36935.84
99	C4H7+O2 = C4H6+HO2	1.00E+09	0	0
100	C4H8-1 = C3H5-A+CH3	5.00E+15	0	70876.86
101	C4H8-1 = C2H3+C2H5	1.00E+19	-1	96602.17
102	C4H8-1 = H+C4H7	4.11E+18	-1	97181.15
103	C4H8-1+H = C4H7+H2	5.00E+13	0	3893.28
104	C4H8-1+OH = C4H7+H2O	2.25E+13	0	2213.16
105	PC4H9 = C2H5+C2H4	7.50E+17	-1.41	29528.68
106	PC4H9 = C4H8-1+H	1.16E+17	-1.17	38093.81
107	CH3COCH3 = CH3CO+CH3	1.22E+23	-1.99	83804.4
108	CH3COCH3+OH = CH3COCH2+H2O	3.38E+07	1.74	828.56
109	CH3COCH2 = CH2CO+CH3	1.00E+14	0	30946.24
110	C2H5CO = C2H5+CO	1.83E+15	-0.73	12887.6
111	C2H5CHO+H = C2H5CO+H2	4.00E+13	0	4192.67
112	C2H5CHO+O = C2H5CO+OH	5.00E+12	0	1786.96
113	C2H5CHO+OH = C2H5CO+H2O	2.69E+10	0.76	-339.36
114	C2H5CHO = C2H5+HCO	9.85E+18	-0.73	81568.3
115	C5H10-1 = C2H5+C3H5-A	9.17E+20	-1.63	73861.67
116	C5H10-1+H = C5H9+H2	2.80E+13	0	3993.12
117	C5H10-1+O = C5H9+OH	2.54E+05	2.56	-1128.08
118	C5H10-1+OH = C5H9+H2O	5.12E+06	2	-297.52
119	H2O2+H = H2+HO2	4.82E+13	0	7936.24
120	CH3+OH = CH2+H2O	3.00E+06	2	2495.68
121	CH3OH(+M) = CH2OH+H(+M)	2.69E+16	-0.08	98768.4
122	C2H4+O = CH2CHO+H	3.39E+06	1.88	178.68
123	C3H6+O2 = C3H5-T+HO2	1.40E+12	0	60594.72
124	C5H11-1 = C2H4+NC3H7	7.97E+17	-1.44	29738.32
125	C5H11-1 = H+C5H10-1	3.48E+15	-0.66	37814.29
126	C2H5O+M = CH3+CH2O+M	1.35E+38	-6.96	23758.72
127	SC2H4OH+O2 = CH3CHO+HO2	3.81E+06	2	1638.12

128	H2O2+O2 = 2HO2	1.84E+14	-0.66	39471.42
129	C2H3+O2 = CH2CHO+O	3.50E+14	-0.61	5250.88
130	C2H5O2 = C2H5+O2	4.93E+50	-11.5	42176.72
131	CH3O2+M = CH3+O2+M	4.34E+27	-3.42	30417.18
132	C3H2+O2 = HCCO+CO+H	5.00E+13	0	0
133	C2H5+HO2 = C2H5O+OH	3.20E+13	0	0
134	CH3O2+CH3 = 2CH3O	7.00E+12	0	-998.24
135	CH3O2+C2H5 = CH3O+C2H5O	7.00E+12	0	-998.24
136	H2O2+OH = H2O+HO2	5.80E+14	0	9543.36
137	O2C2H4OH = PC2H4OH+O2	3.90E+16	-1	29948
138	O2C2H4OH = OH+2CH2O	1.25E+10	0	18867.2
139	C2H5O2 = C2H4O2H	5.64E+47	-11.44	37255.27
140	CH3CO3 = CH3CO+O2	4.62E+19	-1.9	39491.37
141	C2H5O+M = CH3CHO+H+M	1.16E+35	-5.89	25226.16
142	C2H4O2H = C2H4+HO2	9.29E+30	-6.1	19895.44
143	C3H6OOH1-2 = C3H6+HO2	5.50E+14	-0.85	15233.57
144	CH3+OH = CH2(S)+H2O	2.65E+13	0	2182.16
145	CH3OH+O2 = CH2OH+HO2	2.05E+13	0	44822.12
146	NC3H7O2 = C3H6OOH1-2	2.00E+11	0	26803.44
147	NC3H7O2 = NC3H7+O2	3.36E+19	-1.32	35697.97
148	C4H8-1+O = C3H6+CH2O	7.23E+05	2.34	-1048.24
149	C4H8-1+O = CH3CHO+C2H4	1.30E+13	0	848.56
150	C4H8-1+O = CH3CO+C2H5	1.30E+13	0	848.56
151	C4H8-1+O = C2H5CHO+CH2	1.30E+13	0	848.56
152	C4H8-1+O = C2H5CO+CH3	1.30E+13	0	848.56
153	C4H8OOH1-3O2 = C4H8OOH1-3+O2	5.60E+22	-2.23	37894.16
154	C4H8OOH1-3O2 = NC4KET13+OH	2.50E+10	0	21362.88
155	C4H8OOH1-3 = OH+CH2O+C3H6	6.64E+13	-0.16	29848.16
156	PC4H9O2 = C4H8OOH1-3	2.50E+10	0	20813.84
157	CH3COCH2O2 = CH3COCH2+O2	8.09E+15	-1.11	27402.38
158	C2H5O2 = C2H4+HO2	3.37E+55	-13.42	44592.53
159	C2H4O2H = C2H5+O2	2.15E+37	-8.21	27971.37
160	C3H4-A+HO2 = C3H3+H2O2	3.00E+13	0	13975.68
161	CH3CHO+OH = CH3+HOCHO	3.00E+15	-1.08	0
162	C3H5-T+O2 = C3H4-A+HO2	1.89E+30	-5.59	15513.07
163	C3H6+O2 = C3H5-A+HO2	4.00E+12	0	39830.8
164	C3H5-A+H = C3H4-A+H2	1.81E+13	0	0
165	C3H5-T+O2 = CH3COCH2+O	3.81E+17	-1.36	5570.34
166	C3H4-A+M = C3H3+H+M	1.14E+17	0	69878.6

167	C3H4-A = C3H4-P	1.20E+15	0	92239.75
168	C3H4-A+O2 = C3H3+HO2	4.00E+13	0	39092.08
169	C3H3+H = C3H2+H2	5.00E+13	0	0
170	C3H4-A+OH = C3H3+H2O	1.00E+07	2	998.24
171	C3H5-A = C3H4-A+H	6.66E+15	-0.43	63110.35
172	C3H5-T = C3H4-A+H	3.51E+14	-0.44	40819.09
173	C3H4-P+M = C3H3+H+M	1.14E+17	0	69878.6
174	C3H4-P+O2 = C3H3+HO2	2.00E+13	0	41527.84
175	C3H4-P+OH = C3H3+H2O	1.00E+07	2	998.24
176	C3H5-T = C3H4-P+H	1.08E+15	-0.6	38423.26
177	C3H3+OH = C3H2+H2O	1.00E+13	0	0
178	C3H3+O2 = CH2CO+HCO	3.01E+10	0	2865.04
179	PC4H9O2 = PC4H9+O2	6.16E+19	-1.38	35448.4
180	CH2CHO = CH2CO+H	3.09E+15	-0.26	50731.86
181	CH2CHO+O2 = CH2O+CO+OH	2.00E+13	0	4192.67
182	NC4KET13 = CH3CHO+CH2CHO+OH	1.05E+16	0	41527.84
183	C3H5-A+O2 = C3H4-A+HO2	2.18E+21	-2.85	30706.66
184	C3H5-A+O2 = C2H2+CH2O+OH	9.72E+29	-5.71	21412.79
185	HCCO+O2 = CO2+HCO	2.40E+11	0	-852.56
186	CH2CO+OH = CH2OH+CO	3.73E+12	0	-1011.24
187	C3H5-T+O2 = CH2O+CH3CO	3.71E+25	-3.96	7030.84
188	TC3H6OH = CH3COCH3+H	5.00E+13	0	21822.08
189	TC3H6OH = IC3H5OH+H	6.20E+15	-0.66	40270.05
190	IC3H5OH = C3H5-T+OH	7.37E+19	-0.94	108910.8
191	C3H6+H = C3H5-T+H2	4.05E+05	2.5	9777.04
192	NC3H7CHO+OH = NC3H7CO+H2O	2.69E+10	0.76	-339.36
193	NC3H7CHO+H = NC3H7CO+H2	4.00E+13	0	4192.67
194	NC3H7CHO+O = NC3H7CO+OH	5.00E+12	0	1786.96
195	NC3H7CO = NC3H7+CO	5.32E+15	-0.86	13376.8
196	C2H5COCH3+OH = CH2CH2COCH3+H2O	7.55E+09	0.97	1583.28
197	C2H5COCH3+OH = CH3CHCOCH3+H2O	8.45E+11	0	-227.68
198	C2H5COCH3+OH = C2H5COCH2+H2O	5.10E+11	0	1189.92
199	C2H5COCH3+HO2 = CH3CHCOCH3+H2O2	2.00E+11	0	8682.96
200	C2H5COCH3+O = CH2CH2COCH3+OH	2.25E+13	0	7686.68
201	C2H5COCH3+O = CH3CHCOCH3+OH	3.07E+13	0	3394.08

202	C2H5COCH3+O = C2H5COCH2+OH	5.00E+12	0	5951.6
203	C2H5COCH3+O2 = CH3CHCOCH3+HO2	1.55E+13	0	41897.2
204	CH3CHCO+OH = C2H5+CO2	1.73E+12	0	-1008.24
205	CH3CHCO+OH = SC2H4OH+CO	2.00E+12	0	-1008.24
206	CH3CHCO+O = CH3CHO+CO	3.20E+12	0	-436.2
207	CH2CH2COCH3 = C2H4+CH3CO	5.97E+12	0	20694
208	C2H5COCH2 = CH2CO+C2H5	1.57E+13	0	29948
209	CH3CHCOCH3 = C2H3COCH3+H	3.42E+16	-0.82	41697.54
210	CH3CHCOCH3 = CH3CHCO+CH3	1.41E+15	-0.44	38273.5
211	C2H5COC2H4P = C2H5CO+C2H4	1.55E+17	-1.46	27791.68
212	NC3H7COCH2 = NC3H7+CH2CO	1.23E+18	-1.4	43374.64
213	NC4H9CHO+O2 = NC4H9CO+HO2	2.00E+13	0.5	42126.81
214	NC4H9CHO+OH = NC4H9CO+H2O	2.69E+10	0.76	-339.36
215	NC4H9CHO+H = NC4H9CO+H2	4.00E+13	0	4192.67
216	NC4H9CHO+O = NC4H9CO+OH	5.00E+12	0	1786.96
217	NC4H9CO = PC4H9+CO	1.00E+11	0	9583.36
218	HOCHO+M = CO2+H2+M	1.50E+16	0	56901.14
219	HOCHO = HCO+OH	4.59E+18	-0.46	108112.2
220	HOCHO+OH = H2O+CO2+H	2.62E+06	2.06	914.4
221	HOCHO+OH = H2O+CO+OH	1.85E+07	1.51	-960.4
222	HOCHO+H = H2+CO2+H	4.24E+06	2.1	4859.52
223	HOCHO+H = H2+CO+OH	6.03E+13	-0.35	2982.88
224	HOCHO+HO2 = H2O2+CO+OH	1.00E+12	0	11899.36
225	HOCHO+O = CO+2OH	1.77E+18	-1.9	2969.88
226	CH2(S)+M = CH2+M	1.00E+13	0	0
227	CH2(S)+O2 = CO+OH+H	7.00E+13	0	0
228	CH2(S)+CO2 = CH2O+CO	3.00E+12	0	0
229	C6H12-1+OH = C5H11-1+CH2O	1.00E+11	0	-3993.12
230	C6H12-1 = NC3H7+C3H5-A	1.00E+16	0	70876.86
231	NC7H16 = C5H11-1+C2H5	8.10E+77	-17.62	120191.2
232	NC7H16 = PC4H9+NC3H7	1.42E+78	-17.71	120490.7
233	NC7H16+H = C7H15-1+H2	1.88E+05	2.75	6269.12
234	NC7H16+H = C7H15-2+H2	2.60E+06	2.4	4463.31
235	NC7H16+H = C7H15-3+H2	2.60E+06	2.4	4463.31
236	NC7H16+H = C7H15-4+H2	1.30E+06	2.4	4463.31
237	NC7H16+O = C7H15-1+OH	1.93E+05	2.68	3709.6
238	NC7H16+O = C7H15-2+OH	9.54E+04	2.71	2102.32
239	NC7H16+O = C7H15-3+OH	9.54E+04	2.71	2102.32
240	NC7H16+O = C7H15-4+OH	4.77E+04	2.71	2102.32

241	NC7H16+OH = C7H15-1+H2O	1.05E+10	0.97	1587.28
242	NC7H16+OH = C7H15-2+H2O	9.40E+07	1.61	-35
243	NC7H16+OH = C7H15-3+H2O	9.40E+07	1.61	-35
244	NC7H16+OH = C7H15-4+H2O	4.70E+07	1.61	-35
245	NC7H16+HO2 = C7H15-1+H2O2	1.68E+13	0	20404.53
246	NC7H16+HO2 = C7H15-2+H2O2	1.12E+13	0	17659.28
247	NC7H16+HO2 = C7H15-3+H2O2	1.12E+13	0	17659.28
248	NC7H16+HO2 = C7H15-4+H2O2	5.60E+12	0	17659.28
249	NC7H16+O2 = C7H15-1+HO2	6.00E+13	0	52708.42
250	NC7H16+O2 = C7H15-2+HO2	4.00E+13	0	50063.02
251	NC7H16+O2 = C7H15-3+HO2	4.00E+13	0	50063.02
252	NC7H16+O2 = C7H15-4+HO2	2.00E+13	0	50063.02
253	NC7H16+CH3O = C7H15-1+CH3OH	3.16E+11	0	6987.84
254	NC7H16+CH3O = C7H15-2+CH3OH	2.19E+11	0	4991.36
255	NC7H16+CH3O = C7H15-3+CH3OH	2.19E+11	0	4991.36
256	NC7H16+CH3O = C7H15-4+CH3OH	1.10E+11	0	4991.36
257	NC7H16+C2H3 = C7H15-1+C2H4	1.00E+12	0	17968.8
258	NC7H16+C2H3 = C7H15-2+C2H4	8.00E+11	0	16770.88
259	NC7H16+C2H3 = C7H15-3+C2H4	8.00E+11	0	16770.88
260	NC7H16+C2H3 = C7H15-4+C2H4	4.00E+11	0	16770.88
261	NC7H16+C7H15-1 = C7H15-2+NC7H16	1.00E+11	0	10381.92
262	NC7H16+C7H15-1 = C7H15-3+NC7H16	1.00E+11	0	10381.92
263	NC7H16+C7H15-1 = C7H15-4+NC7H16	5.00E+10	0	10381.92
264	NC7H16+C7H15-2 = C7H15-3+NC7H16	1.00E+11	0	10381.92
265	NC7H16+C7H15-2 = C7H15-4+NC7H16	5.00E+10	0	10381.92
266	NC7H16+C7H15-3 = C7H15-4+NC7H16	5.00E+10	0	10381.92
267	C7H15-1 = C5H11-1+C2H4	8.16E+17	-1.42	30786.53
268	C7H15-2 = PC4H9+C3H6	2.22E+16	-0.89	30077.73
269	C7H15-3 = C4H8-1+NC3H7	9.63E+17	-1.42	30526.96
270	C7H15-3 = C6H12-1+CH3	1.03E+14	-0.42	28640.24
271	C7H15-4 = C2H5+C5H10-1	5.43E+16	-0.89	30536.93
272	C7H15-1 = C7H15-3	1.39E+09	0.98	33701.44
273	C7H15-1 = C7H15-4	2.54E+09	0.35	19725.76
274	C7H15-2 = C7H15-3	9.59E+08	1.39	39631.15
275	C7H15-1 = C7H15-2	5.48E+08	1.62	38692.8
276	C7H15O2-1 = C7H15-1+O2	2.66E+20	-1.67	35338.58

277	C7H15O2-2 = C7H15-2+O2	1.36E+23	-2.36	37604.68
278	C7H15O2-3 = C7H15-3+O2	9.88E+21	-1.97	37794.34
279	C7H15O2-4 = C7H15-4+O2	1.36E+23	-2.36	37604.68
280	C7H15O2-1 = C7H14OOH1-3	2.50E+10	0	20813.84
281	C7H15O2-1 = C7H14OOH1-4	3.12E+09	0	19016.96
282	C7H15O2-2 = C7H14OOH2-4	2.50E+10	0	20813.84
283	C7H15O2-2 = C7H14OOH2-5	3.12E+09	0	19016.96
284	C7H15O2-3 = C7H14OOH3-1	3.75E+10	0	24357.68
285	C7H15O2-3 = C7H14OOH3-5	2.50E+10	0	20813.84
286	C7H15O2-3 = C7H14OOH3-6	3.12E+09	0	19016.96
287	C7H15O2-4 = C7H14OOH4-2	5.00E+10	0	20813.84
288	C7H14OOH1-4 = C7H14O1-4+OH	9.38E+09	0	6987.84
289	C7H14OOH2-4 = C7H14O2-4+OH	7.50E+10	0	15223.6
290	C7H14OOH2-5 = C7H14O2-5+OH	9.38E+09	0	6987.84
291	C7H14OOH3-6 = C7H14O2-5+OH	9.38E+09	0	6987.84
292	C7H14OOH4-2 = C7H14O2-4+OH	7.50E+10	0	15223.6
293	C7H14OOH1-3 = OH+CH2O+C6H12-1	8.12E+13	-0.14	31036.08
294	C7H14OOH2-4 = OH+CH3CHO+C5H10-1	5.36E+17	-1.4	26703.6
295	C7H14OOH3-1 = OH+NC4H9CHO+C2H4	2.21E+19	-1.67	26933.21
296	C7H14OOH3-5 = OH+C2H5CHO+C4H8-1	2.47E+18	-1.55	26973.12
297	C7H14OOH4-2 = OH+NC3H7CHO+C3H6	1.30E+18	-1.49	26753.52
298	C7H14OOH1-3O2 = C7H14OOH1-3+O2	1.37E+23	-2.37	37574.72
299	C7H14OOH2-4O2 = C7H14OOH2-4+O2	1.39E+23	-2.38	37534.78
300	C7H14OOH2-5O2 = C7H14OOH2-5+O2	1.39E+23	-2.38	37534.78
301	C7H14OOH3-1O2 = C7H14OOH3-1+O2	3.32E+20	-1.65	35218.82
302	C7H14OOH3-5O2 = C7H14OOH3-5+O2	1.39E+23	-2.38	37534.78
303	C7H14OOH3-6O2 = C7H14OOH3-6+O2	1.39E+23	-2.38	37534.78
304	C7H14OOH4-2O2 = C7H14OOH4-2+O2	6.97E+22	-2.38	37534.78
305	C7H14OOH1-3O2 = NC7KET13+OH	2.50E+10	0	21362.88
306	C7H14OOH2-4O2 = NC7KET24+OH	1.25E+10	0	17819.04
307	C7H14OOH2-5O2 = NC7KET25+OH	1.56E+09	0	16022.16
308	C7H14OOH3-5O2 = NC7KET35+OH	1.25E+10	0	17819.04

309	C7H14OOH3-6O2 = NC7KET36+OH	1.56E+09	0	16022.16
310	C7H14OOH4-2O2 = NC7KET42+OH	1.25E+10	0	17819.04
311	NC7KET13 = NC4H9CHO+CH2CHO+OH	1.05E+16	0	41527.84
312	NC7KET24 = NC3H7CHO+CH3COCH2+OH	1.05E+16	0	41527.84
313	NC7KET25 = C2H5CHO+CH2CH2COCH3+OH	1.05E+16	0	41527.84
314	NC7KET35 = C2H5CHO+C2H5COCH2+OH	1.05E+16	0	41527.84
315	NC7KET36 = CH3CHO+C2H5COC2H4P+OH	1.05E+16	0	41527.84
316	NC7KET42 = CH3CHO+NC3H7COCH2+OH	1.05E+16	0	41527.84
317	C7H14O1-4+OH = C5H10-1+CH2CHO+H2O	2.50E+12	0	0
318	C7H14O2-4+OH = CH3CO+C5H10-1+H2O	2.50E+12	0	0
319	C7H14O2-5+OH = CH3COCH2+C4H8-1+H2O	2.50E+12	0	0
320	C7H14O1-4+OH = C2H4+NC3H7COCH2+H2O	2.50E+12	0	0
321	C7H14O2-4+OH = C3H6+NC3H7CO+H2O	2.50E+12	0	0
322	C7H14O2-5+OH = C3H6+C2H5COCH2+H2O	2.50E+12	0	0
323	NC4H9COCH3+OH = NC4H9COCH2+H2O	5.10E+11	0	1189.92
324	NC4H9COCH3+HO2 = NC4H9COCH2+H2O2	2.38E+04	2.55	14664.56
325	NC4H9COCH2 = PC4H9+CH2CO	1.55E+18	-1.41	43065.17
326	C7H14OOH1-4 = C5H10-1+C2H4+HO2	2.44E+16	-1.08	29398.96
327	C7H14OOH1-4 = C5H9OOH1-5+C2H5	1.66E+18	-1.75	27512.16
328	C7H14OOH2-4 = C5H9OOH1-4+C2H5	1.67E+18	-1.75	27622
329	C7H14OOH2-5 = C6H11OOH1-5+CH3	5.28E+12	0.17	30227.52
330	C7H14OOH3-5 = C6H11OOH1-4+CH3	5.28E+12	0.17	30227.52

APPENDIX B:

Reduced mechanism of GRI mechanism for Natural gas fuel

Rate coefficients are expressed in the form:

$$K = A \times T^{b} \times \exp(-\frac{E}{RT})$$

For concentration units mol/cm3 and time in s. E is given in cal/mol.

Species:

CH4, CO, HO2, H2O, H2, N2, O2, CO2, C2H6, AR, CH3, H2O2, HCO, CH2O, CH3O, CH3OH, H, OH, O

Reaction number	Reaction	A	b	E
1.	O+CH3=H+CH2O	5.06E+13	0.00	0.00
2.	O+CH4=OH+CH3	1.02E+09	1.50	8599.06
3.	O2+CH2O=HO2+HCO	1.00E+14	0.00	39995.67
4.	H+2O2=HO2+O2	2.08E+19	-1.24	0.00
5.	H+O2+H2O=HO2+H2O	1.13E+19	-0.76	0.00
6.	H+O2+N2=HO2+N2	2.60E+19	-1.24	0.00
7.	H+O2=O+OH	2.65E+16	-0.67	17039.16
8.	H+CH4=CH3+H2	6.60E+08	1.62	10838.83
9.	H+CH2O(+M)=CH3O(+M)	5.40E+11	0.45	2599.71
10.	H+CH2O=HCO+H2	5.74E+07	1.90	2741.70
11.	OH+H2=H+H2O	2.16E+08	1.51	3429.62
12.	2OH(+M)=H2O2(+M)	7.40E+13	-0.37	0.00
13.	2OH=O+H2O	3.57E+04	2.40	-2109.78
14.	OH+HO2=O2+H2O	1.45E+13	0.00	-499.95
15.	OH+H2O2=HO2+H2O	2.00E+12	0.00	426.95
16.	OH+H2O2=HO2+H2O	1.70E+18	0.00	29406.81
17.	OH+CH4=CH3+H2O	1.00E+08	1.60	3119.67
18.	OH+CO=H+CO2	4.76E+07	1.23	70.00
19.	OH+CH2O=HCO+H2O	3.43E+09	1.18	-446.96
20.	OH+CH3OH=CH3O+H2O	6.30E+06	2.00	1499.85
21.	2HO2=O2+H2O2	1.30E+11	0.00	-1629.82
22.	2HO2=O2+H2O2	4.20E+14	0.00	11998.70
23.	HO2+CH3=O2+CH4	1.00E+12	0.00	0.00

24.	HO2+CH3=OH+CH3O	3.78E+13	0.00	0.00
25.	HO2+CO=OH+CO2	1.50E+14	0.00	23597.43
26.	HO2+CH2O=HCO+H2O2	5.60E+06	2.00	11998.70
27.	CH3+O2=O+CH3O	3.56E+13	0.00	30476.69
28.	CH3+O2=OH+CH2O	2.31E+12	0.00	20312.80
29.	CH3+H2O2=HO2+CH4	2.45E+04	2.47	5179.43
30.	2CH3(+M)=C2H6(+M)	6.77E+16	-1.18	653.92
31.	CH3+CH2O=HCO+CH4	3.32E+03	2.81	5859.36
32.	CH3+CH3OH=CH3O+CH4	1.00E+07	1.50	9938.91
33.	HCO+H2O=H+CO+H2O	1.50E+18	-1.00	16998.15
34.	HCO+M=H+CO+M	1.87E+17	-1.00	16998.15
35.	HCO+O2=HO2+CO	1.34E+13	0.00	399.96
36.	CH3O+O2=HO2+CH2O	4.28E-13	7.60	-3529.61
37.	O+CH3=>H+H2+CO	3.37E+13	0.00	0.00
38.	OH+HO2=O2+H2O	5.00E+15	0.00	17328.11
39.	OH+CH3=>H2+CH2O	8.00E+09	0.50	-1754.82

APPENDIX C:

Reduced mechanism of Golovitchev mechanism for n-heptane fuel

Rate coefficients are expressed in the form:

$$K = A \times T^{b} \times \exp(-\frac{E}{RT})$$

For concentration units mol/cm3 and time in s. E is given in cal/mol.

Species:

CH4, CO, HO2, H2O, H2, N2, O2, CO2, C2H6 , AR , CH2, CH2(S), CH3, H2O2, C, HCO, CH2O, CH, CH2OH, CH3O, CH3OH, C2H, C2H2, C2H3, C2H4, C2H5, HCCO , CH2CO, HCCOH, H, N, NH, NH2, NH3, NNH , NO, NO2, N2O, HNO, CN, HCN, H2CN, HCNN, HCNO, HOCN, HNCO, NCO , OH, C3H7 , C3H8, CH2CHO, CH3CHO, O

Reaction number	Reaction	A	b	E
1	C7H16+O2 = C7H15-2+HO2	2.80E+14	0	47174.88
2	C7H16+H = C7H15-1+H2	5.60E+07	2	7666.16
3	C7H16+H = C7H15-2+H2	4.38E+07	2	4749.49
4	C7H16+OH = C7H15-1+H2O	8.60E+09	1.1	1814.81
5	C7H16+OH = C7H15-2+H2O	4.80E+09	1.3	690.42
6	C7H16+HO2 = C7H15-1+H2O2	8.00E+12	0	19297.9
7	C7H16+HO2 = C7H15-2+H2O2	1.00E+13	0	16948.16
8	C7H16+CH3 = C7H15-1+CH4	1.30E+12	0	11598.73
9	C7H16+CH3 = C7H15-2+CH4	8.00E+11	0	9498.97
10	C7H16 = C4H9+C3H7	2.00E+16	0	80701.25
11	C7H15-1+O2 = C7H15O2	2.00E+12	0	0
12	C7H15-2+O2 = C7H15O2	2.00E+12	0	0
13	C7H15O2 = C7H14O2H	6.00E+11	0	20377.8
14	C7H14O2H+O2 = C7H14O2HO2	2.34E+11	0	0
15	C7H14O2HO2 = C7KET21+OH	2.96E+13	0	26697.11
16	C7KET21 = C5H11CO+CH2O+OH	1.00E+16	0	42395.41
17	C5H11CO = C5H11+CO	1.00E+11	0	9598.96
18	C5H11 = C2H5+C3H6	3.20E+13	0	28296.93
19	C7H15-1 = C2H4+C5H11	2.50E+13	0	28806.87
20	C7H15-2 = CH3+C6H12	3.00E+13	0	29796.77
21	C6H12 = C3H7+C3H5	1.00E+16	0	67992.62

22	C7H15-2 = C4H9+C3H6	1.20E+13	0	29596.78
23	C7H15-1 = C7H15-2	2.00E+11	0	18098.03
24	C4H9 = C3H6+CH3	2.23E+17	-1.4	30826.66
25	C4H9 = C2H5+C2H4	2.50E+13	0	28806.87
26	C3H7 = C2H4+CH3	9.60E+13	0	30946.65
27	C3H7 = C3H6+H	1.25E+14	0	36896.01
28	C3H6 = C2H3+CH3	6.15E+15	0	85490.73
29	C3H6+H = C3H5+H2	5.00E+12	0	1499.85
30	C3H6+CH3 = C3H5+CH4	9.00E+12	0	8479.09
31	C3H6+OH = CH3CHO+CH3	3.50E+11	0	0
32	C3H5 = C3H4+H	4.00E+13	0	69752.42
33	C3H5+O2 = C3H4+HO2	6.00E+11	0	9998.92
34	C3H4+OH = C2H3+CH2O	1.00E+12	0	0
35	C3H4+OH = C2H4+HCO	1.00E+12	0	0
36	C2H4+HO2 = CH3CHO+OH	2.20E+13	0	17198.14
37	C2H4+CH3O2 = CH3CHO+CH3O	7.00E+13	0	14498.42
38	CH3CHO = CH3+HCO	7.08E+15	0	81751.12
39	CH3CO+M = CH3+CO+M	1.80E+16	0	14398.44
40	CH3CHO+OH = CH3CO+H2O	1.00E+13	0	0
41	CH3O+CO = CH3+CO2	1.57E+14	0	11798.73
42	CH3O+O2 = CH2O+HO2	1.20E+11	0	2599.71
43	CH3O(+M) = CH2O+H(+M)	2.00E+13	0	27417.02
44	CH3+HO2 = CH3O+OH	4.30E+13	0	0
45	CH3+O2 = CH3O+O	3.67E+13	0	29996.75
46	CH3+O2 = CH2O+OH	4.80E+10	0	8999.02
47	CH3+O2 = CH3O2	3.02E+59	-15	17202.13
48	CH3O2+O = CH3O+O2	3.61E+13	0	0
49	CO+OH = CO2+H	3.51E+07	1.3	-757.92
50	CO+O2 = CO2+O	1.60E+13	0	40995.55
51	HO2+CO = CO2+OH	5.80E+13	0	22927.52
52	H2+OH = H2O+H	1.17E+09	1.3	3625.6
53	O+OH = O2+H	4.00E+14	-0.5	0
54	O+OH+M = HO2+M	1.00E+16	0	0
55	H+O2+H2O = HO2+H2O	1.13E+19	-0.76	0
56	H+O2+N2 = HO2+N2	2.60E+19	-1.24	0
57	OH+HO2 = H2O+O2	7.50E+12	0	0
58	H+HO2 = 2OH	1.70E+14	0	874.9
59	2OH = O+H2O	6.00E+08	1.3	0
60	H+HO2 = H2+O2	1.25E+13	0	0

61	2HO2 = H2O2+O2	2.00E+12	0	0
62	2OH(+M) = H2O2(+M)	7.60E+13	-0.37	0
63	H2O2+OH = H2O+HO2	1.00E+13	0	1799.8
64	CH2O+O2 = HCO+HO2	6.20E+13	0	38995.77
65	CH2O+O = HCO+OH	4.10E+11	0.57	2759.7
66	CH2O+H = HCO+H2	2.19E+08	1.8	2999.67
67	CH2O+OH = HCO+H2O	2.43E+10	1.18	-446.96
68	CH2O+HO2 = HCO+H2O2	3.00E+12	0	7999.13
69	HCO+O2 = HO2+CO	3.30E+13	-0.4	0
70	HCO+M = H+CO+M	1.87E+17	-1	16998.15
71	HCO+HO2 = CO2+OH+H	3.00E+13	0	0
72	CH4+OH = CH3+H2O	1.60E+06	2.1	2459.73
73	CH4+HO2 = CH3+H2O2	1.00E+13	0	18697.97
74	CH3+H = CH4	1.90E+36	-7	9049.02
75	2CH3(+M) = C2H6(+M)	2.12E+16	-0.97	619.92
76	C2H4+H = C2H3+H2	1.10E+14	0	8499.07
77	C2H4+O = C2H3+OH	1.51E+07	1.91	3789.59
78	C2H4+OH = CH2O+CH3	6.00E+13	0	959.9
79	C2H4+OH = C2H3+H2O	6.02E+13	0	5954.36
80	C2H6+O2 = C2H5+HO2	1.00E+13	0	48954.69
81	C2H5+O2 = C2H4+HO2	2.00E+10	0	-2199.77
82	C2H3+O2 = CH2O+HCO	4.00E+12	0	-249.96
83	O+CH3CHO => OH+CH3+CO	2.92E+12	0	1807.81
84	O2+CH3CHO => HO2+CH3+CO	3.01E+13	0	39145.75
85	H+CH3CHO => CH3+H2+CO	2.05E+09	1.16	2404.75
86	OH+CH3CHO => CH3+H2O+CO	2.34E+10	0.73	-1112.88
87	HO2+CH3CHO => CH3+H2O2+CO	3.01E+12	0	11921.7
88	CH3+CH3CHO => CH3+CH4+CO	2.72E+06	1.77	5919.35
89	C3H8(+M) = C2H5+CH3(+M)	9.90E+22	-1.6	84419.84
90	O+C3H8 = OH+C3H7	1.93E+05	2.68	3715.59
91	OH+C3H8 = C3H7+H2O	3.16E+07	1.8	933.89
92	C3H7+H2O2 = HO2+C3H8	3.78E+02	2.72	1499.85
93	HO2+C3H7 => OH+C2H5+CH2O	2.41E+13	0	0
94	C3H6+C2H5 = C3H5+C2H6	2.23E+00	3.5	6639.28
95	C3H6+O = CH3+CH3CO	6.80E+04	2.56	-1129.87

APPENDIX D:

Reduced mechanism for Natural gas and n-heptane blended fuel

Rate coefficients are expressed in the form:

$$K = A \times T^{b} \times \exp(-\frac{E}{RT})$$

For concentration units mol/cm3 and time in s. E is given in cal/mol.

Species:

CH4,CO, HO2, H2O, H2, N2, O2, CO2, C2H6, AR, C7H16, H2O2, OH, CH3, CH3O, CH2O, CH3O2, HCO, C7H15-1, C7H15-2, C7H15O2, C7H14O2H, C7H14O2HO2, C7KET21, C6H12, C5H11CO, C5H11, C4H9, C3H7, C3H6, C3H5, C3H4, C2H3, C2H4, C2H5, O, C3H8, CH3CHO, CH3CO, H, CH3OH

Reaction number	Reaction	A	b	E
1	O+CH3 = H+CH2O	5.49E+13	0	0
2	O+CH4 = OH+CH3	1.14E+09	1.74	7606.07
3	O2+CH2O = HO2+HCO	8.25E+13	0	38984.97
4	H+2O2 = HO2+O2	2.04E+19	-1.52	0
5	H+O2+H2O = HO2+H2O	1.24E+19	-0.79	0
6	H+O2+N2 = HO2+N2	2.90E+19	-1.43	0
7	H+O2 = O+OH	3.08E+16	-0.65	14340.87
8	H+CH4 = CH3+H2	8.09E+08	1.3	13164.33
9	H+CH2O(+M) = CH3O(+M)	5.53E+11	0.41	2607.11
10	H+CH2O = HCO+H2	4.81E+07	2.1	2878.12
11	OH+H2 = H+H2O	2.59E+08	1.22	3272.11
12	2OH(+M) = H2O2(+M)	9.55E+13	-0.46	0
13	2OH = O+H2O	4.06E+04	3.05	-2195.79
14	OH+HO2 = O2+H2O	1.50E+13	0	-552.1
15	OH+H2O2 = HO2+H2O	1.97E+12	0	399.73
16	OH+H2O2 = HO2+H2O	2.00E+18	0	30458.92
17	OH+CH4 = CH3+H2O	1.00E+08	2.02	2688.28
18	OH+CO = H+CO2	5.52E+07	1.14	78.85
19	OH+CH2O = HCO+H2O	4.30E+09	1.35	-556.74
20	OH+CH3OH = CH3O+H2O	5.87E+06	2.45	1672.05
21	2HO2 = O2+H2O2	1.19E+11	0	-1710.63
22	2HO2 = O2+H2O2	3.97E+14	0	13605.87

23	HO2+CH3 = O2+CH4	1.06E+12	0	0
24	HO2+CH3 = OH+CH3O	4.82E+13	0	0
25	HO2+CO = OH+CO2	1.92E+14	0	25650.48
26	HO2+CH2O = HCO+H2O2	4.75E+06	2.45	12850.24
27	CH3+O2 = O+CH3O	4.48E+13	0	33758.55
28	CH3+O2 = OH+CH2O	2.37E+12	0	23949.83
29	CH3+H2O2 = HO2+CH4	2.30E+04	2.79	6136.86
30	2CH3(+M) = C2H6(+M)	5.79E+16	-1.52	691.5
31	CH3+CH2O = HCO+CH4	4.05E+03	2.71	4733.53
32	CH3+CH3OH = CH3O+CH4	1.21E+07	1.53	11144.43
33	HCO+H2O = H+CO+H2O	1.43E+18	-1.24	18077.12
34	HCO+M = H+CO+M	2.25E+17	-1.27	13747.65
35	HCO+O2 = HO2+CO	1.44E+13	0	326.79
36	CH3O+O2 = HO2+CH2O	3.97E-13	7.74	-3292.88
37	O+CH3 => H+H2+CO	3.38E+13	0	0
38	OH+HO2 = O2+H2O	4.99E+15	0	15922.03
39	OH+CH3 => H2+CH2O	6.84E+09	0.46	-2043.38
40	C7H16+O2 = C7H15-2+HO2	2.29E+14	0	58158.34
41	C7H16+H = C7H15-1+H2	5.28E+07	2.05	8647.95
42	C7H16+H = C7H15-2+H2	4.60E+07	2.41	3889.83
43	C7H16+OH = C7H15-1+H2O	6.97E+09	1.24	2149.51
44	C7H16+OH = C7H15-2+H2O	4.71E+09	1.62	589.25
45	C7H16+HO2 = C7H15-1+H2O2	8.01E+12	0	24195.18
46	C7H16+HO2 = C7H15-2+H2O2	8.11E+12	0	19261.98
47	C7H16+CH3 = C7H15-1+CH4	1.04E+12	0	13057.51
48	C7H16+CH3 = C7H15-2+CH4	7.45E+11	0	11884.42
49	C7H16 = C4H9+C3H7	2.14E+16	0	101180.6
50	C7H15-1+O2 = C7H15O2	2.19E+12	0	0
51	C7H15-2+O2 = C7H15O2	2.13E+12	0	0
52	C7H15O2 = C7H14O2H	6.17E+11	0	26447.1
53	C7H14O2H+O2 = C7H14O2HO2	2.92E+11	0	0
54	C7H14O2HO2 = C7KET21+OH	3.78E+13	0	30984.48
55	C7KET21 = C5H11CO+CH2O+OH	8.56E+15	0	47263.6
56	C5H11CO = C5H11+CO	9.11E+10	0	8213.03
57	C5H11 = C2H5+C3H6	2.61E+13	0	27115.93
58	C7H15-1 = C2H4+C5H11	2.39E+13	0	36480.39
59	C7H15-2 = CH3+C6H12	2.96E+13	0	28495.4
60	C6H12 = C3H7+C3H5	9.16E+15	0	88224.75
61	C7H15-2 = C4H9+C3H6	1.25E+13	0	33050.39

62	C7H15-1 = C7H15-2	2.16E+11	0	15616.39
63	C4H9 = C3H6+CH3	1.92E+17	-1.23	38301.66
64	C4H9 = C2H5+C2H4	2.88E+13	0	28007.31
65	C3H7 = C2H4+CH3	1.14E+14	0	38773.51
66	C3H7 = C3H6+H	1.42E+14	0	35158.92
67	C3H6 = C2H3+CH3	6.86E+15	0	98761.19
68	C3H6+H = C3H5+H2	4.21E+12	0	1596.28
69	C3H6+CH3 = C3H5+CH4	9.92E+12	0	10545.1
70	C3H6+OH = CH3CHO+CH3	3.05E+11	0	0
71	C3H5 = C3H4+H	4.03E+13	0	76895.57
72	C3H5+O2 = C3H4+HO2	5.82E+11	0	11160.07
73	C3H4+OH = C2H3+CH2O	1.21E+12	0	0
74	C3H4+OH = C2H4+HCO	1.08E+12	0	0
75	C2H4+HO2 = CH3CHO+OH	2.10E+13	0	13824.34
76	C2H4+CH3O2 = CH3CHO+CH3O	7.74E+13	0	12981.25
77	CH3CHO = CH3+HCO	6.98E+15	0	94315.52
78	CH3CO+M = CH3+CO+M	1.99E+16	0	17756.47
79	CH3CHO+OH = CH3CO+H2O	8.07E+12	0	0
80	CH3O+CO = CH3+CO2	1.61E+14	0	9959.27
81	CH3+O2 = CH3O2	2.77E+59	-15.65	19874.31
82	CH3O2+O = CH3O+O2	4.50E+13	0	0
83	CO+O2 = CO2+O	2.02E+13	0	41229.5
84	O+OH+M = HO2+M	1.22E+16	0	0
85	H+HO2 = 2OH	2.20E+14	0	923.56
86	H+HO2 = H2+O2	1.07E+13	0	0
87	CH2O+O = HCO+OH	4.43E+11	0.72	2755.81
88	HCO+HO2 = CO2+OH+H	3.49E+13	0	0
89	CH3+H = CH4	2.17E+36	-7.61	8935.91
90	C2H4+H = C2H3+H2	1.19E+14	0	7820.93
91	C2H4+O = C2H3+OH	1.53E+07	1.94	3189.94
92	C2H4+OH = CH2O+CH3	6.94E+13	0	1103.54
93	C2H4+OH = C2H3+H2O	5.93E+13	0	5212.42
94	C2H6+O2 = C2H5+HO2	1.01E+13	0	44603.73
95	C2H5+O2 = C2H4+HO2	2.16E+10	0	-1966.44
96	C2H3+O2 = CH2O+HCO	3.54E+12	0	-264.42
97	O+CH3CHO => OH+CH3+CO	3.05E+12	0	1999.62
98	O2+CH3CHO => HO2+CH3+CO	2.71E+13	0	39278.15
99	H+CH3CHO => CH3+H2+CO	1.69E+09	1.51	2283.04
100	OH+CH3CHO => CH3+H2O+CO	1.95E+10	0.91	-1375.01

101	HO2+CH3CHO => CH3+H2O2+CO	2.46E+12	0	11940.25
102	CH3+CH3CHO => CH3+CH4+CO	2.36E+06	1.75	7352.55
103	C3H8(+M) = C2H5+CH3(+M)	8.13E+22	-1.5	106447.9
104	O+C3H8 = OH+C3H7	2.24E+05	2.73	4094.93
105	OH+C3H8 = C3H7+H2O	2.63E+07	1.67	1198.72
106	C3H7+H2O2 = HO2+C3H8	3.42E+02	2.59	1804.04
107	HO2+C3H7 => OH+C2H5+CH2O	2.13E+13	0	0
108	C3H6+C2H5 = C3H5+C2H6	2.23E+00	4.19	8492.34
109	C3H6+O = CH3+CH3CO	8.46E+04	3.03	-1001.48